Title
Investigations of Metabolic Pathways in Mycobacterium tuberculosis

Author
Hatzios, Stavroula

Publication Date
2010

Peer reviewed|Thesis/dissertation

Investigations of Metabolic Pathways in *Mycobacterium tuberculosis*

by

Stavroula K Hatzios

A dissertation submitted in partial satisfaction of the

requirements for the degree of

Doctor of Philosophy

in

Chemistry

in the

Graduate Division

of the

University of California, Berkeley

Committee in charge:

Professor Carolyn R. Bertozzi, Chair
Professor Matthew B. Francis
Professor Tom Alber

Fall 2010

Investigations of Metabolic Pathways in *Mycobacterium tuberculosis*

By Stavroula K Hatzios

Abstract

Investigations of Metabolic Pathways in *Mycobacterium tuberculosis*

by

Stavroula K Hatzios

Doctor of Philosophy in Chemistry

University of California, Berkeley

Professor Carolyn R. Bertozzi, Chair

Mycobacterium tuberculosis (*Mtb*), the bacterium that causes tuberculosis in humans, infects roughly two billion people worldwide. However, less than one percent of infected individuals are symptomatic. Most have a latent infection characterized by dormant, non-replicating bacteria that persist within a mass of immune cells in the lung called the granuloma. The granuloma provides a protective barrier between infected cells and surrounding tissue. When host immunity is compromised, the granuloma can deteriorate and reactivate the disease.

In order to mount a latent infection, *Mtb* must survive in alveolar macrophages, the host's primary line of defense against this intracellular pathogen. By evading typical bactericidal processes, *Mtb* is able to replicate and stimulate granuloma formation. The mechanisms by which *Mtb* persists in macrophages are ill defined; thus, elucidating the factors responsible for this hallmark of *Mtb* pathogenesis is an important area of research.

This thesis explores three discrete metabolic pathways in *Mtb* that are likely to mediate its interactions with host immune cells. The first three chapters examine the sulfate assimilation pathway of *Mtb* and its regulation by the phosphatase CysQ. Chapter 1 provides a general overview of the transcriptional, biochemical, and molecular levels of sulfur metabolism regulation in *Mtb*, while Chapters 2 and 3 present a detailed analysis of how CysQ may influence sulfur transactions in the cell. Chapter 4 explores the biosynthesis of the cell wall glycolipid Polyacyltrehalose, which is exclusively synthesized by pathogenic mycobacteria and may mediate host-pathogen interactions. Finally, Chapter 5 describes a novel osmoregulatory pathway in *Mtb* that affects the pathogen's response to osmotic stress and its production of the well-characterized virulence factor EspA.

This dissertation is dedicated to my father, who is tragically unable to witness the summit, but inspired the climb.

Investigations of Metabolic Pathways in *Mycobacterium tuberculosis*

Table of Contents

List of Figures

List of Tables

List of Schemes

Acknowledgements

I have many people to thank for their guidance, support, and encouragement these last five years. My advisor, Dr. Carolyn Bertozzi, has been a stalwart supporter of my career since I joined the lab. She gave me the scientific freedom to explore offbeat ideas, even those truly peripheral to the group's research, and provided the resources to help guide me down the rabbit hole. Those research experiences have done so much to bolster my confidence as a scientist. I think most people, myself included, confront feelings of insecurity during graduate school, often questioning whether or not they can excel in their chosen field. Carolyn has always made me feel like I can excel as a scientist, and for that I am truly grateful. I admire her positive attitude, her exceptional ability to communicate complex ideas, and knack for mitigating seemingly epic research disasters into minor misfortunes. She has been a tremendous role model, and I have learned so much during my time in her lab.

I would like to thank the members of the Bertozzi group, past and present, for their enduring scientific and emotional support over the years. I would especially like to thank the denizens of room 817, Mike Boyce, Jessica Seeliger, and Gaby de Almeida, for always offering a sympathetic ear during episodes of grad school catharsis and for providing such a positive work environment, not to mention a hip soundtrack for the daily grind. I am particularly indebted to Mike, who has always been so generous with his time and advised me through many scientific and personal challenges. He is a great friend, and I know I am a better scientist because of him. I would also like to express my sincere gratitude to Jessica, an invaluable compatriot of the TB subgroup who has provided me with an abundance of helpful feedback and whose diligence and professionalism I greatly admire. I am grateful to Jessica, Sarah Gilmore, Kim Sogi, and Michael Schelle for helping me brave the TB landscape and for truly appreciating the daily struggle of hours spent working in a respirator without a bathroom break. I would also like to thank Pam Chang, whom I met only once during our undergraduate years at MIT, but who became one of my closest friends at Berkeley. She was always willing to talk me through the ups and downs of graduate school, often over a late-night brownie sundae at Fentons. I am also grateful to Brian Carlson, who spent many patient hours showing me the ropes as a first-year and has remained a good friend. I can always count on him to inject a healthy dose of humor into minor life crises like having your car radio stolen (three times!). Jason Rush, Matt Hangauer, and Pete Woodruff were my labmates in room 831 during my first few years of graduate school, and I thank them for their good company, humor, and practical jokes (of which I was often the target, but silly string and Nerf guns make for sweet revenge). I also thank Jason for many introspective discussions en route to Strada, which provided a welcome respite from the (occasional) tedium of the lab. I am grateful to Jeremy Baskin, whom I befriended at MIT, for helping me transition to life at Berkeley, for all his support over the years, and for motivating me to make time for my oboe. I also thank Sloan Siegrist and Kimberly Beatty for their friendship and for reminding me to smile more often. I am indebted to the amazing support staff of the Bertozzi lab, especially Asia Avelino, Karen Carkhuff, and Olga Martinez, for deftly managing the administrative and technical demands of our enormous group and for slashing through reams of red tape on my behalf. I would also like to thank

Lisa Prach, the director of the biosafety level 3 facility, for expertly taming such a high-maintenance monster of a lab.

I have worked with numerous collaborators over the course of my graduate research and am truly grateful for their guidance, expertise, and time. I owe tremendous thanks to Professor David Sherman and Tige Rustad at Seattle Biomedical Research Institute for teaching me the art of microarray analysis, providing me with invaluable TB-related advice, and for being so generous with their time these last two years. I am grateful to several mass spectrometry collaborators who made pivotal contributions to my thesis research: Cindy Holsclaw and Professor Julie Leary at UC Davis; Tony Iavarone at UC Berkeley; David King and Arnold Falick at the HHMI Mass Spectrometry Laboratory. I would also like to thank Gerald Newton and Professor Robert Fahey at UC San Diego, as well as Professor Tom Alber and his graduate student Christina Baer at UC Berkeley, for their expert advice and technical contributions to my research. I am grateful to the Portnoy, Doudna, and M. Chang labs at UC Berkeley for being so generous with their equipment, and also to Professor Dan Portnoy for advising me during the postdoctoral application process.

I would like to thank the Chemical Biology Graduate Program for giving me the opportunity to rotate in three exceptional labs. I am grateful to each of my rotation advisors (Professors Carolyn Bertozzi, Michael Marletta, and Tom Alber) for welcoming me into their research groups and for their continued support throughout my years at UC Berkeley. I would also like to thank the members of my thesis committee (Professors Matt Francis, Jennifer Doudna, Jamie Doudna Cate, and Tom Alber) for their time and support. I had the good fortune of working with Professor Francis as a graduate student instructor and thank him for his guidance and for being such an exceptional teacher. I am also grateful to the National Institutes of Health, Lawrence Berkeley National Lab, and Howard Hughes Medical Institute for funding my graduate research.

I have been actively involved in science outreach programs since high school and was able to continue that tradition through graduate school with the help of Community Resources for Science (CRS), a non-profit organization that connects scientists with local elementary schools to improve science literacy through hands-on demonstrations. I have worked closely with CRS personnel over the last five years to expand the program's presence on campus and would like to express my sincere thanks to them for championing such an important cause. In particular, I would like to thank the former program director, Anne Jennings, the current campus coordinator, Heidi Williamson, and Professor Bob Bergman, who has been a strong advocate for the program since its inception. I would also like to thank the many members of the Bertozzi outreach team who have volunteered their time over the last four years (and counting!) to mentor kids in our community.

I am also grateful to the many role models who were instrumental in my decision to attend graduate school. I would like to thank my high school chemistry teacher, Mrs. Grady, and calculus teacher, Ms. Helms, for all their support and encouragement. I would like to thank Professor JoAnne Stubbe, one of my biochemistry professors at MIT, whose devotion to teaching and science I greatly admire. I would also like to thank my undergraduate research advisor, Professor Sarah O'Connor, for taking me under her wing and molding me into a capable researcher.

Finally, I would like to thank my friends and family, the unsung heroes of graduate school whose support has been as essential to my success as the science itself. Most of all, I am grateful to my mom, my sister, and Anna, our closest family friend, for their love, strength, and unwavering faith in me.

I would like to close by thanking my dad, the late Dr. Kriton Hatzios, who never got the chance to see me go to graduate school, but inspired me every step of the way.

Chapter 1: Regulation of sulfur metabolism in *Mycobacterium tuberculosis*

Introduction

Tuberculosis poses a critical threat to global health. It is estimated that one-third of the world's population is infected with *Mycobacterium tuberculosis (Mtb)*, the disease-causing bacterium (*1*). However, less than one percent of those infected with *Mtb* show signs of active disease (*2*). The majority of infected individuals have a latent infection characterized by dormant, non-replicating bacteria that persist within a mass of immune cells in the lung (*3*). Collectively, these cells form a protective barrier between the bacteria and surrounding tissue known as the granuloma (*4, 5*). When an infected host becomes immunocompromised, the granuloma deteriorates, liberating the confined bacteria and reactivating the disease.

In order to mount a latent infection, *Mtb* must withstand phagocytosis by alveolar macrophages, the host's primary line of defense against airborne pathogens (*5*). By evading typical bactericidal processes, *Mtb* is able to replicate and eventually induce granuloma formation (*3*). The mechanisms by which *Mtb* persists in the hostile phagosomal environment and orchestrates the transition to latency are ill defined. Elucidating the molecular machinery and metabolic pathways that facilitate these pivotal events is crucial to identifying new therapeutic targets for this global human pathogen.

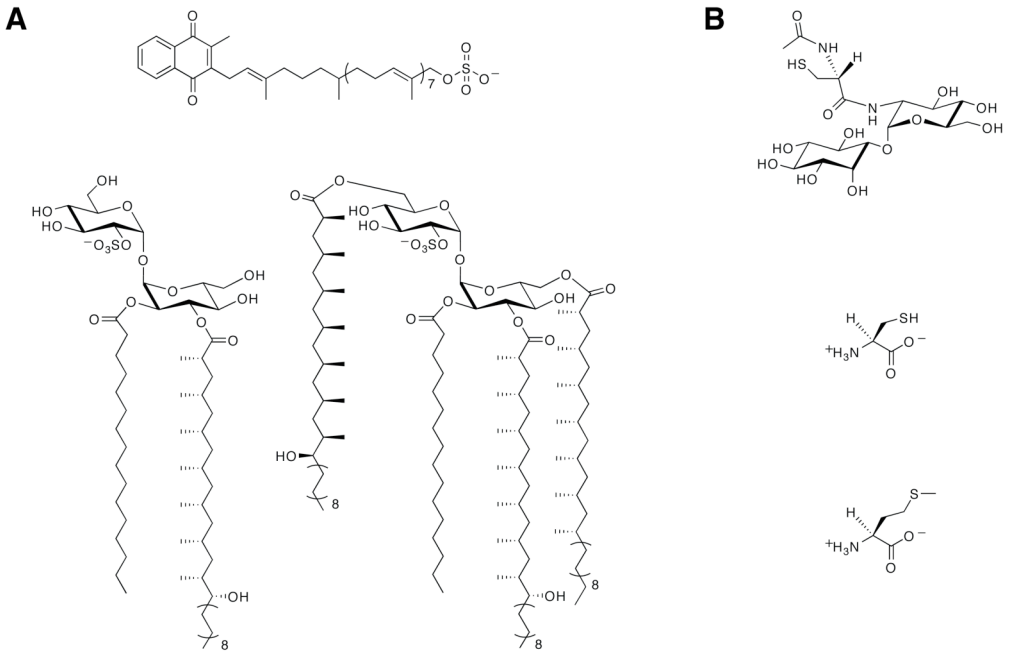

FIGURE 1-1. Sulfur-containing metabolites from *M. tuberculosis*. (**A**) Sulfated compounds, clockwise from top: S881, Sulfolipid-1, SL_{1278}. (**B**) Reduced sulfur compounds, from top to bottom: mycothiol, cysteine, methionine.

There is a growing body of evidence that supports a role for sulfur-containing metabolites in *Mtb* pathogenesis (*6, 7*). Sulfated molecules from *Mtb* have been intimately linked to bacterial virulence (Figure 1-1A) (*8-10*). For example, the prominent cell wall-associated glycolipid Sulfolipid-1 is only produced by pathogenic species of mycobacteria (*8, 11*), and its biosynthetic precursor SL_{1278} has been shown to elicit cytokine production in human tuberculosis patients (*10*). On the contrary, biosynthesis of the sulfated menaquinone S881 suppresses bacterial virulence (*9*). Reduced sulfur compounds (Figure 1-1B), such as the proteogenic amino acids cysteine and methionine, also contribute to *Mtb* pathogenesis (*6*). Disabling their biosynthesis dramatically attenuates bacterial virulence and persistence during the chronic phase of infection in mice (*12*). Mycothiol (MSH), the primary thiol-containing small molecule of mycobacteria (*13*), has also been shown to facilitate bacterial survival *in vitro* (*14*). Biosynthesis of these important sulfur-containing metabolites relies on the sulfate assimilation pathway (*15*).

The sulfate assimilation pathway (Figure 1-2) is composed of a group of enzymes that catalyze the uptake and metabolism of inorganic sulfate from the host (*7*). This pathway commences with the active import of sulfate, which is subsequently adenylated by ATP sulfurylase, an enzyme containing both GTPase and sulfurylase domains (*16*). The resulting product, adenosine 5'-phosposulfate (APS), can be reduced to sulfite by APS reductase for the biosynthesis of reduced sulfur species via the reductive branch of the pathway (*17*). Alternatively, because APS constitutes a metabolic branchpoint, it can be phosphorylated at the 3'-position by APS kinase to generate 3'-phosphoadenosine 5'-phosphosulfate (PAPS), the universal sulfate donor in the cell (*15*). PAPS is a substrate for sulfotransferases, enzymes that catalyze the transfer of its sulfate group onto bacterial metabolites (*11*). Collectively, these reactions constitute the sulfation branch of the sulfate assimilation pathway.

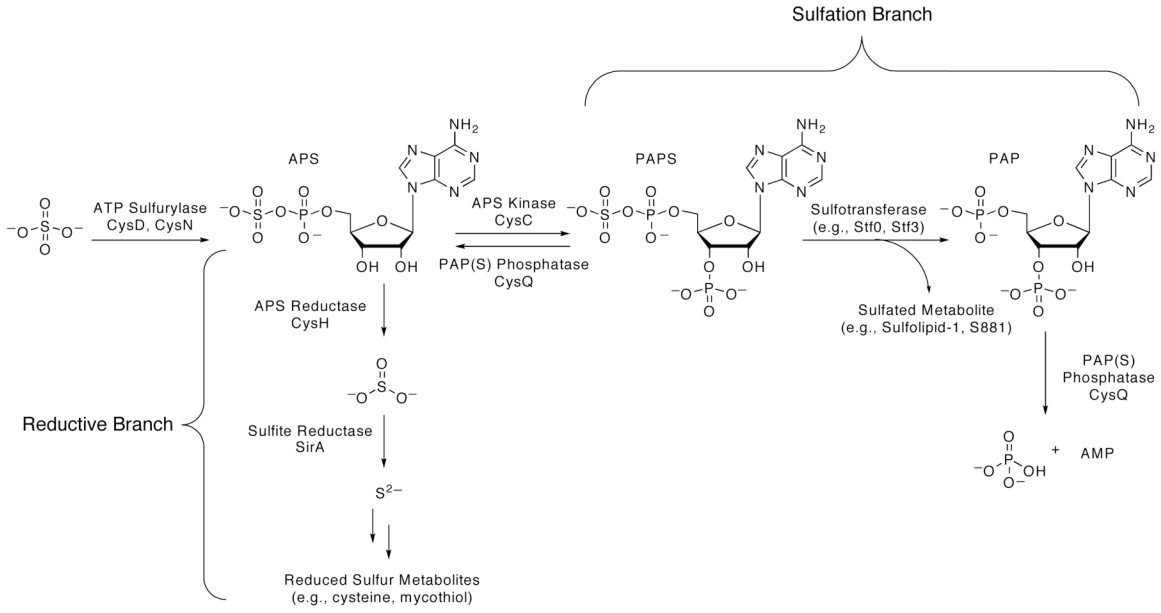

FIGURE 1-2. Sulfate assimilation pathway of *M. tuberculosis*.

The regulation of *Mtb* sulfur metabolism relies on the transcriptional response of sulfate assimilation enzymes to diverse environmental cues and regulatory proteins that influence flux through the sulfate assimilation pathway. Further, models of small molecule regulation from other bacteria suggest similar mechanisms may modulate related transcriptional circuits in *Mtb*. In this chapter, the influence of each of these regulatory elements on *Mtb* sulfur assimilation is discussed in an effort to guide our understanding of how this essential pathway facilitates bacterial adaptation to the host.

Transcriptional regulation of sulfur metabolism genes

Transcriptional profiling has demonstrated that *Mtb* sulfur metabolism genes are dynamically regulated by diverse environmental cues (Table 1-1) (*18-27*). This is perhaps not surprising given the demonstrated importance of the sulfate assimilation pathway to bacterial survival (*6*) and the hostile conditions encountered by bacteria in the phagosome (*28*). For example, upon phagocytosis, bacteria are exposed to oxidative stress and deprived of essential nutrients (*28, 29*). Microarray analysis has shown that these conditions elicit the upregulation of key genes from the sulfate assimilation pathway (Table 1-1) (*19, 20, 24, 25*). Genes encoding the primary sulfate transport complex of *Mtb* are induced following treatment with hydrogen peroxide (*cysT*) and nutrient starvation (*cysA1*, *cysT*, *cysW*, *subI*), conditions which also induce the ATP sulfurylase genes *cysD* and *cysN*, as well as the *cysC* gene that encodes APS kinase (in *Mtb*, *cysC* is fused to *cysN*, yielding a bifunctional *cysNC* gene (*16*)). Given that these genes coordinate the first few steps of the sulfate assimilation pathway, their induction is most likely accompanied by an increase in the biosynthesis of sulfur-containing metabolites that protect the pathogen during the course of infection. Notably, *cysD* and *cysNC* are also induced during macrophage infection, underscoring the importance of sulfur metabolism to intracellular survival (*19, 23*). Indeed, reduced sulfur compounds have been shown to play a critical role in facilitating bacterial persistence *in vivo* (*12*). Genes contributing to the biosynthesis of these metabolites, such as *cysH* and *sirA*, which direct the reduction of APS to sulfide (*17, 30*), and *cysK2* and *cysM*, which participate in cysteine biosynthesis (*31, 32*), are also among those induced by hydrogen peroxide and nutrient starvation. Collectively, these genes are likely to facilitate bacterial adaptation to the phagosomal environment.

Hypoxia is another environmental cue that has been correlated with the upregulation of genes from the sulfate assimilation pathway (*21, 22*). Transcription of *cysD*, *cysNC*, *cysK2*, and *cysM* is induced by hypoxia, suggesting ATP sulfurylase and cysteine biosynthesis may facilitate bacterial adaptation to oxygen-limiting conditions. Because the granuloma has been shown to harbor regions of low oxygen tension (*4*), it is plausible that sulfur metabolism may be important in the transition to latency. The finding that reduced sulfur compounds are critical to the onset of chronic *Mtb* infection in mice lends additional support to this hypothesis (*12*).

TABLE 1-1. Sulfur metabolism genes from *M. tuberculosis* induced by various conditions of environmental stress

Stress Condition	Genes Induced	Reference
5-chloropyrazinamide	*cysN*	(*18*)
Hydrogen peroxide	*cysD*, *cysNC*[a], *cysK2*, *cysM*, *cysT*	(*19, 20*)
Hypoxia	*cysD*, *cysK2*, *cysN*, *cysM*	(*21, 22*)
Macrophage infection	*cysD*, *cysN*	(*19, 23*)
Menadione	*cysA1*, *cysT*, *cysW*, *subI*	(*18*)
Nutrient starvation	*cysA1*, *cysD*, *cysH*, *cysN*, *cysQ*, *cysT*, *cysW*, *sirA*, *subI*	(*24, 25*)
Sodium dodecyl sulfate (SDS)	*cysD*, *cysN*	(*26*)
Vancomycin	*cysD*, *cysK2*, *cysNC*	(*27*)

[a] The *cysN* and *cysC* genes of *Mtb* are fused into a single, bifunctional *cysNC* gene (*20*). However, the transcript is often reported as *cysN* in microarray data.

Certain antibiotics have also been shown to affect the transcription of sulfur metabolism genes. Vancomycin, an inhibitor of peptidoglycan biosynthesis, induces expression of *cysK2*, *cysD*, and *cysNC* (*27*). The *cysNC* gene is also induced by 5-chloropyrazinamide, a pyrazinamide analog that irreversibly inhibits fatty acid biosynthesis *in vitro* (*18, 33*). Furthermore, *cysA1*, *cysT*, *cysW*, and *subI* are collectively induced by menadione, a synthetic vitamin K precursor that promotes the formation of reduced oxygen species (*18, 34*). These data suggest that sulfur metabolism may modulate the bacterial response to these drugs, possibly through the involvement of sulfur-containing compounds in drug detoxification pathways.

In all likelihood, one or more transcriptional regulators mediate the transcriptional response of the sulfate assimilation pathway to extracellular signals. The alternative sigma factor SigH, which is induced by phagocytosis and stress conditions including acidic pH and exposure to diamide, a thiol oxidizer, has been shown to regulate the transcription of several sulfur metabolism genes (e.g., *cysA1*, *cysT*, *cysW, cysD*, and *cysNC*) following diamide treatment (*35*). SigH activity is regulated by the redox-sensitive anti-sigma factor RshA (*36*). Interestingly, the alternative sigma factor SigR from *Streptomyces coelicolor*, a related actinomycete, is also induced by diamide and regulated by the redox-sensitive anti-sigma factor RsrA (Figure 1-3) (*37*). SigR and RsrA have been shown to modulate MSH production in *S. coelicolor* in response to intracellular MSH levels (*37*). The strong dependence of MSH biosynthesis on the sulfate assimilation pathway suggests that SigH and RshA might similarly regulate the biosynthesis of this ubiquitous thiol in mycobacteria.

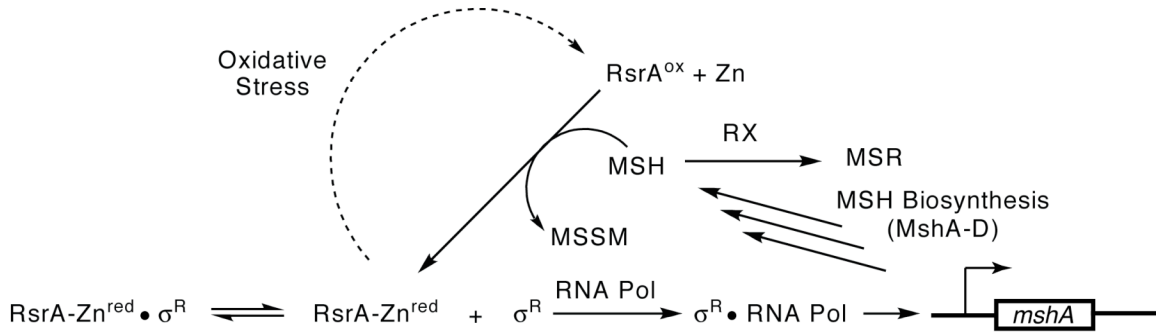

FIGURE 1-3. Feedback regulation of RsrA activity and SigR (σ^R)-mediated transcription by MSH in *S. coelicolor*. The zinc-binding anti-sigma factor RsrA binds the alternative sigma factor σ^R in its reduced state, preventing the association of σ^R with RNA polymerase (RNA Pol). Under conditions of oxidative stress (e.g., hydrogen peroxide or diamide treatment), the zinc-binding cysteine residues of RsrA form disulfide bonds, releasing zinc and liberating σ^R. Upon binding σ^R, RNA polymerase induces transcription of *mshA*, which encodes the first enzyme in the MSH biosynthetic pathway. MSH reduces oxidized RsrA, suppressing its own biosynthesis. However, when oxidizing or alkylating agents (RX) deplete MSH levels, RsrA remains oxidized, facilitating σ^R-mediated transcription and enhancing MSH biosynthesis (*37, 54*).

In *Escherichia coli*, the majority of sulfate assimilation genes belong to the cysteine (*cys*) regulon that is positively regulated by the transcription factor CysB (*38*). In the absence of inorganic sulfate, a second transcription factor, Cbl, induces a series of sulfate starvation-inducible (SSI) genes that coordinate the uptake and subsequent metabolism of organosulfur compounds for the generation of sulfite (*39, 40*). Comparable transcriptional regulators have not yet been identified in mycobacteria.

Though the enzymes involved in sulfur metabolism are largely conserved between these two prokaryotes, there are some key differences in the organization of their respective sulfate assimilation pathways. In *Mtb*, the reductive branch of the pathway emanates from APS, whereas *E. coli* initiates the biosynthesis of reduced sulfur metabolites from PAPS (*15*). *Mtb* also encodes four eukaryotic-like sulfotransferases (*stf0*, *stf1*, *stf2*, and *stf3*), which are not present in *E. coli* (*11, 41*). Further, *Mtb* encodes two independent pathways for cysteine biosynthesis: the traditional pathway, which utilizes L-serine as in *E. coli*, and a novel route that utilizes *O*-phospho-L-serine (*31, 32, 42*). While these distinctions do not rule out the possibility of a CysB-like master regulator in *Mtb*, they do suggest that the transcriptional regulation of mycobacterial sulfur-metabolizing enzymes may diverge considerably from that of *E. coli*. Additional studies are needed to elucidate the transcriptional machinery mediating the expression of these enzymes in *Mtb*. Notably, a functional analog of CysB was recently identified in *Corynebacterium glutamicum*, a gram-positive bacterium belonging to the same suborder as *Mtb*, which will likely facilitate the search for related proteins in mycobacteria (*43*).

Biochemical regulation of sulfur metabolism

In addition to the various environmental conditions that modulate sulfur metabolism at the transcriptional level, several proteins are poised to regulate the metabolic pipeline by mediating the availability of sulfate and its flux through the sulfate assimilation pathway. The first of these are the sulfate transporters, which enable the uptake of extracellular sulfate. The primary sulfate permease of *Mtb* is an ABC transporter encoded by the *subI-cysTWA1* operon (*44*). Genetic disruption of the *cysA1* gene in *Mycobacterium bovis* completely inhibits sulfate uptake *in vitro* and renders the mutant auxotrophic for methionine, yet does not impair bacterial survival in mice (*44*). This implies either a strong reliance on methionine transport *in vivo*, or the presence of other sulfate transporters that can compensate for the loss of SubI-CysTWA activity during infection. Notably, *Mtb* encodes two additional putative sulfate transporters, Rv1739c and Rv1707, whose genes are induced 24 hours post infection of activated macrophages (*19, 45*). Rv1739c expression in *E. coli* has been shown to enhance sulfate uptake, though complementation of the *M. bovis cysA1* mutant with the *Rv1739c* gene is not sufficient to restore sulfate prototrophy (*45*). In contrast, little is known about the *Rv1707* gene product. Assuming all three of these transporters are functional, it is possible they modulate sulfate uptake in response to discrete environmental signals.

The sulfatases are a second class of proteins that likely contribute to the intracellular concentration of free sulfate. These enzymes catalyze the hydrolysis of sulfate esters from sulfated proteins, peptides, and small molecules (*46*). Type I sulfatases are characterized by an active-site formylglycine residue that is critical for catalysis (*47*). The formylglycine is either co- or post-translationally installed by a formylglycine-generating (FGE) enzyme via oxidation of a conserved cysteine (Figure 1-4). The *Mtb* genome encodes six type I sulfatases, yet little is known about their biochemistry (*47*). One of these, AtsG, was recently shown to possess arylsulfatase activity, but its native substrate has not been identified (*48*). In the absence of FGE, *Mtb* exhibits residual sulfatase activity that may be attributed to FGE-independent type II and type III sulfatases (*47*). It is possible that some of these enzymes are secreted and facilitate sulfate scavenging from the host. Alternatively, they may hydrolyze sulfate from endogenous metabolites to redirect the biosynthesis of sulfur-containing compounds in response to evolving cellular needs. In either scenario, these sulfatases are likely to regulate sulfur metabolism by affecting sulfate availability.

FIGURE 1-4. Modification of the active site cysteine of type I sulfatases by formylglycine-generating enzyme (FGE).

Another enzyme poised to regulate *Mtb* sulfur metabolism is CysQ, a 3'-phosphoadenosine-5'-phosphatase. Unlike sulfate permeases and sulfatases, whose

activity directly influences the availability of free sulfate, CysQ has the ability to modulate the levels of intermediates that may affect flux through the sulfate assimilation pathway. Specifically, CysQ dephosphorylates 3'-phosphoadenosine 5'-phosphate (PAP), a byproduct of sulfotransferase reactions, and its sulfated counterpart, PAPS (*49*). Since PAP inhibits at least one *Mtb* sulfotransferase (*50*), and PAPS accumulation is believed to be cytotoxic (*51*), the degradation of these pathway intermediates by CysQ is likely to promote sulfation and balance sulfur transactions in the cell. Interestingly, CysQ activity is inhibited by alkali metal cations *in vitro*, including physiological concentrations of sodium, and a homologous enzyme from *Streptococcus mutans* confers resistance to superoxide stress (*49, 52*). These findings suggest that CysQ may be sensitive to changes in the ionic composition of the cytosol or to oxidative stress encountered during the course of infection. If so, CysQ may modulate sulfur metabolism in response to evolving environmental conditions.

Molecular mechanisms of sulfur metabolism regulation

Small molecule regulation of sulfur metabolism is another important mechanism directing the biosynthesis of sulfur-containing metabolites in bacteria. Though this phenomenon has not been thoroughly investigated in *Mtb*, several paradigms have emerged from other bacteria that may yet prove functional in mycobacteria. In *Salmonella typhimurium*, cysteine, sulfide, and thiosulfate have all been shown to inhibit sulfate assimilation (*38*). Cysteine does so by inhibiting serine acetyltransferase, which catalyzes the formation of *O*-acetylserine, the biosynthetic precursor of cysteine. In contrast, sulfide and thiosulfate bind the CysB transcriptional regulator, repressing the transcription of genes that facilitate sulfide biosynthesis or in the case of thiosulfate, its uptake from outside the cell. In *E. coli*, APS has been shown to inhibit Cbl-mediated transcription, preventing the induction of SSI genes that facilitate sulfur metabolism in the absence of inorganic sulfate (*53*). Thus, APS may serve as a molecular barometer of sulfate assimilation that modulates gene expression in response to sulfate availability. While similar feedback mechanisms remain to be elucidated in *Mtb*, they are likely to play an important role in regulating sulfur metabolism. Consistent with this hypothesis, transcription of the *cysDNC* operon of *Mtb* increases in response to sulfur limitation and decreases following treatment with exogenous cysteine (*20*).

MSH is also likely to trigger transcriptional regulation of sulfur-metabolizing enzymes in *Mtb*. As mentioned previously, the alternative sigma factor SigR from *S. coelicolor* has been shown to modulate the biosynthesis of MSH in response to the intracellular MSH concentration (*37, 54*). The current model of MSH regulation revolves around the redox-sensitive anti-sigma factor RsrA, which binds SigR in its reduced state, sequestering the sigma factor and preventing it from binding RNA polymerase (Figure 1-3). MSH facilitates this activity by maintaining RsrA in its reduced state. Thus, when MSH is abundant, RsrA remains active, suppressing MSH biosynthesis. However, when thiol-reactive toxins overwhelm the cell's MSH supply, RsrA is no longer maintained in its reduced form, freeing SigR to induce MSH biosynthesis. Given the importance of MSH in maintaining the reducing environment of the cytosol and promoting resistance to toxic oxidants (*55*), it is likely that a similar regulatory network is in place to regulate its biosynthesis in mycobacteria.

Summary

The sulfate assimilation pathway of *Mtb* is responsible for the biosynthesis of sulfur-containing metabolites that influence bacterial pathogenesis. The transcriptional regulation of this pathway in response to multifarious environmental cues, including those typically encountered in the phagosome, likely facilitates adaptation to host immune cells. In addition, several proteins that mediate the flux of sulfate through the pathway, such as sulfate permeases, sulfatases, and the phosphatase CysQ, are poised to modulate the biosynthesis of sulfur-containing compounds in response to the evolving metabolic demands of the cell. Finally, the potential for small molecule regulation of *Mtb* sulfur metabolism abounds; the metabolites produced by the sulfate assimilation pathway are themselves candidate regulators of this network, as is the case with cysteine and MSH in other bacteria. Realizing the extent of this regulation remains an outstanding challenge in the field, as does identifying the transcriptional proteins that orchestrate this pathway's response to the bacterial environment. Elucidating these regulatory elements will not only advance our understanding of sulfur metabolism in *Mtb*, but may also reveal a molecular linchpin whose inhibition may dismantle an essential metabolic pathway in this ubiquitous human pathogen.

Thesis overview

Mtb has evolved into a highly successful human pathogen. It deftly subverts the bactericidal mechanisms of alveolar macrophages, ultimately inducing granuloma formation and establishing long-term residence in the host. These hallmarks of *Mtb* infection are facilitated by the metabolic adaptation of the pathogen to its surroundings and the biosynthesis of molecules that mediate its interactions with host immune cells. The subsequent chapters of this thesis present detailed explorations of three such mechanisms from *Mtb*. Chapters 2 and 3 describe the biochemical characterization of a phosphatase from the sulfate assimilation pathway of *Mtb* and its ability to modulate the biosynthesis of virulence-associated sulfated glycolipids derived from this pathway. The biosynthesis of Polyacyltrehalose (PAT), a cell wall glycolipid that bears a strong structural resemblance to these sulfated glycolipids, is the subject of Chapter 4. Specifically, the biochemical characterization of PapA3, an acyltransferase required for PAT assembly, is described. Finally, Chapter 5 uncovers the presence of a novel osmoregulatory pathway in *Mtb* that mediates its response to osmotic stress. Collectively, these findings advance our understanding of complex mechanisms that may aid this notorious intracellular pathogen in its expert manipulation of the host immune response.

References

1. World Health Organization (www.who.int/tb/en/).

2. Ginsberg, A. M., and Spigelman, M. (2007) Challenges in tuberculosis drug research and development, *Nat. Med. 13*, 290-294.

3. Lin, P. L., and Flynn, J. L. (2010) Understanding latent tuberculosis: a moving target, *J. Immunol. 185*, 15-22.

4. Russell, D. G. (2007) Who puts the tubercle in tuberculosis?, *Nat. Rev. Microbiol. 5*, 39-47.

5. Russell, D. G. (2001) *Mycobacterium tuberculosis*: here today, and here tomorrow, *Nat. Rev. Mol. Cell Biol. 2*, 569-577.

6. Bhave, D. P., Muse, W. B., 3rd, and Carroll, K. S. (2007) Drug targets in mycobacterial sulfur metabolism, *Infect. Disord. Drug Targets 7*, 140-158.

7. Schelle, M. W., and Bertozzi, C. R. (2006) Sulfate metabolism in mycobacteria, *Chembiochem 7*, 1516-1524.

8. Gangadharam, P. R., Cohn, M. L., and Middlebrook, G. (1963) Infectivity, pathogenicity and sulpholipid fraction of some Indian and British strains of tubercle bacilli, *Tubercle 44*, 452-455.

9. Mougous, J. D., Senaratne, R. H., Petzold, C. J., Jain, M., Lee, D. H., Schelle, M. W., Leavell, M. D., Cox, J. S., Leary, J. A., Riley, L. W., and Bertozzi, C. R. (2006) A sulfated metabolite produced by *stf3* negatively regulates the virulence of *Mycobacterium tuberculosis*, *Proc. Natl. Acad. Sci. U. S. A. 103*, 4258-4263.

10. Gilleron, M., Stenger, S., Mazorra, Z., Wittke, F., Mariotti, S., Bohmer, G., Prandi, J., Mori, L., Puzo, G., and De Libero, G. (2004) Diacylated sulfoglycolipids are novel mycobacterial antigens stimulating CD1-restricted T cells during infection with *Mycobacterium tuberculosis*, *J. Exp. Med. 199*, 649-659.

11. Mougous, J. D., Green, R. E., Williams, S. J., Brenner, S. E., and Bertozzi, C. R. (2002) Sulfotransferases and sulfatases in mycobacteria, *Chem. Biol. 9*, 767-776.

12. Senaratne, R. H., De Silva, A. D., Williams, S. J., Mougous, J. D., Reader, J. R., Zhang, T., Chan, S., Sidders, B., Lee, D. H., Chan, J., Bertozzi, C. R., and Riley, L. W. (2006) 5'-Adenosinephosphosulphate reductase (CysH) protects *Mycobacterium tuberculosis* against free radicals during chronic infection phase in mice, *Mol. Microbiol. 59*, 1744-1753.

13. Newton, G. L., Arnold, K., Price, M. S., Sherrill, C., Delcardayre, S. B., Aharonowitz, Y., Cohen, G., Davies, J., Fahey, R. C., and Davis, C. (1996) Distribution of thiols in microorganisms: mycothiol is a major thiol in most actinomycetes, *J. Bacteriol. 178*, 1990-1995.

14. Sareen, D., Newton, G. L., Fahey, R. C., and Buchmeier, N. A. (2003) Mycothiol is essential for growth of *Mycobacterium tuberculosis* Erdman, *J. Bacteriol. 185*, 6736-6740.

15. Williams, S. J., Senaratne, R. H., Mougous, J. D., Riley, L. W., and Bertozzi, C. R. (2002) 5'-Adenosinephosphosulfate lies at a metabolic branch point in mycobacteria, *J. Biol. Chem. 277*, 32606-32615.

16. Sun, M., Andreassi, J. L., 2nd, Liu, S., Pinto, R., Triccas, J. A., and Leyh, T. S. (2005) The trifunctional sulfate-activating complex (SAC) of *Mycobacterium tuberculosis*, *J. Biol. Chem. 280*, 7861-7866.

17. Carroll, K. S., Gao, H., Chen, H., Stout, C. D., Leary, J. A., and Bertozzi, C. R. (2005) A conserved mechanism for sulfonucleotide reduction, *PLoS Biol. 3*, e250.

18. Boshoff, H. I., Myers, T. G., Copp, B. R., McNeil, M. R., Wilson, M. A., and Barry, C. E., 3rd. (2004) The transcriptional responses of *Mycobacterium tuberculosis* to inhibitors of metabolism: novel insights into drug mechanisms of action, *J. Biol. Chem. 279*, 40174-40184.

19. Schnappinger, D., Ehrt, S., Voskuil, M. I., Liu, Y., Mangan, J. A., Monahan, I. M., Dolganov, G., Efron, B., Butcher, P. D., Nathan, C., and Schoolnik, G. K. (2003) Transcriptional adaptation of *Mycobacterium tuberculosis* within macrophages: insights into the phagosomal environment, *J. Exp. Med. 198*, 693-704.

20. Pinto, R., Tang, Q. X., Britton, W. J., Leyh, T. S., and Triccas, J. A. (2004) The *Mycobacterium tuberculosis cysD* and *cysNC* genes form a stress-induced operon that encodes a tri-functional sulfate-activating complex, *Microbiology 150*, 1681-1686.

21. Voskuil, M. I., Visconti, K. C., and Schoolnik, G. K. (2004) *Mycobacterium tuberculosis* gene expression during adaptation to stationary phase and low-oxygen dormancy, *Tuberculosis 84*, 218-227.

22. Rustad, T. R., Harrell, M. I., Liao, R., and Sherman, D. R. (2008) The enduring hypoxic response of *Mycobacterium tuberculosis*, *PLoS ONE 3*, e1502.

23. Fontan, P., Aris, V., Ghanny, S., Soteropoulos, P., and Smith, I. (2008) Global transcriptional profile of *Mycobacterium tuberculosis* during THP-1 human macrophage infection, *Infect. Immun*. *76,* 717-725.

24. Hampshire, T., Soneji, S., Bacon, J., James, B. W., Hinds, J., Laing, K., Stabler, R. A., Marsh, P. D., and Butcher, P. D. (2004) Stationary phase gene expression of *Mycobacterium tuberculosis* following a progressive nutrient depletion: a model for persistent organisms?, *Tuberculosis 84*, 228-238.

25. Betts, J. C., Lukey, P. T., Robb, L. C., McAdam, R. A., and Duncan, K. (2002) Evaluation of a nutrient starvation model of *Mycobacterium tuberculosis* persistence by gene and protein expression profiling, *Mol. Microbiol. 43*, 717-731.

26. Manganelli, R., Voskuil, M. I., Schoolnik, G. K., and Smith, I. (2001) The *Mycobacterium tuberculosis* ECF sigma factor sigmaE: role in global gene expression and survival in macrophages, *Mol. Microbiol. 41*, 423-437.

27. Provvedi, R., Boldrin, F., Falciani, F., Palu, G., and Manganelli, R. (2009) Global transcriptional response to vancomycin in *Mycobacterium tuberculosis*, *Microbiology 155*, 1093-1102.

28. Rohde, K., Yates, R. M., Purdy, G. E., and Russell, D. G. (2007) *Mycobacterium tuberculosis* and the environment within the phagosome, *Immunol. Rev. 219*, 37-54.

29. Appelberg, R. (2006) Macrophage nutriprive antimicrobial mechanisms, *J. Leukoc. Biol. 79*, 1117-1128.

30. Pinto, R., Harrison, J. S., Hsu, T., Jacobs, W. R., Jr., and Leyh, T. S. (2007) Sulfite reduction in mycobacteria, *J. Bacteriol. 189*, 6714-6722.

31. O'Leary, S. E., Jurgenson, C. T., Ealick, S. E., and Begley, T. P. (2008) O-phospho-L-serine and the thiocarboxylated sulfur carrier protein CysO-COSH are substrates for CysM, a cysteine synthase from *Mycobacterium tuberculosis*, *Biochemistry 47*, 11606-11615.

32. Schnell, R., and Schneider, G. (2010) Structural enzymology of sulphur metabolism in *Mycobacterium tuberculosis*, *Biochem. Biophys. Res. Commun. 396*, 33-38.

33. Boshoff, H. I., Mizrahi, V., and Barry, C. E., 3rd. (2002) Effects of pyrazinamide on fatty acid synthesis by whole mycobacterial cells and purified fatty acid synthase I, *J. Bacteriol. 184*, 2167-2172.

34. Criddle, D. N., Gillies, S., Baumgartner-Wilson, H. K., Jaffar, M., Chinje, E. C., Passmore, S., Chvanov, M., Barrow, S., Gerasimenko, O. V., Tepikin, A. V., Sutton, R., and Petersen, O. H. (2006) Menadione-induced reactive oxygen species generation via redox cycling promotes apoptosis of murine pancreatic acinar cells, *J. Biol. Chem. 281*, 40485-40492.

35. Mehra, S., and Kaushal, D. (2009) Functional genomics reveals extended roles of the *Mycobacterium tuberculosis* stress response factor sigmaH, *J. Bacteriol. 191*, 3965-3980.

36. Park, S. T., Kang, C. M., and Husson, R. N. (2008) Regulation of the SigH stress response regulon by an essential protein kinase in *Mycobacterium tuberculosis*, *Proc. Natl. Acad. Sci. U. S. A. 105*, 13105-13110.

37. Park, J. H., and Roe, J. H. (2008) Mycothiol regulates and is regulated by a thiol-specific antisigma factor RsrA and sigma(R) in *Streptomyces coelicolor*, *Mol. Microbiol. 68*, 861-870.

38. Kredich, N. M. (1992) The molecular basis for positive regulation of *cys* promoters in *Salmonella typhimurium* and *Escherichia coli*, *Mol. Microbiol. 6*, 2747-2753.

39. Iwanicka-Nowicka, R., and Hryniewicz, M. M. (1995) A new gene, *cbl*, encoding a member of the LysR family of transcriptional regulators belongs to *Escherichia coli cys* regulon, *Gene 166*, 11-17.

40. Stec, E., Witkowska-Zimny, M., Hryniewicz, M. M., Neumann, P., Wilkinson, A. J., Brzozowski, A. M., Verma, C. S., Zaim, J., Wysocki, S., and Bujacz, G. D. (2006) Structural basis of the sulphate starvation response in *E. coli*: crystal structure and mutational analysis of the cofactor-binding domain of the Cbl transcriptional regulator, *J. Mol. Biol. 364*, 309-322.

41. Mougous, J. D., Petzold, C. J., Senaratne, R. H., Lee, D. H., Akey, D. L., Lin, F. L., Munchel, S. E., Pratt, M. R., Riley, L. W., Leary, J. A., Berger, J. M., and Bertozzi, C. R. (2004) Identification, function and structure of the mycobacterial sulfotransferase that initiates Sulfolipid-1 biosynthesis, *Nat. Struct. Mol. Biol. 11*, 721-729.

42. Burns, K. E., Baumgart, S., Dorrestein, P. C., Zhai, H., McLafferty, F. W., and Begley, T. P. (2005) Reconstitution of a new cysteine biosynthetic pathway in *Mycobacterium tuberculosis*, *J. Am. Chem. Soc. 127*, 11602-11603.

43. Ruckert, C., Milse, J., Albersmeier, A., Koch, D. J., Puhler, A., and Kalinowski, J. (2008) The dual transcriptional regulator CysR in *Corynebacterium glutamicum* ATCC 13032 controls a subset of genes of the McbR regulon in response to the availability of sulphide acceptor molecules, *BMC Genomics 9*, 483.

44. Wooff, E., Michell, S. L., Gordon, S. V., Chambers, M. A., Bardarov, S., Jacobs, W. R., Jr., Hewinson, R. G., and Wheeler, P. R. (2002) Functional genomics reveals the sole sulphate transporter of the *Mycobacterium tuberculosis* complex and its relevance to the acquisition of sulphur *in vivo*, *Mol. Microbiol. 43*, 653-663.

45. Zolotarev, A. S., Unnikrishnan, M., Shmukler, B. E., Clark, J. S., Vandorpe, D. H., Grigorieff, N., Rubin, E. J., and Alper, S. L. (2008) Increased sulfate uptake by *E. coli* overexpressing the SLC26-related SulP protein Rv1739c from

Mycobacterium tuberculosis, *Comp. Biochem. Physiol. A Mol. Integr. Physiol. 149*, 255-266.

46. Bojarova, P., and Williams, S. J. (2008) Sulfotransferases, sulfatases and formylglycine-generating enzymes: a sulfation fascination, *Curr. Opin. Chem. Biol. 12*, 573-581.

47. Carlson, B. L., Ballister, E. R., Skordalakes, E., King, D. S., Breidenbach, M. A., Gilmore, S. A., Berger, J. M., and Bertozzi, C. R. (2008) Function and structure of a prokaryotic formylglycine generating enzyme, *J. Biol. Chem*. *283,* 20117-20125.

48. Hossain, M. M., Kawarabayasi, Y., Kimura, M., and Kakuta, Y. (2009) Expression and functional analysis of a predicted AtsG arylsulphatase identified from *Mycobacterium tuberculosis* genomic data, *J. Biochem. 146*, 767-769.

49. Hatzios, S. K., Iavarone, A. T., and Bertozzi, C. R. (2008) Rv2131c from *Mycobacterium tuberculosis* is a CysQ 3'-phosphoadenosine-5'-phosphatase, *Biochemistry 47,* 5823-5831.

50. Pi, N., Hoang, M. B., Gao, H., Mougous, J. D., Bertozzi, C. R., and Leary, J. A. (2005) Kinetic measurements and mechanism determination of Stf0 sulfotransferase using mass spectrometry, *Anal. Biochem. 341*, 94-104.

51. Neuwald, A. F., Krishnan, B. R., Brikun, I., Kulakauskas, S., Suziedelis, K., Tomcsanyi, T., Leyh, T. S., and Berg, D. E. (1992) *cysQ*, a gene needed for cysteine synthesis in *Escherichia coli* K-12 only during aerobic growth, *J. Bacteriol. 174*, 415-425.

52. Zhang, J., and Biswas, I. (2009) A pAp-phosphatase activity is required for superoxide stress tolerance in *Streptococcus mutans*, *J. Bacteriol. 191,* 4330-4340.

53. Bykowski, T., van der Ploeg, J. R., Iwanicka-Nowicka, R., and Hryniewicz, M. M. (2002) The switch from inorganic to organic sulphur assimilation in *Escherichia coli*: adenosine 5'-phosphosulphate (APS) as a signalling molecule for sulphate excess, *Mol. Microbiol. 43*, 1347-1358.

54. Newton, G. L., and Fahey, R. C. (2008) Regulation of mycothiol metabolism by sigma(R) and the thiol redox sensor anti-sigma factor RsrA, *Mol. Microbiol. 68*, 805-809.

55. Buchmeier, N. A., Newton, G. L., and Fahey, R. C. (2006) A mycothiol synthase mutant of *Mycobacterium tuberculosis* has an altered thiol-disulfide content and limited tolerance to stress, *J. Bacteriol. 188*, 6245-6252.

Chapter 2: Biochemical characterization of the *Mycobacterium tuberculosis* CysQ[a]

Introduction

Many sulfur-containing metabolites have been implicated in *Mycobacterium tuberculosis* (*Mtb*) pathogenesis, suggesting the sulfate assimilation pathway may serve as a reservoir of molecules intimately linked to the virulence and survival of the bacterium (*1, 2*). Notable examples include Sulfolipid-1, a glycolipid constituent of the *Mtb* cell wall that has been correlated with virulence (*3*), and mycothiol, an abundant low molecular mass thiol whose antioxidant activity may facilitate bacterial survival in the host (*4-6*). In addition, disruption of the reductive branch of the sulfate assimilation pathway has been shown to attenuate *Mtb* virulence and persistence during the chronic phase of infection in mice (*7*). Genes involved in the sulfate assimilation pathway are frequently upregulated under conditions that mimic the latent stage of the *Mtb* life cycle; some of these genes lack a human counterpart, making them attractive drug targets (*1, 8, 9*). Since dormant mycobacteria are impervious to antibiotics that rely on active cell division, the machinery used by these bacteria in the metabolism of sulfur may represent new targets for therapeutic intervention.

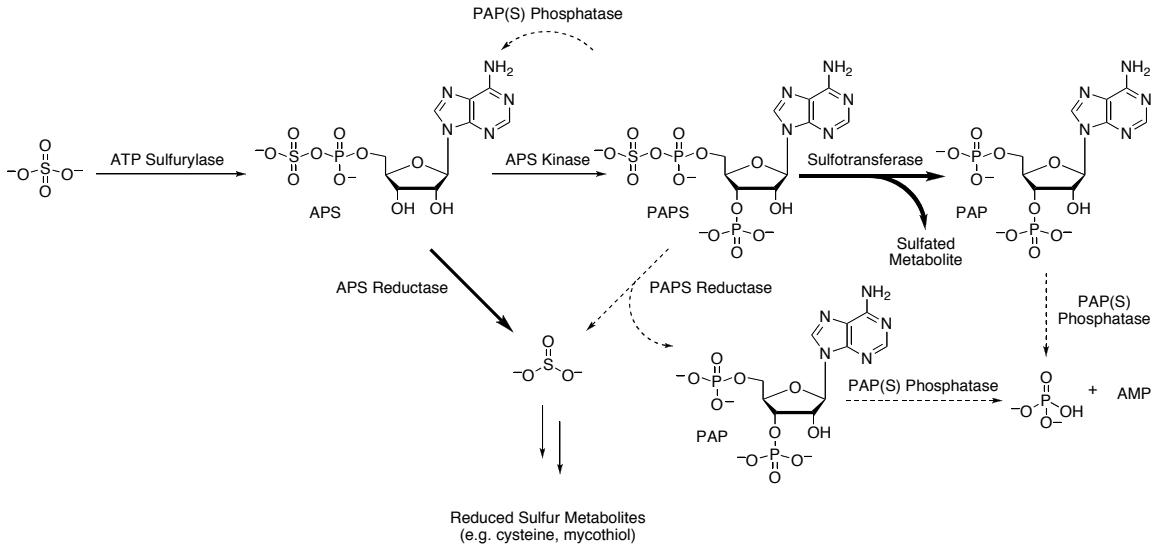

FIGURE 2-1. Sulfate assimilation pathways of *E. coli* and *M. tuberculosis*. Arrows with dotted lines designate enzymatic reactions specific to *E. coli*. Bolded arrows designate those specific to *Mtb*.

The sulfate assimilation pathway of *Mtb* is analogous to the prototypical pathway of *E. coli* (Figure 2-1) (*10-12*). It begins with the uptake of inorganic sulfate, which is subsequently activated by condensation with ATP in a reaction catalyzed by ATP sulfurylase. This enzyme, encoded by the genes *cysD* and *cysN*, is a heterodimeric G-protein that couples GTP hydrolysis with the sulfurylation of ATP to generate adenosine

[a] Anthony T. Iavarone contributed to the work presented in this chapter.

5'-phosphosulfate (APS). APS is then phosphorylated at the 3'-position by APS kinase (CysC) to give 3'-phosphoadenosine 5'-phosphosulfate (PAPS). In *E. coli*, this intermediate is reduced to sulfite and 3'-phosphoadenosine 5'-phosphate (PAP) by PAPS reductase (CysH), which uses thioredoxin as an electron donor. Sulfite is then reduced to sulfide, which is incorporated into several reduced sulfur-containing metabolites, such as cysteine, methionine, and mycothiol, by other enzymes in the *cys* regulon. In *Mtb*, however, this reduction cascade emanates from APS, which is reduced to sulfite by APS reductase (also termed CysH) (*12, 13*). This leaves PAPS to serve as the sulfuryl group donor for a set of eukaryotic-like sulfotransferases, which generate sulfated metabolites believed to mediate host-pathogen interactions and signaling pathways in the bacterium (*14-16*).

One regulator of sulfate assimilation in *E. coli* is the phosphatase CysQ (*17, 18*). Mutations in the *cysQ* gene result in cysteine and sulfite auxotrophy under aerobic conditions, which supports a key role for this enzyme in sulfur metabolism. CysQ is believed to regulate the intracellular level of PAPS, which may be cytotoxic at high concentrations (*17, 19*). In addition, CysQ is thought to modulate PAP levels in the cell (*19, 20*), an activity that might further regulate the biosynthesis of reduced sulfur-containing metabolites since PAP is a competitive inhibitor of PAPS reductase. Interestingly, PAP accumulation negatively regulates the activity of other important bacterial enzymes (*21*). Examples include oligoribonuclease, an exonuclease which degrades small ribonucleotides, and phosphopantetheinyltransferase, an enzyme which transfers the 4-phosphopantetheine group of coenzyme A to acyl carrier protein during fatty acid biosynthesis and the production of secondary metabolites (*22*). Thus, CysQ may not only regulate the cell's ability to metabolize sulfur, but could also play a role in other essential bacterial processes. Yet, no homolog of the *E. coli* CysQ has been characterized in *Mtb*.

Given the many parallels between sulfur metabolism in *E. coli* and *Mtb*, we reasoned that a CysQ-like phosphatase could be functional in mycobacteria. Upon searching the *Mtb* genome, we discovered a gene, *Rv2131c*, whose encoded protein shares 31% amino acid sequence identity with the *E. coli* CysQ (*23*). However, a recent report by Gu and coworkers (*24*) indicated the encoded enzyme may serve as a bifunctional inositol monophosphatase and fructose-1,6-bisphosphatase, a finding that supports a role for *Rv2131c* in *myo*-inositol biosynthesis and challenges its assignment to the mycobacterial sulfate assimilation pathway.

In this chapter, we clarify the physiological role of *Rv2131c* by providing conclusive evidence that the gene product can function as a CysQ phosphatase. Genetic complementation of an *E. coli* Δ*cysQ* mutant with the *Mtb* gene unequivocally establishes its ability to dephosphorylate PAP and PAPS *in vivo*. In addition, following the heterologous expression of *Rv2131c* in *E. coli*, the enzyme was purified and characterized to obtain kinetic parameters for PAP, *myo*-inositol-1-phosphate (IMP), and fructose-1,6-bisphosphate (FBP). The data confirm that PAP is the preferred *in vitro* substrate of *Rv2131c*, redefining the substrate specificity of this enzyme and validating its assignment as a CysQ phosphatase. Taken together, these findings suggest that *Rv2131c* may serve as an important regulator of sulfur metabolism in *Mtb.* With the potential to manipulate sulfation levels in the cell and regulate the biosynthesis of essential reduced sulfur-containing metabolites, CysQ may be an attractive target for antibiotic therapy.

Results and Discussion

Identification of CysQ homolog Rv2131c in the M. tuberculosis *genome*

BLAST analysis was used to identify a CysQ homolog in *M. tuberculosis* with 31% amino acid sequence identity to *E. coli* CysQ (UniProtKB entry P22255). The corresponding gene, *Rv2131c*, was annotated as a "possible monophosphatase *cysQ*" in the published genome (*23*). The encoded protein bears the conserved metal-binding motif of the phosphomonoesterase protein family (Figure 2-2), which includes the *S. cerevisiae* Hal2p (UnitProtKB P32179), a well-characterized 3'-phosphoadenosine-5'-phosphatase (*20, 25, 26*).

FIGURE 2-2. Multiple sequence alignment of enzymes from the phosphomonoesterase protein family. Sequences were aligned using ClustalW and shading of conserved residues was performed using Jalview. The underlined residues constitute the conserved metal-binding motif of the phosphomonoesterase protein family. Abbreviations are as follows: Mtb_Rv2131c, Rv2131c from *Mtb* (UniProtKB entry P65163); Ecoli_CysQ, CysQ from *E. coli* (UniProtKB entry P22255); Scer_Hal2, 3' (2'),5'-bisphosphate nucleotidase from *S. cerevisae* (UniProtKB entry P32179); Osat_RHL, 3'(2'),5'-diphosphonucleoside 3'(2')-phosphohydrolase from *O. sativa* (UniProtKB entry P0C5A3); Ecoli_SuhB, inositol-1-monophosphatase from *E. coli* (UniProtKB entry P0ADG4); Ecoli_FBPase, fructose-1,6-bisphosphatse from *E. coli* (UniProtKB entry P0A993).

Heterologous expression of Rv2131c in E. coli

Rv2131c was expressed in *E. coli* BL21(DE3) with an N-terminal His_6 tag. Initial attempts to purify the protein using the procedure described by Gu *et al.* (*24*) were unsuccessful. Significant impurities were retained following elution of the protein from the column. To improve the purification process, a substrate-affinity purification step was introduced. PAP-agarose resin pre-equilibrated with calcium, an inhibitor of homologous phosphatases, was used to enrich the *Rv2131c* gene product by preventing hydrolysis of the immobilized substrate (*18*). The protein was eluted using an excess of PAP and further purified by size exclusion chromatography. The protein was stable in gel filtration buffer lacking NaCl, an inhibitor of certain CysQ homologs (*27, 28*). For this reason, NaCl was omitted from subsequent activity assays. SDS-PAGE analysis revealed an apparent molecular mass of 30 kDa for the purified protein. Electrospray ionization mass spectrometry was used to confirm the identity of the protein, whose measured mass (30,578 ± 1 Da) was in agreement with the predicted molecular mass of the protein lacking the N-terminal methionine (30,578.5 Da). In addition, tryptic

digestion and mass fingerprinting of the purified protein sample generated approximately 83% sequence coverage, providing further confirmation of the protein's identity.

Defining optimal conditions for PAP phosphatase activity

Once the purified *Rv2131c* gene product was found to dephosphorylate PAP, its activity with the substrate was measured as a function of pH, various metal ions, and Mg^{2+} concentration (Figure 2-3). The pH-dependent activity profile was determined by calculating the specific activity of the enzyme in the presence of 100 μM PAP and 0.5 mM $MgCl_2$ at pH 6.0, 6.5, 7.0, 7.5, 8.0, 8.5, 9.0, and 10.0. The optimum pH was found to be between 8.5 and 9.5 (Figure 2-3A), similar to that of other CysQ homologs (*19, 29*).

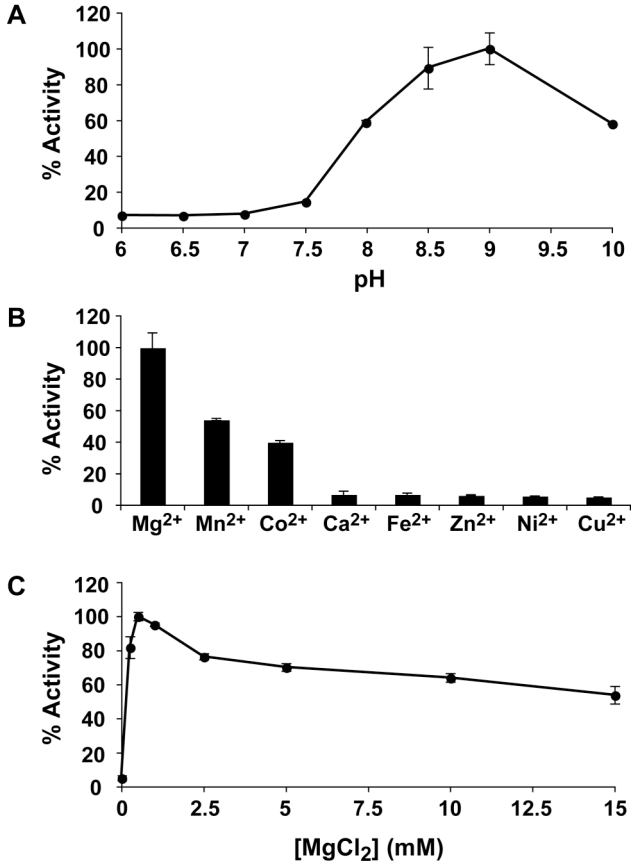

FIGURE 2-3. pH, Metal, and Mg^{2+} dependence of Rv2131c PAP phosphatase activity. Rv2131c activity as a function of pH (**A**), various divalent metal ions (**B**), or $MgCl_2$ concentration (**C**). Conditions: 100 μM PAP, 50 mM Tris buffer, pH 8.5, 0.5 mM $MgCl_2$, 5 nM enzyme, 30 °C. For (**A**) through (**C**), the corresponding conditions were varied. Activities are expressed as a percentage of the maximum observed activity. These data represent the average of three independent experiments. Error bars indicate the corresponding standard deviation.

To determine its divalent metal ion dependence, the enzyme was assayed with 100 μM PAP in the presence of 50 mM Tris buffer (pH 8.5) and 0.5 mM $MgCl_2$, $MnCl_2$, $CoCl_2$, $CaCl_2$, $FeCl_2$, $ZnCl_2$, $NiCl_2$, or $CuCl_2$. As anticipated, the enzyme was most active with Mg^{2+}, the preferred cofactor of the phosphomonoesterase protein family (*25*). Mn^{2+} afforded roughly 50% of the activity observed with Mg^{2+}, while 40% activity was retained in the presence of Co^{2+}. Less than 7% activity was observed with the remaining metal ions (Figure 2-3B). This trend may be explained by variations in the pK_a of metal-coordinated water, which likely participates in phosphoryl group transfer (*30*). The pK_a's of Mg^{2+}-, Mn^{2+}-, and Co^{2+}-coordinated water are between 10.2 and 11.4, whereas those of water coordinated to the remaining divalent metal ions deviate markedly from these values (*31*). The microenvironment defined by the enzyme's active site appears to favor hydrolysis by water with a pK_a that falls within this narrow range.

Once Mg^{2+} was identified as the optimal metal cofactor for PAP-phosphatase activity, different concentrations of the metal ion (from 0 to 15 mM) were assayed in the presence of 100 μM PAP and 50 mM Tris buffer (pH 8.5). Maximal activity was observed with 0.5 mM $MgCl_2$, comparable to the *E. coli* CysQ and related enzymes (*19, 29, 32*). Only a small amount of the metal ion was needed to activate the enzyme, which maintained significant activity at higher Mg^{2+} concentrations, though a gradual decline in activity was observed above 1 mM $MgCl_2$ (Figure 2-3C).

Sensitivity of Rv2131c to alkali metal cations

Proteins belonging to the phosphomonoesterase protein family are universally inhibited by lithium, often at submillimolar concentrations (*25*). In addition, the PAP phosphatase activity of CysQ homologs is commonly affected by two other alkali metal cations: Na^+ and K^+ (*19, 20, 26*). Some enzymes are inhibited by both of these cations (*28, 29*), whereas others are inhibited by sodium but activated by potassium (*20, 26*). It is likely that the variable cation sensitivity of CysQ homologs results from structural differences in their alkali metal-binding sites (*26*).

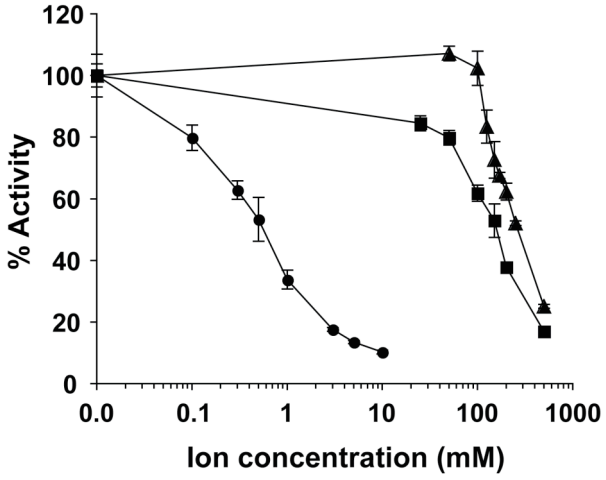

FIGURE 2-4. Inhibition of Rv2131c PAP phosphatase activity by Li^+, Na^+, and K^+. Rv2131c activity as a function of LiCl (●), NaCl (■), or KCl (▲) concentration.

Conditions: 100 μM PAP, 50 mM Tris buffer, pH 8.5, 0.5 mM $MgCl_2$, 5 nM enzyme, variable amounts of LiCl, NaCl, or KCl, 30 °C. Activities are expressed as a percentage of the activity observed in the absence of monovalent cations. These data represent the average of three independent experiments. Error bars indicate the corresponding standard deviation.

To evaluate the sensitivity of the *Rv2131c*-encoded enzyme to these cations, PAP phosphatase activity was measured using 100 μM PAP in the presence of 50 mM Tris buffer (pH 8.5), 0.5 mM $MgCl_2$, and various concentrations of LiCl (0 to 10 mM), NaCl (0 to 500 mM), or KCl (0 to 500 mM). Lithium was the most potent inhibitor of Rv2131c, with a half-maximal inhibition concentration (IC_{50}) of approximately 0.5 mM (Figure 2-4). Sodium and potassium also inhibited PAP hydrolysis, but had higher IC_{50} values (150 mM and 250 mM, respectively).

Electrospray ionization mass spectrometry assay

Previous efforts to assay CysQ-type activity have frequently relied on colorimetric inorganic phosphate detection or HPLC-based methods (*19, 20, 28*). However, the limited sensitivity of these techniques has frustrated attempts to accurately measure kinetic parameters for substrates with low micromolar K_m values (*20, 33*). Methods involving radiolabeled materials have been successfully employed to obtain the kinetic parameters for such substrates (*18, 33*), but are often cumbersome. This is especially true when radioactive substrates must be synthesized due to a lack of commercial availability, as is the case with PAP. For these reasons, and because initial attempts to characterize PAP using the malachite green assay indicated the K_m was below 20 μM, we used a mass spectrometry-based assay for the steady-state kinetic analysis of this substrate. This approach has been successfully applied to bacterial sulfotransferases, generating kinetic parameters that are in excellent agreement with those obtained using a radiolabel transfer assay (*34, 35*).

To quantify product formation by mass spectrometry, an internal standard must be used whose mass spectral intensity can be compared to that of the product ion (*34*). For this comparison to be valid, the structure and ionization efficiency of the internal standard must approximate those of the product. With this in mind, we selected GMP as our internal standard because of its structural similarities to the PAP reaction product, AMP. A mixture containing known concentrations of AMP and GMP was prepared and analyzed by electrospray ionization mass spectrometry (ESI-MS) to obtain the intensities of the product and internal standard ions. These values were then used to calculate a single-point normalization factor R using eq 1. An average R value of 1.5 ± 0.1 was obtained using a series of samples prepared and analyzed at different times over a three-week period. This value was used to calculate the amount of AMP generated in subsequent assays using eq 2.

Initially, a reaction progress curve was generated to define the linear range of enzyme activity (Figure 2-5). Product formation was monitored as a function of time by taking aliquots of a reaction mixture containing 25 μM PAP and 5 nM enzyme over a 30-minute period. Each aliquot was quenched with a 10% HCl solution and then mixed with

the internal standard prior to analysis by ESI-MS. Acid was used to stop the reaction because the internal standard was not soluble in methanol, the organic solvent traditionally used as a quenching agent in this assay (*34, 35*). The linear portion of the progress curve was defined between 0 and 6 minutes with an R^2 value of 0.993 (Figure 2-5, inset). A reaction time of 4 minutes was used in subsequent kinetic assays, corresponding to approximately 37% conversion of substrate to product.

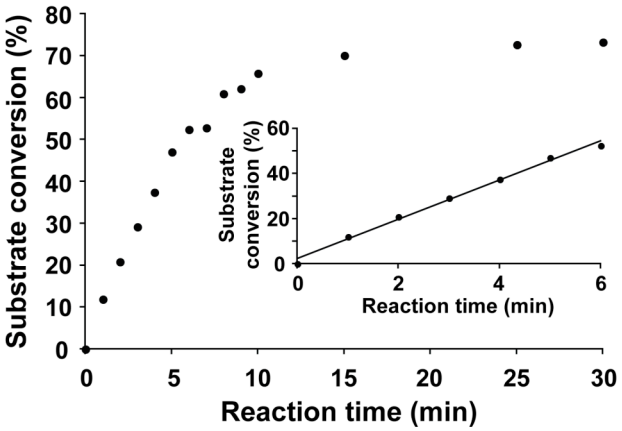

FIGURE 2-5. Reaction progress curve for determining the linear range of Rv2131c PAP phosphatase activity. Conditions: 25 μM PAP, 50 mM Tris buffer, pH 8.5, 0.5 mM $MgCl_2$, 5 nM enzyme, 30 °C. The inset shows the linear portion of the curve from 0 to 6 min.

It is noteworthy that unlike previous applications of this method (*34, 35*), samples were prepared under entirely aqueous conditions and without altering the biochemical matrix of the reaction. Tris buffer was used at a concentration of 50 mM in each reaction, demonstrating the ability of this assay to quantify the products of enzymatic processes in complex biochemical mixtures. The sensitivity of these measurements was somewhat limited by the ion suppression effect of Tris buffer, however, which made it difficult to obtain accurate reaction progress curves at low substrate concentrations. For this reason, we were unable to confirm whether enzyme activity was still linear after four minutes under these reaction conditions. Thus, the initial rates calculated at low PAP concentrations may be slightly underestimated and the K_m for this substrate may be even lower than reported.

Steady-state kinetic assays

The kinetics of PAP phosphatase activity were measured by reacting various amounts of substrate with Rv2131c and quantifying product formation by the ESI-MS assay (Figure 2-6). Reaction velocity was plotted as a function of substrate concentration (Figure 2-7), and Michaelis-Menten parameters were derived using KaleidaGraph.

As anticipated, the K_m for PAP is in the low micromolar range and compares favorably with those of the *E. coli* CysQ (1.1 μM) and *S. cerevisiae* Hal2p (0.72 μM) (Table 2-1) (*18*). These values are consistent with the reportedly low levels of PAP in the

cell (less than 10 μM) (*27*). The catalytic efficiency of the *Rv2131c*-encoded enzyme for PAP is also comparable to those of its homologous enzymes (*18*). The similar biochemical profiles of these enzymes support the assignment of the *Rv2131c* gene product as a PAP-specific phosphatase.

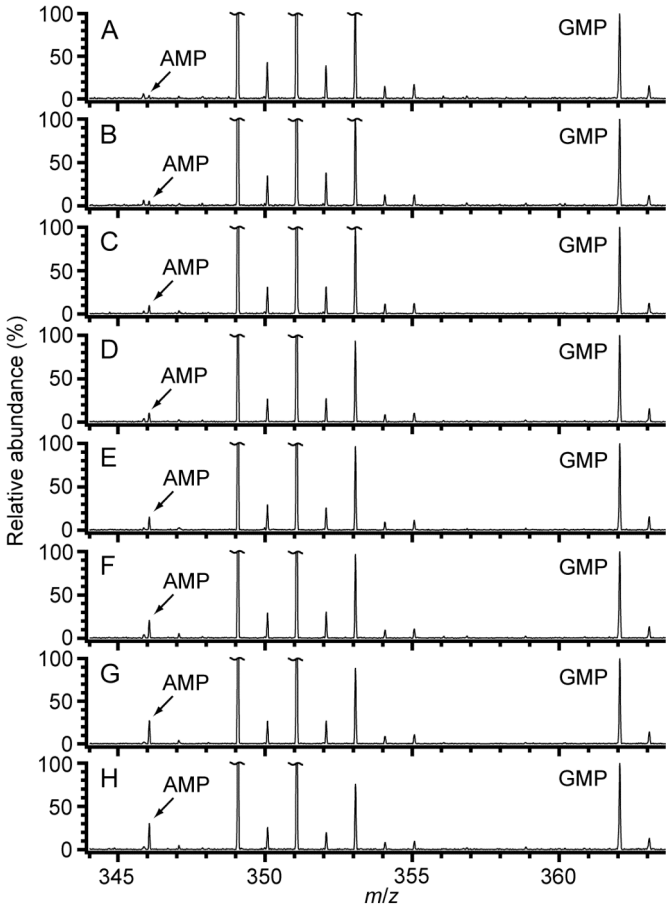

FIGURE 2-6. Sample mass spectra from the kinetic study of Rv2131c with PAP as the substrate. A series of reaction mixtures containing (**A**) 0.625, (**B**) 1.25, (**C**) 2.5, (**D**) 3.5, (**E**) 5, (**F**) 12.5, (**G**) 25, and (**H**) 50 μM PAP were prepared. Reactions were quenched after 4 min and mixed with an internal standard solution containing 6.25 μM GMP prior to analysis by ESI-MS. Conditions: 50 mM Tris buffer, pH 8.5, 0.5 mM $MgCl_2$, 5 nM enzyme, 30 °C. The $(M-H)^-$ ions of AMP and GMP are denoted by "AMP" and "GMP," respectively. Mass spectral intensities are normalized to the intensity of the $(M-H)^-$ ion of GMP (at *m*/*z* 362.1).

In concurrence with the previous biochemical study of *Rv2131c* (*24*), the encoded enzyme was found to dephosphorylate IMP and FBP. However, the catalytic efficiencies for these substrates are over three orders of magnitude lower than the corresponding second-order rate constant for PAP, indicating that PAP is the preferred substrate for Rv2131c. These findings suggest the enzyme exhibits only nominal activity with IMP and FBP *in vivo*. While isolated activity with certain inositol phosphates has been

described for a number of CysQ homologs, PAP is widely defined as the superior substrate (*18, 28, 32, 33, 36*). The slight promiscuity of these enzymes can possibly be attributed to the structural similarities between these substrates and the conservation of a common metal-binding motif and core fold among members of the phosphomonoesterase protein family, which includes various inositol phosphatases, fructose 1,6-bisphosphatase, and the *E. coli* CysQ (*25*).

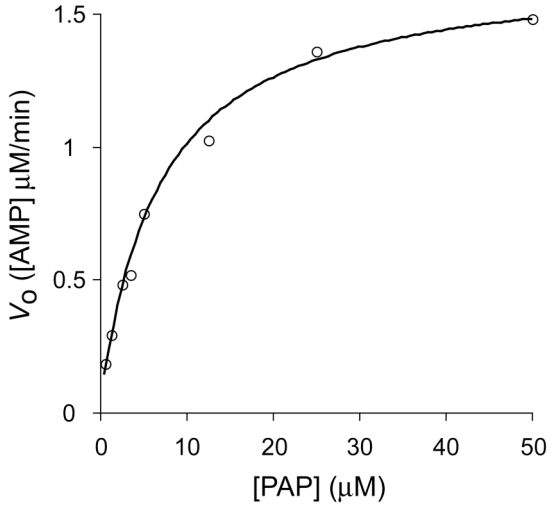

FIGURE 2-7. Steady-state kinetics of Rv2131c with PAP as the substrate. A plot of V_o versus [PAP]. Conditions: 0.625 to 50 μM PAP, 50 mM Tris buffer, pH 8.5, 0.5 mM $MgCl_2$, 5 nM enzyme, 30 °C.

TABLE 2-1. Michaelis-Menten parameters for Rv2131c

Substrate	K_m (μM)[a]	k_{cat} (s^{-1})[a]	k_{cat}/K_m (μM^{-1} min^{-1})
PAP	8.1 ± 3.1	5.4 ± 1.1	42 ± 8
IMP	7110 ± 1070	0.31 ± 0.13	0.0027 ± 0.0015
FBP	566 ± 107	0.24 ± 0.05	0.025 ± 0.001

[a]KaleidaGraph (version 4.03) was used to extract K_m and k_{cat} from initial velocity data. Conditions for PAP: 0.625 to 50 μM PAP, 50 mM Tris buffer, pH 8.5, 0.5 mM $MgCl_2$, 5 nM enzyme. Conditions for IMP and FBP: IMP (1 to 5.5 mM) or FBP (90 to 900 μM), 50 mM Tris buffer, pH 9.0, 10 mM $MgCl_2$, 110 nM enzyme. All reactions were performed at 30 °C. These data represent the average of three independent experiments.

PAP phosphatases have also been shown to exhibit activity with PAPS, another intermediate of the sulfate assimilation pathway (*20, 28, 33, 36*). Unfortunately, the phosphosulfate bond of this substrate is prone to rapid hydrolysis, which results in conversion to PAP (*33, 37*). Consequently, the kinetic analysis of this substrate is complicated by the presence of a competing substrate. In addition, commercial PAPS (Sigma, EMD Biosciences) is supplied as a lithium salt. Since lithium is a potent inhibitor of this enzyme class (*25, 26*), ion-exchange chromatography must be used to

purify the substrate prior to its use in biochemical assays. This purification process results in significant decomposition of the compound to PAP and sulfate (*33*), precluding its accurate kinetic characterization. For these reasons, attempts to obtain kinetic parameters for PAPS that would enable a comparison with the other substrates in this study were unsuccessful. However, a qualitative assessment of [^{35}S]PAPS hydrolysis by Rv2131c using thin-layer chromatography and Phosphorimager analysis suggests that PAPS is a substrate for the enzyme (data not shown).

Genetic complementation of an E. coli *Δ*cysQ *mutant*

Given the similarities in sequence and substrate selectivity between the *Rv2131c*-encoded enzyme and the *E. coli* CysQ, we chose to validate the function of *Rv2131c* through genetic complementation studies in *E. coli.* A mutant strain of *E. coli* lacking CysQ was transformed with *Rv2131c* in a pBAD18 plasmid under the control of an arabinose-inducible promoter. Disruption of the *cysQ* gene in *E. coli* results in a growth requirement for sulfite or cysteine (Figure 2-8, A) (*17*). Thus, following growth on LB agar with ampicillin and kanamycin, isolated colonies of the transformed cells were plated onto M9 minimal medium containing sulfate as the sole sulfur source. Arabinose was also included in the medium to enable overexpression of the *Mtb* gene. Complementation of the mutant strain clearly demonstrated the ability of the *Rv2131c* gene product to restore prototrophy *in vivo* (Figure 2-8, B). Growth of the mutant strain was restored to levels observed in the presence of sulfite after just 24 hours of growth. Importantly, the vector control maintained cysteine and sulfite auxotrophy (Figure 2-8, C). These results support our hypothesis that *Rv2131c* encodes a functional CysQ *in vivo*.

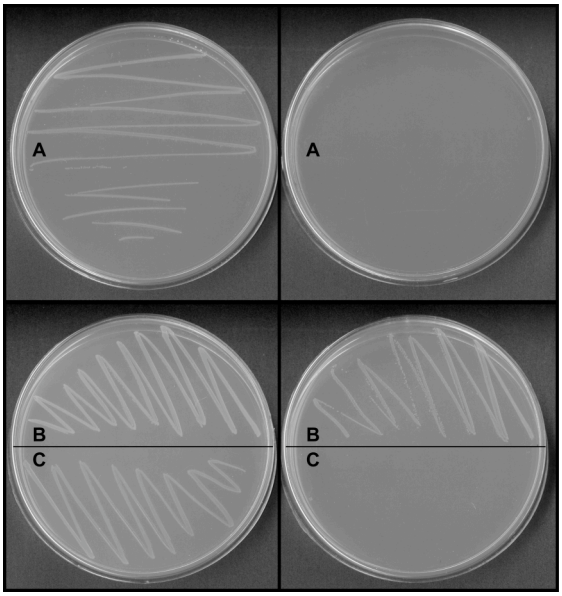

FIGURE 2-8. Complementation of Δ*cysQ* sulfite auxotrophy in *E. coli*. An *E. coli* strain with the native *cysQ* disrupted by a transposon insertion (**A**) was transformed with the *Rv2131c* gene in a pBAD18 vector (**B**) or with the vector alone (**C**). Individual

colonies were plated onto M9 minimal medium containing 0.2% arabinose and incubated at 37 °C for 24 h. Plates on the left contained 0.5 mM sulfite.

Conclusions

In recent years, a framework for mycobacterial sulfur metabolism has emerged reflecting analogous pathways in *E. coli* (*1, 2, 11*). Many key genes of the Cys regulon, including the *cysDNC* genes and *cysH*, have been identified and characterized (*12, 13, 38, 39*). We now augment the current picture of sulfur metabolism in *Mtb* to include CysQ, a PAP phosphatase encoded by the *Rv2131c* gene.

Following its identification by homology to the *E. coli* CysQ, *Rv2131c* was recombinantly expressed and purified from *E. coli*. Biochemical studies of the *Rv2131c* enzyme revealed its ability to dephosphorylate PAP in a magnesium-dependent manner that was sensitive to inhibition by lithium, sodium, and potassium ions. The enzyme exhibited optimal activity with 0.5 mM $MgCl_2$ at pH 8.5 to 9.5. A sensitive ESI-MS assay was used to extract the kinetic parameters for PAP, which were comparable to those of the *E. coli* CysQ. PAP was the substrate utilized most efficiently by the enzyme, which exhibited relatively little activity with IMP and FBP. Genetic complementation studies in *E. coli* confirmed its ability to dephosphorylate PAP and PAPS *in vivo*, reaffirming its place in the sulfate assimilation pathway of *Mtb*.

While the *Rv2131c* enzyme was originally classified as a bifunctional inositol monophosphatase and fructose-1,6-bisphosphatase, our findings suggest its primary physiological role relates to mycobacterial sulfur metabolism and not to the biosynthesis of *myo*-inositol. By controlling the pools of PAP and PAPS in the cell, Rv2131c is poised to serve as a key regulator of the sulfate assimilation pathway. This enzyme, which we rename CysQ in accordance with its genomic annotation, has the potential to manipulate sulfation levels in the cell and control the biosynthesis of essential reduced sulfur-containing metabolites.

Materials and Methods

Materials

Pfu DNA polymerase was from Stratagene (La Jolla, CA). Oligonucleotides were from Elim Biopharmaceuticals, Inc. (Hayward, CA). Restriction enzymes and calf intestinal alkaline phosphatase (CIP) were from New England Biolabs (Ipswich, MA). QIAGEN kits were used for plasmid DNA purification and the extraction of DNA from agarose gels. T4 DNA ligase and BL21(DE3) chemically competent cells were purchased from Invitrogen (Carlsbad, CA). Vectors were obtained from Novagen (pET28b; Madison, WI) and the American Type Culture Collection (pBAD18; Manassas, VA). DNA sequencing was performed by Elim Biopharmaceuticals, Inc. All chemicals were purchased from Sigma-Aldrich (St. Louis, MO) and were used without further purification, including 3'-phosphoadenosine 5'-phosphate (PAP), guanosine 5'-monophosphate (GMP), adenosine 5'-monophosphate (AMP), D-*myo*-inositol-1-monophosphate (IMP), and D-fructose-1,6-bisphosphate (FBP). Assay mixtures were prepared in water that was doubly distilled and deionized using a Milli-Q system

(Millipore; Billerica, MA). All other materials used in this work were obtained from sources cited within the text.

Preparation of expression vector

The *Rv2131c* gene was PCR-amplified from *Mtb* H37Rv genomic DNA with the primers 5'-TTACGTAGGACATATGGTGGTGAGCCCTGCCGCACC-3' (NdeI) and 5'-TAGTATAAGCGGATCCTCAGCGCCACGCGTCGGCGA-3' (BamHI). The resulting 0.8-kilobase fragment was digested with NdeI and BamHI and ligated into a similarly-digested and CIP-treated pET28b vector with an N-terminal His_6 tag. DNA sequencing was used to confirm the successful construction of the pET28b_2131c plasmid.

Preparation of E. coli *complementation vector*

The *Rv2131c* gene was PCR-amplified from *Mtb* H37Rv genomic DNA with the primers 5'-CACAGTTACGTCTAGAAGGAGGTACTGAATGGTGAGCCCTGCCGCAC-3' (XbaI) and 5'-ACATGACTCTAAGCTTTCAGCGCCACGCGTCGGCGA-3' (HindIII). A ribosome binding site was added by PCR and is shown in boldface type. The PCR product was digested with XbaI and HindIII and ligated into a similarly-digested and CIP-treated pBAD18 vector with an ampicillin resistance marker and an arabinose-inducible promoter (*40*). DNA sequencing was used to confirm the successful construction of the pBAD18_2131c plasmid.

Expression of Rv2131c in E. coli

pET28b_2131c was transformed into *E. coli* strain BL21(DE3). Transformants were used to inoculate 1-L cultures of LB medium containing 50 mg/L kanamycin, which were incubated at 37 °C for approximately 2.5 h with shaking until an OD_{600} of 0.6-0.8 was reached. Protein expression was induced by the addition of isopropyl β-D-thiogalactoside (IPTG) to a final concentration of 100 μM. The cultures were grown for an additional 20 h at 18 °C before the cells were harvested by centrifugation (6000 rpm, 4 °C, 15 min). The collected cells (~5 g/L) were suspended in 20 mL of PAP-agarose buffer (50 mM Tris buffer, pH 7.5, 10 mM $CaCl_2$, and 50 mM KCl) supplemented with 5 μg/mL lysozyme, 5 μg/mL DNase, and 1 complete, EDTA-free protease inhibitor cocktail tablet (Roche) at 4 °C. Cells were lysed by ultrasonication (Misonix Sonicator 3000) or using a high-pressure homogenizer (Avestin EmulsiFlex-C5). The cell lysate was cleared by centrifugation (18,500 rpm, 4 °C, 20 min) and the protein was purified from the supernatant as previously described (*18*). Briefly, ~1.5 mL of PAP-agarose resin (Sigma) were swelled in PAP-agarose buffer and added to the supernatant, which was rocked gently with the beads for 2 h at 4 °C. The supernatant was applied to a chromatography column and collected by gravity flow. The resin was washed with 20 mL of PAP-agarose buffer containing 500 mM NaCl, followed by 20 mL of PAP-agarose buffer. To elute the protein, 3 mL of elution buffer (PAP-agarose buffer containing 300 μM PAP) were allowed to equilibrate with the column for 20 min before 0.5-mL

fractions were collected. SDS-PAGE was used to identify column fractions containing the desired protein, which were concentrated and further purified by size exclusion chromatography. The protein was loaded onto a HiPrep 16/60 Sephacryl S-300 High Resolution gel filtration column (GE Healthcare Biosciences Corp.) equilibrated with gel filtration buffer (50 mM Tris buffer, pH 7.5, 10% glycerol, 1 mM dithiothreitol). Fractions (2 mL each) were analyzed by SDS-PAGE and those containing pure protein were concentrated by centrifugation and stored at -80 °C.

To confirm the protein's identity, the purified sample was desalted on a microbore reversed phase column (Bruker Agilent) and characterized using a Bruker Hewlett-Packard ESI-Ion Trap mass spectrometer. Tryptic digestion and mass fingerprinting using an Applied Biosystems 4800 MALDI-TOF were used to provide further confirmation of the protein's identity. Protein concentration was determined by UV absorption at 280 nm using a calculated extinction coefficient of 46,350 M^{-1} cm^{-1}.

Activity assays

The Baykov malachite green method (*41*) was used to establish phosphatase activity with PAP as the substrate and to determine the optimal conditions for catalysis. A standard reaction mixture contained 50 mM Tris buffer, pH 8.5, 100 μM PAP, 0.5 mM $MgCl_2$, and 5 nM enzyme in a 200 μL volume. The reaction was preincubated for 5 min at 30 °C prior to the addition of enzyme and quenched 5 min thereafter by adding one-fourth volume of acidic malachite green dye solution. After 10 min, the absorbance of the reaction at 630 nm was determined using a Molecular Devices SpectraMax 190 UV-visible plate reader. A standard curve generated using monobasic potassium phosphate was used to correlate the absorbance of the reaction mixture with the concentration of inorganic phosphate in solution. Since enzyme activity was determined to be linear under these reaction conditions, the initial rate of the reaction was calculated by dividing the concentration of liberated phosphate by the reaction time. Control reactions without enzyme were treated identically and used to account for background hydrolysis of the substrate. For the determination of the optimum pH range, metal cofactor, and $MgCl_2$ concentration, the corresponding factors were varied. To evaluate the effect of various alkali metal cations on enzyme activity, increasing amounts of each cation were added to the standard reaction mixture.

Enzyme kinetics

The kinetic parameters for PAP were determined using a previously described ESI-MS assay (*34, 35*) with some modifications, as described below.

Mass spectrometry

Mass spectra were acquired using a quadrupole time-of-flight (Q-Tof) mass spectrometer equipped with a Z-spray electrospray ionization (ESI) source (Q-Tof Premier™, Waters, Beverly, MA). Sample solutions were infused from a 250 μL Gastight® syringe (Hamilton, Reno, NV) into the ESI probe at a flow rate of 5 μL/min

using a syringe pump. The electrospray was emitted from a stainless steel capillary with an inner diameter of 127 μm. The ion source parameters were as follows: ESI capillary voltage 2.4 kV, nebulizing gas (nitrogen) flow rate 800 L/hr, sample cone voltage 35 V, extraction cone and ion guide voltages 5 V, source block temperature 80 ºC, and nebulizing gas temperature 200 ºC. No cone gas was used. The pressures in the different stages of the instrument were as follows: first pumping stage 1.5 mbar, ion transfer stage 5×10^{-4} mbar, quadrupole analyzer 2×10^{-5} mbar, argon-filled cell 8×10^{-3} mbar, and Tof analyzer 9×10^{-7} mbar. The Tof analyzer was operated in "V" mode. Under these conditions, a mass resolving power (*42*) of 10,000 was routinely achieved. For each sample, mass spectra were recorded in the negative ion mode for a period of 4 min. The electrospray emitter was rinsed with deionized water after each measurement to avoid cross-contamination between samples. External mass calibration was performed immediately prior to measurements, using solutions of sodium formate. Mass spectra were processed using MassLynx software (version 4.1, Waters).

Single-point normalization factor

Guanosine 5'-monophosphate (GMP) was selected as the internal standard due to its structural similarities to the product of PAP dephosphorylation, AMP. A solution containing 5 μM AMP in 50 mM Tris buffer, pH 8.5, and 0.5 mM $MgCl_2$ was prepared. A 25-μL aliquot of the solution was mixed with 100 μL water containing 6.25 μM GMP. The intensities of the product ion (I_P) and internal standard ion (I_{IS}) measured by ESI-MS were used to obtain the corresponding single-point normalization factor R. R relates the intensity ratio, I_P/I_{IS}, to the concentration ratio of the respective analytes as described in eq 1.

$$R = (I_P/I_{IS})/([\text{product}]/[\text{internal standard}]) \quad (1)$$

This equation can be rearranged to calculate the product concentration when R, (I_P/I_{IS}), and the concentration of the internal standard are known (eq 2). If the initial rate of a reaction is desired, the product concentration can be divided by the reaction time (T_R) provided that enzyme activity is linear during that time (eq 3).

$$[\text{product}] = (I_P/I_{IS})[\text{internal standard}]/R \quad (2)$$

$$V_o = [\text{product}]/T_R \quad (3)$$

Reaction progress curve

To establish the linear range of PAP phosphatase activity, a reaction progress curve was generated. A 421-μL reaction mixture containing 50 mM Tris buffer, pH 8.5, 0.5 mM $MgCl_2$, and 25 μM PAP was preincubated for 5 min at 30 °C. Prior to the addition of enzyme, a 25-μL aliquot was removed and quenched with 5 μL of 10% HCl to obtain a 0 min time point. To initiate the reaction, 4 μL of a 500 nM enzyme stock were added to the mixture for a final enzyme concentration of 5 nM. The reaction

proceeded at 30 °C for 30 min, during which 25-μL aliquots were removed and quenched as described above. A 25-μL aliquot from each quenched sample was then mixed with 100 μL of internal standard solution (6.25 μM GMP in water) and analyzed by ESI-MS. The concentration of AMP in each sample was calculated as described above and used to determine the extent of substrate conversion as a function of time.

Determination of Michaelis-Menten parameters for PAP

Attempts to characterize the kinetic parameters for PAP using the malachite green assay suggested that the K_m was below 20 μM (data not shown). Because this is near the detection limit of the assay, a more sensitive method was required for the kinetic analysis of this substrate. Eight reaction mixtures (198 μL each) containing 50 mM Tris buffer, pH 8.5, 0.5 mM $MgCl_2$, and a variable concentration of PAP (0.625 to 50 μM) were prepared. Following a 5-min incubation at 30 °C, the reactions were initiated by adding 2 μL of a 500 nM enzyme stock for a final enzyme concentration of 5 nM. After 4 min at 30 °C, the reactions were quenched using 40 μL 10% HCl. Samples for ESI-MS analysis were prepared by combining 25 μL of each quenched reaction with 100 μL of internal standard solution. Using the calculated AMP concentration for each sample, the corresponding initial rates were determined and plotted against PAP concentration using KaleidaGraph (version 4.03) to obtain Michaelis-Menten parameters.

Determination of Michaelis-Menten parameters for IMP and FBP

The kinetic parameters for IMP and FBP were determined using the malachite green assay (*41*). Reaction mixtures were prepared using the optimal conditions for catalysis reported previously for these substrates (*24*). Mixtures containing 50 mM Tris buffer, pH 9.0, 10 mM $MgCl_2$, 110 nM enzyme, and a variable concentration of IMP (1 to 5.5 mM) or FBP (90 to 900 μM) were prepared in a 100 μL volume. The substrate concentrations used in these studies were based on the previously reported K_m values for IMP (220 μM) and FBP (450 μM) (*24*). However, initial experiments revealed that the K_m for IMP was much greater than expected, necessitating the use of a higher concentration range. Because substrate inhibition was observed for both IMP and FBP, the highest substrate concentrations used in the kinetic analysis of these substrates were 5.5 mM and 900 μM, respectively. The reactions were preincubated for 5 min at 30 °C prior to the addition of enzyme and quenched 15 min thereafter by adding one-fourth volume of acidic malachite green dye solution. Enzyme activity was determined to be in the linear regime under these reaction conditions. Control reactions without enzyme were used to account for the background hydrolysis of each substrate. The amount of inorganic phosphate in each sample was quantified as described above and used to determine the initial rates corresponding to each substrate concentration. KaleidaGraph was used to determine the kinetic parameters for these substrates.

Genetic complementation in E. coli

An *E. coli* mutant with a Tn5Kan-I-SceI transposon in the *cysQ* gene was obtained from the *E. coli* Genome Project at the University of Wisconsin-Madison. Cells cultured overnight in 2 mL of LB medium with 50 mg/L kanamycin were used to inoculate 1 L of LB/kanamycin medium and grown for approximately 3 h at 37 °C with shaking to an OD_{600} of ~0.6. The cells were then cooled to 4 °C and made electrocompetent by washing them four times, twice in ice-cold water and twice in ice-cold 10% glycerol, and resuspending them in 0.5 mL of 10% glycerol. Electroporation with a Bio-Rad Gene Pulser was used to transform plasmid DNA into the cells following the manufacturer's protocol. Transformants were grown on LB agar containing 50 mg/L kanamycin and 100 mg/L ampicillin. Individual colonies were streaked onto M9 minimal medium (10 g/L M9 minimal salts (Sigma), 15 g/L Bacto™ Agar, 0.2% glycerol, 1 mM $MgSO_4$, and 0.1 mM $CaCl_2$) containing arabinose (0.2%) and 50 mg/L kanamycin. Certain plates also contained 100 mg/L ampicillin and/or 0.5 mM Na_2SO_3. The antibiotics, $MgSO_4$, $CaCl_2$, arabinose, and Na_2SO_3 were sterile-filtered individually and added following autoclave sterilization of the remaining media. Plates were incubated at 37 °C for 24 h.

References

1. Bhave, D. P., Muse, W. B., 3rd, and Carroll, K. S. (2007) Drug targets in mycobacterial sulfur metabolism, *Infect. Disord. Drug Targets 7*, 140-158.

2. Schelle, M. W., and Bertozzi, C. R. (2006) Sulfate metabolism in mycobacteria, *Chembiochem 7*, 1516-1524.

3. Gangadharam, P. R., Cohn, M. L., and Middlebrook, G. (1963) Infectivity, pathogenicity and sulpholipid fraction of some Indian and British strains of tubercle bacilli, *Tubercle 44*, 452-455.

4. Newton, G. L., and Fahey, R. C. (2002) Mycothiol biochemistry, *Arch. Microbiol. 178*, 388-394.

5. Buchmeier, N. A., Newton, G. L., Koledin, T., and Fahey, R. C. (2003) Association of mycothiol with protection of *Mycobacterium tuberculosis* from toxic oxidants and antibiotics, *Mol. Microbiol. 47*, 1723-1732.

6. Sareen, D., Newton, G. L., Fahey, R. C., and Buchmeier, N. A. (2003) Mycothiol is essential for growth of *Mycobacterium tuberculosis* Erdman, *J. Bacteriol. 185*, 6736-6740.

7. Senaratne, R. H., De Silva, A. D., Williams, S. J., Mougous, J. D., Reader, J. R., Zhang, T., Chan, S., Sidders, B., Lee, D. H., Chan, J., Bertozzi, C. R., and Riley, L. W. (2006) 5'-Adenosinephosphosulphate reductase (CysH) protects

Mycobacterium tuberculosis against free radicals during chronic infection phase in mice, *Mol. Microbiol. 59*, 1744-1753.

8. Pinto, R., Tang, Q. X., Britton, W. J., Leyh, T. S., and Triccas, J. A. (2004) The *Mycobacterium tuberculosis cysD* and *cysNC* genes form a stress-induced operon that encodes a tri-functional sulfate-activating complex, *Microbiology 150*, 1681-1686.

9. Hampshire, T., Soneji, S., Bacon, J., James, B. W., Hinds, J., Laing, K., Stabler, R. A., Marsh, P. D., and Butcher, P. D. (2004) Stationary phase gene expression of *Mycobacterium tuberculosis* following a progressive nutrient depletion: a model for persistent organisms?, *Tuberculosis 84*, 228-238.

10. Kredich, N. M. (1992) The molecular basis for positive regulation of *cys* promoters in *Salmonella typhimurium* and *Escherichia coli*, *Mol. Microbiol. 6*, 2747-2753.

11. Neidhardt, F. C., and Curtiss, R. (1996) Escherichia coli *and Salmonella: cellular and molecular biology*, 2nd ed., ASM Press, Washington, D.C.

12. Williams, S. J., Senaratne, R. H., Mougous, J. D., Riley, L. W., and Bertozzi, C. R. (2002) 5'-Adenosinephosphosulfate lies at a metabolic branch point in mycobacteria, *J. Biol. Chem. 277*, 32606-32615.

13. Carroll, K. S., Gao, H., Chen, H., Stout, C. D., Leary, J. A., and Bertozzi, C. R. (2005) A conserved mechanism for sulfonucleotide reduction, *PLoS Biol. 3*, e250.

14. Mougous, J. D., Green, R. E., Williams, S. J., Brenner, S. E., and Bertozzi, C. R. (2002) Sulfotransferases and sulfatases in mycobacteria, *Chem. Biol. 9*, 767-776.

15. Mougous, J. D., Petzold, C. J., Senaratne, R. H., Lee, D. H., Akey, D. L., Lin, F. L., Munchel, S. E., Pratt, M. R., Riley, L. W., Leary, J. A., Berger, J. M., and Bertozzi, C. R. (2004) Identification, function and structure of the mycobacterial sulfotransferase that initiates Sulfolipid-1 biosynthesis, *Nat. Struct. Mol. Biol. 11*, 721-729.

16. Mougous, J. D., Senaratne, R. H., Petzold, C. J., Jain, M., Lee, D. H., Schelle, M. W., Leavell, M. D., Cox, J. S., Leary, J. A., Riley, L. W., and Bertozzi, C. R. (2006) A sulfated metabolite produced by *stf3* negatively regulates the virulence of *Mycobacterium tuberculosis*, *Proc. Natl. Acad. Sci. U. S. A. 103*, 4258-4263.

17. Neuwald, A. F., Krishnan, B. R., Brikun, I., Kulakauskas, S., Suziedelis, K., Tomcsanyi, T., Leyh, T. S., and Berg, D. E. (1992) *cysQ*, a gene needed for cysteine synthesis in *Escherichia coli* K-12 only during aerobic growth, *J. Bacteriol. 174*, 415-425.

18. Spiegelberg, B. D., Xiong, J. P., Smith, J. J., Gu, R. F., and York, J. D. (1999) Cloning and characterization of a mammalian lithium-sensitive bisphosphate 3'-nucleotidase inhibited by inositol 1,4-bisphosphate, *J. Biol. Chem. 274*, 13619-13628.

19. Peng, Z., and Verma, D. P. (1995) A rice *HAL2*-like gene encodes a Ca(2+)-sensitive 3'(2'),5'-diphosphonucleoside 3'(2')-phosphohydrolase and complements yeast *met22* and *Escherichia coli cysQ* mutations, *J. Biol. Chem. 270*, 29105-29110.

20. Murguia, J. R., Belles, J. M., and Serrano, R. (1995) A salt-sensitive 3'(2'),5'-bisphosphate nucleotidase involved in sulfate activation, *Science 267*, 232-234.

21. Mechold, U., Ogryzko, V., Ngo, S., and Danchin, A. (2006) Oligoribonuclease is a common downstream target of lithium-induced pAp accumulation in *Escherichia coli* and human cells, *Nucleic Acids Res. 34*, 2364-2373.

22. Walsh, C. T., Gehring, A. M., Weinreb, P. H., Quadri, L. E., and Flugel, R. S. (1997) Post-translational modification of polyketide and nonribosomal peptide synthases, *Curr. Opin. Chem. Biol. 1*, 309-315.

23. Cole, S. T., Brosch, R., Parkhill, J., Garnier, T., Churcher, C., Harris, D., Gordon, S. V., Eiglmeier, K., Gas, S., Barry, C. E., 3rd, Tekaia, F., Badcock, K., Basham, D., Brown, D., Chillingworth, T., Connor, R., Davies, R., Devlin, K., Feltwell, T., Gentles, S., Hamlin, N., Holroyd, S., Hornsby, T., Jagels, K., Krogh, A., McLean, J., Moule, S., Murphy, L., Oliver, K., Osborne, J., Quail, M. A., Rajandream, M. A., Rogers, J., Rutter, S., Seeger, K., Skelton, J., Squares, R., Squares, S., Sulston, J. E., Taylor, K., Whitehead, S., and Barrell, B. G. (1998) Deciphering the biology of *Mycobacterium tuberculosis* from the complete genome sequence, *Nature 393*, 537-544.

24. Gu, X., Chen, M., Shen, H., Jiang, X., Huang, Y., and Wang, H. (2006) Rv2131c gene product: an unconventional enzyme that is both inositol monophosphatase and fructose-1,6-bisphosphatase, *Biochem. Biophys. Res. Commun. 339*, 897-904.

25. York, J. D., Ponder, J. W., and Majerus, P. W. (1995) Definition of a metal-dependent/Li(+)-inhibited phosphomonoesterase protein family based upon a conserved three-dimensional core structure, *Proc. Natl. Acad. Sci. U. S. A. 92*, 5149-5153.

26. Albert, A., Yenush, L., Gil-Mascarell, M. R., Rodriguez, P. L., Patel, S., Martinez-Ripoll, M., Blundell, T. L., and Serrano, R. (2000) X-ray structure of yeast Hal2p, a major target of lithium and sodium toxicity, and identification of framework interactions determining cation sensitivity, *J. Mol. Biol. 295*, 927-938.

27. Murguia, J. R., Belles, J. M., and Serrano, R. (1996) The yeast *HAL2* nucleotidase is an *in vivo* target of salt toxicity, *J. Biol. Chem. 271*, 29029-29033.

28. Gil-Mascarell, R., Lopez-Coronado, J. M., Belles, J. M., Serrano, R., and Rodriguez, P. L. (1999) The Arabidopsis *HAL2*-like gene family includes a novel sodium-sensitive phosphatase, *Plant J. 17*, 373-383.

29. Aggarwal, M., Bansal, P. K., and Mondal, A. K. (2005) Molecular cloning and biochemical characterization of a 3'(2'),5'-bisphosphate nucleotidase from *Debaryomyces hansenii*, *Yeast 22*, 457-470.

30. Patel, S., Martinez-Ripoll, M., Blundell, T. L., and Albert, A. (2002) Structural enzymology of Li(+)-sensitive/Mg(2+)-dependent phosphatases, *J. Mol. Biol. 320*, 1087-1094.

31. Breslow, R. (2005) *Artificial enzymes*, Wiley-VCH, Weinheim.

32. Fukuda, C., Kawai, S., and Murata, K. (2007) NADP(H) phosphatase activities of archaeal inositol monophosphatase and eubacterial 3'-phosphoadenosine 5'-phosphate phosphatase, *Appl. Environ. Microbiol. 73*, 5447-5452.

33. Lopez-Coronado, J. M., Belles, J. M., Lesage, F., Serrano, R., and Rodriguez, P. L. (1999) A novel mammalian lithium-sensitive enzyme with a dual enzymatic activity, 3'-phosphoadenosine 5'-phosphate phosphatase and inositol-polyphosphate 1-phosphatase, *J. Biol. Chem. 274*, 16034-16039.

34. Pi, N., Armstrong, J. I., Bertozzi, C. R., and Leary, J. A. (2002) Kinetic analysis of NodST sulfotransferase using an electrospray ionization mass spectrometry assay, *Biochemistry 41*, 13283-13288.

35. Pi, N., Hoang, M. B., Gao, H., Mougous, J. D., Bertozzi, C. R., and Leary, J. A. (2005) Kinetic measurements and mechanism determination of Stf0 sulfotransferase using mass spectrometry, *Anal. Biochem. 341*, 94-104.

36. Quintero, F. J., Garciadeblas, B., and Rodriguez-Navarro, A. (1996) The *SAL1* gene of Arabidopsis, encoding an enzyme with 3'(2'),5'-bisphosphate nucleotidase and inositol polyphosphate 1-phosphatase activities, increases salt tolerance in yeast, *Plant Cell 8*, 529-537.

37. Robbins, P. W., and Lipmann, F. (1958) Enzymatic synthesis of adenosine-5'-phosphosulfate, *J. Biol. Chem. 233*, 686-690.

38. Sun, M., Andreassi, J. L., 2nd, Liu, S., Pinto, R., Triccas, J. A., and Leyh, T. S. (2005) The trifunctional sulfate-activating complex (SAC) of *Mycobacterium tuberculosis*, *J. Biol. Chem. 280*, 7861-7866.

39. Pinto, R., Harrison, J. S., Hsu, T., Jacobs, W. R., Jr., and Leyh, T. S. (2007) Sulfite reduction in mycobacteria, *J. Bacteriol. 189*, 6714-6722.

40. Guzman, L. M., Belin, D., Carson, M. J., and Beckwith, J. (1995) Tight regulation, modulation, and high-level expression by vectors containing the arabinose PBAD promoter, *J. Bacteriol. 177*, 4121-4130.

41. Baykov, A. A., Evtushenko, O. A., and Avaeva, S. M. (1988) A malachite green procedure for orthophosphate determination and its use in alkaline phosphatase-based enzyme immunoassay, *Anal. Biochem. 171*, 266-270.

42. Marshall, A. G., Hendrickson, C. L., and Jackson, G. S. (1998) Fourier transform ion cyclotron resonance mass spectrometry: a primer, *Mass Spectrom. Rev. 17*, 1-35.

Chapter 3: Exploring the role of the 3'-phosphoadenosine-5'-phosphatase CysQ in *Mycobacterium tuberculosis* sulfur metabolism[a]

Introduction

The sulfate assimilation pathway of *Mycobacterium tuberculosis* (*Mtb*) is responsible for the *de novo* synthesis of sulfur-containing metabolites that mediate the virulence of this global pathogen (*1, 2*). The pathway is comprised of two distinct branches: the reductive branch and the sulfation branch (Figure 3-1). These branches are distinguished by the metabolic fate of adenosine 5'-phosphosulfate (APS), a key intermediate in the pathway. APS can either be reduced to sulfite by APS reductase for the biosynthesis of essential reduced sulfur metabolites (reductive branch), or phosphorylated by APS kinase to give 3'-phosphoadenosine 5'-phosphosulfate (PAPS), the universal sulfate donor in the cell (sulfation branch) (*3*). PAPS is a substrate for sulfotransferase enzymes that transfer its 5'-sulfate group onto organic metabolites (*4*). A byproduct of this reaction is 3'-phosphoadenosine 5'-phosphate (PAP), a competitive inhibitor of sulfotransferase activity (*5*). Accumulation of either PAP or PAPS could compromise the cell's ability to metabolize sulfur.

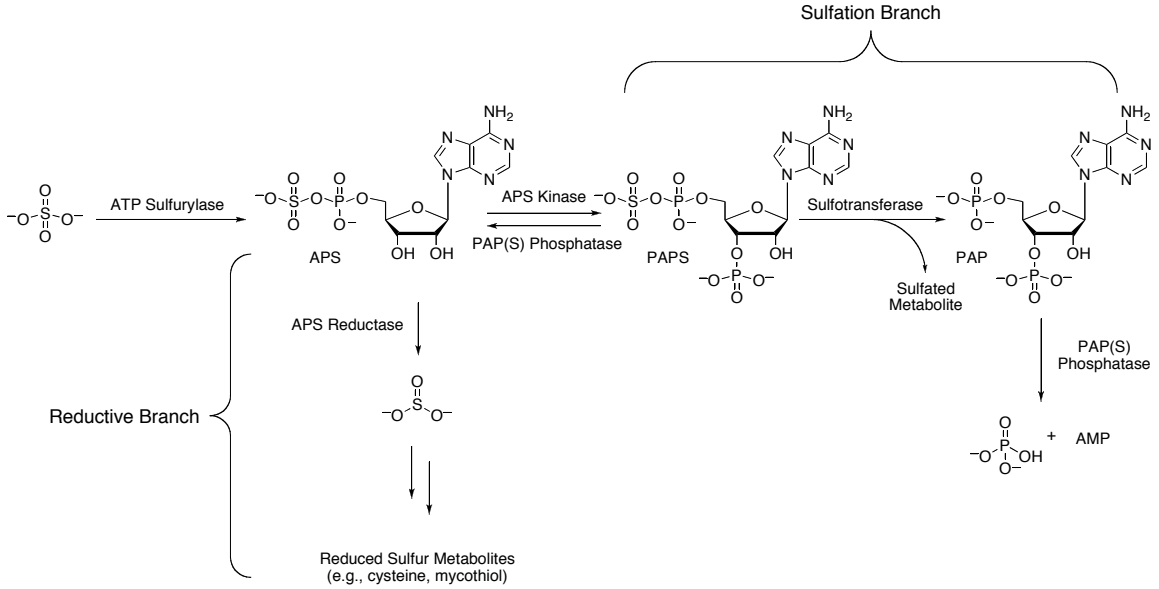

FIGURE 3-1. The sulfate assimilation pathway of *M. tuberculosis*.

In Chapter 2, we demonstrated that *Mtb* encodes a 3'-phosphoadenosine-5'-phosphatase termed CysQ that is capable of dephosphorylating PAP and its sulfated counterpart (*6*). Notably, homologous enzymes have been shown to significantly affect the biosynthesis of sulfur-containing metabolites in *Escherichia coli* and *Saccharomyces cerevisiae* (*7-9*). We hypothesized that CysQ might similarly regulate sulfur metabolism in *Mtb* by modulating the levels of key pathway intermediates.

[a] Michael W. Schelle and Gerald L. Newton contributed to the work presented in this chapter.

In the present chapter, we report the characterization of a *cysQ*-deficient mutant of *Mtb*. We establish that it exhibits attenuated growth *in vitro*, and that this growth defect is not corrected by the addition of exogenous sources of reduced sulfur. Analysis of reduced sulfur species indicates that disruption of *cysQ* does not impact the reductive branch of the sulfate assimilation pathway. In contrast, disabling CysQ activity inhibits the biosynthesis of key sulfated metabolites, suggesting that the enzyme specifically regulates the sulfation branch of the sulfate assimilation pathway.

Results

Disruption of cysQ *attenuates* M. tuberculosis *growth* in vitro

To determine whether *cysQ* disruption affects the growth kinetics of *Mtb*, wild-type, Δ*cysQ*, and Δ*cysQ*::*cysQ* strains were synchronized and their growth monitored for a period of five days. The mutant strain exhibited attenuated growth relative to wild-type *Mtb*, and this phenotype was reverted by complementation (Figure 3-2). Because the growth medium used in these studies, Middlebrook 7H9, is devoid of reduced sulfur species, survival of the cultured bacteria relies on the conversion of sulfate to essential reduced sulfur compounds via the sulfate assimilation pathway. We therefore considered the possibility that the observed attenuation of the mutant strain might reflect an impaired biosynthesis of reduced sulfur compounds in the absence of CysQ. To test this hypothesis, we grew the mutant strain in the presence of either 2 mM cysteine or methionine. Notably, these sulfur-containing amino acids have previously been shown to restore wild-type growth to the APS reductase mutant of *Mtb* (*10*), which is deficient in the *de novo* synthesis of reduced sulfur species and consequently unable to grow in 7H9 medium. In contrast, neither cysteine nor methionine was able to rescue the growth of Δ*cysQ* (Figure 3-2), indicating that a deficiency in reduced sulfur compounds is not responsible for the growth attenuation of the mutant strain.

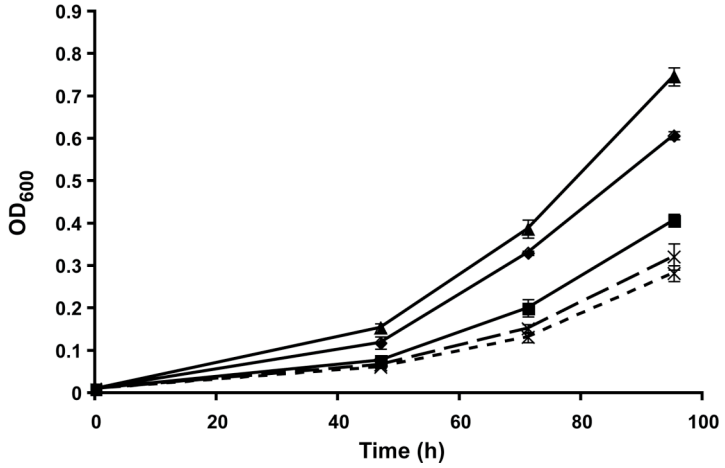

FIGURE 3-2. Disruption of *cysQ* attenuates *M. tuberculosis* growth *in vitro* (◆, wild-type; ■, Δ*cysQ*; ▲, Δ*cysQ*::*cysQ*). Addition of 2 mM cysteine (long dash) or methionine (short dash) does not rescue the growth of Δ*cysQ*.

CysQ does not affect the thiol composition of M. tuberculosis

The monobromobimane assay was used to compare the concentrations of major thiol-containing compounds produced by wild-type, Δ*cysQ*, and Δ*cysQ::cysQ Mtb*. Extracts from exponentially growing bacteria were analyzed for mycothiol, cysteine, CoA, and hydrogen sulfide, a derivative of iron-sulfur proteins. Mycothiol, the most abundant thiol in mycobacteria (*11*), was present at similar levels in all three strains (Figure 3-3A). Further, CoA and hydrogen sulfide content were not affected by *cysQ* disruption (Figures 3-3B and 3-3C). Cysteine levels were very low in all samples (i.e., less than or equal to 0.1 nmol per 10^9 cells) as found previously for wild-type *Mtb* (*12*). Mycothiol, hydrogen sulfide, and CoA concentrations were also similar to those previously reported in the literature (*11*). Only the CoA content of the Δ*cysQ::cysQ* deviated significantly from the other two strains in this analysis. This deviation is most likely a consequence of the variation in cell density among the harvested strains, which has previously been shown to affect CoA levels (*12*). However, the overall homogeneity in the thiol composition of wild-type, Δ*cysQ*, and Δ*cysQ*::*cysQ Mtb* provides further evidence that CysQ does not regulate the biosynthesis of reduced sulfur species in these bacteria.

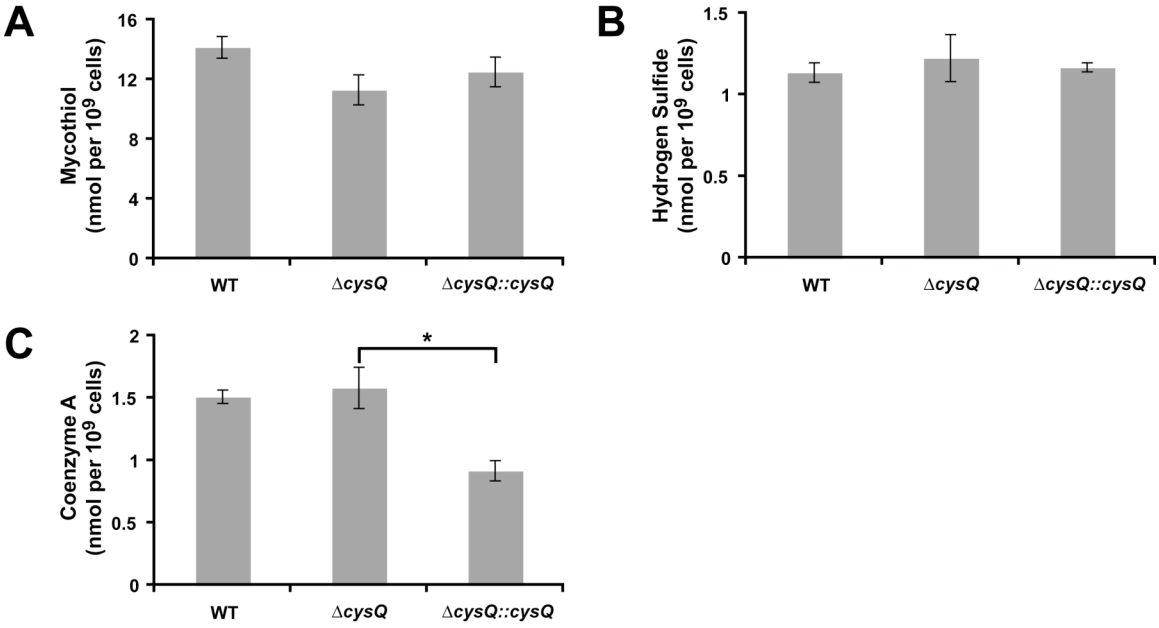

FIGURE 3-3. CysQ does not affect the biosynthesis of mycothiol (**A**), hydrogen sulfide (**B**), or coenzyme A (**C**) as determined by the monobromobimane method. *, $P < 0.01$ by two-tailed Student's *t* test.

SL_{1278} and Sulfolipid-1 (SL-1) biosynthesis are inhibited by the disruption of cysQ

The relative quantities of two major sulfated glycolipids from wild-type, Δ*cysQ*, and Δ*cysQ::cysQ Mtb* were evaluated by metabolic labeling and autoradiography (Figure

3-4A). Equal volumes of total lipid extracts from cells labeled with [^{35}S]sulfate were analyzed by thin-layer chromatography (TLC) for the presence of Sulfolipid-1 (SL-1) and its biosynthetic precursor SL_{1278}. Spots corresponding to these two glycolipids were assigned based on previously published TLC assays (*13*) and confirmed using radiolabeled extracts from the SL-1 biosynthetic mutants Δ*stf0* and Δ*mmpL8* (*14, 15*). Importantly, the Δ*stf0* strain lacks all known precursors in the SL-1 biosynthetic pathway, including SL_{1278}, whereas the Δ*mmpL8* strain accumulates SL_{1278} in the cell wall (*15, 16*). The integrated density of each spot was normalized to the background density of the TLC plate and reported as a percentage of the total integrated density of its respective lane. The averaged data from three independent experiments revealed that both SL_{1278} and SL-1 are present at reduced levels in Δ*cysQ* (Figure 3-4B); the percentage of these metabolites in the mutant strain is approximately one-third that of wild-type *Mtb*. Complementation restored SL-1 to wild-type levels and increased production of SL_{1278}, confirming that the reduction of these metabolites in the mutant can be attributed to the loss of a functional CysQ.

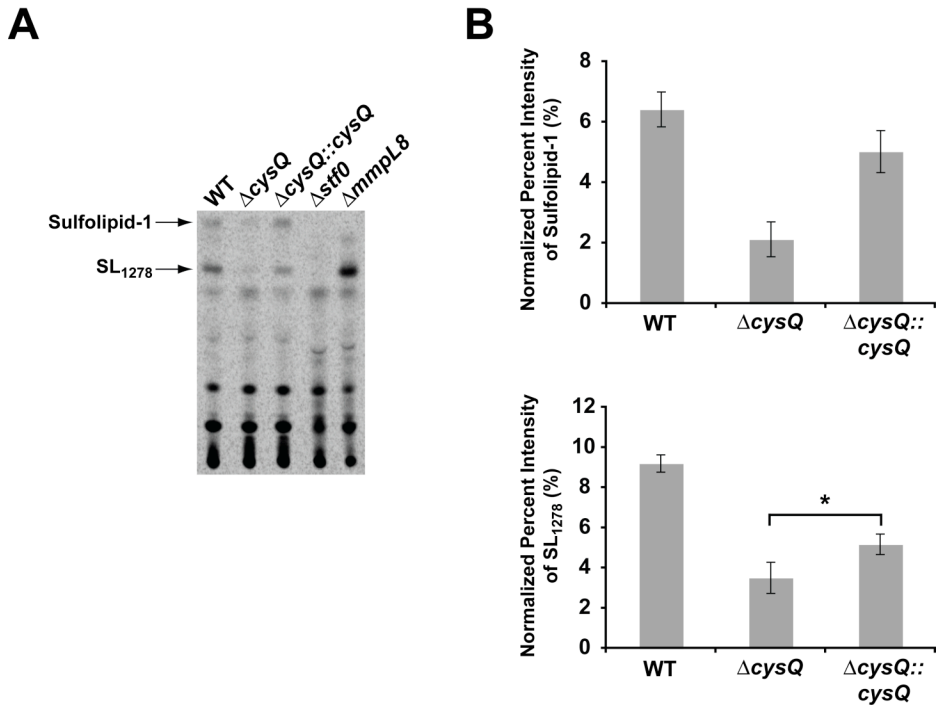

FIGURE 3-4. Loss of CysQ decreases biosynthesis of the sulfated glycolipids Sulfolipid-1 and SL_{1278}. Total lipid extracts from wild-type, Δ*cysQ*, and Δ*cysQ*::*cysQ* *Mtb* labeled with [^{35}S]sulfate were analyzed by TLC (**A**). Relative levels of Sulfolipid-1 and SL_{1278} were determined by densitometry (**B**). *, $P < 0.05$ by two-tailed Student's *t* test.

Discussion

Collectively, the data presented herein support a role for the *Mtb cysQ* in the maintenance of wild-type growth and sulfur metabolism. Disruption of *cysQ* impairs *Mtb* replication *in vitro*, and metabolite analysis indicates that the levels of sulfated glycolipids produced by the Δ*cysQ* strain are markedly reduced relative to wild-type *Mtb*. Notably, the growth attenuation of Δ*cysQ* observed *in vitro* is not reverted by the addition of exogenous reduced sulfur sources, unlike *Mtb* mutants defective in the reduction branch of the sulfate assimilation pathway. Moreover, the thiol composition of *Mtb* remains largely unaffected by *cysQ* disruption. These findings, in accordance with the established biochemical activity of the enzyme, suggest that CysQ may specifically regulate the sulfation branch of the sulfate assimilation pathway.

The ability of CysQ to modulate mycobacterial sulfation likely lies in its ability to degrade PAP, a byproduct and competitive inhibitor of sulfotransferase activity (*5, 6*). Inhibition of a homologous enzyme from *S. cerevisiae*, or disruption of the gene encoding its biosynthesis, has been shown to increase PAP concentration to millimolar levels (*9, 17*). Thus, in the absence of a functional CysQ, sulfotransferase activity is subject to inhibition by PAP accumulation. Inhibition of Stf0, the sulfotransferase responsible for sulfating trehalose in the first committed step of SL-1 biosynthesis (*16*), would result in reduced levels of SL-1 and its precursor SL_{1278}, which is consistent with our findings. Importantly, with the exception of these two glycolipids, the overall labeling of sulfur-containing metabolites in wild-type and Δ*cysQ* extracts by [^{35}S]sulfate appears similar by TLC (Figure 3-4A), suggesting that *cysQ* disruption only affects a small subset of sulfur-containing compounds. Further, a recent study by Movahedzadeh *et al.* (*18*) established that the overall lipid content of *Mtb* is not affected by *cysQ* disruption, indicating that the observed changes in the content of sulfated glycolipids in the Δ*cysQ* strain do not reflect a global reduction in glycolipid production, but rather a specific decline in their biosynthesis.

While there is a clear biochemical basis for the correlation between CysQ activity and mycobacterial sulfation, the relationship between mycobacterial sulfation and growth is not as easily explained. One possibility is that the disruption of *cysQ* inhibits the biosynthesis of one or more sulfated biomolecules required for wild-type growth. The *Mtb* genome encodes four putative sulfotransferases: *stf0*, *stf1*, *stf2*, and *stf3* (*4, 16*). Of these, only *stf0* and *stf3* have been assigned biosynthetic roles; *stf0* sulfates the disaccharide core of SL-1 (*16*), while *stf3* is required for the production of the sulfated menaquinone S881 (*19, 20*). Although the disruption of either of these genes does not impair *Mtb* growth *in vitro* (S. Gilmore, unpublished data; *19*), it is possible that the uncharacterized products of Stf1 and Stf2 influence bacterial growth, or that the simultaneous inhibition of all four sulfotransferases is deleterious to the cell. A second possibility is that the growth attenuation of Δ*cysQ* does not arise from the loss of a sulfated biomolecule, but from the accumulation of the sulfate donor PAPS. In the absence of CysQ, PAP inhibition of sulfotransferase activity could lead to a build-up of this substrate, which previous studies suggest is cytotoxic to *E. coli* (*7*). A third possibility is that the pleiotropic effects of PAP accumulation may be accountable for the growth defect of Δ*cysQ*. In addition to inhibiting sulfotransferases, PAP is known to

negatively regulate other bacterial enzymes including oligoribonucleases (*21*), which degrade small ribonucleotides, and 4'-phosphopantetheinyltransferases (*22*), which activate acyl carrier proteins during the biosynthesis of fatty acids and secondary metabolites. Notably, the *Rv2511* gene, which encodes an oligoribonuclease homolog in *Mtb*, is essential for *Mtb* growth (*23*), and the two 4'-phosphopantetheinyltransferases conserved in mycobacteria are required for the viability of *Mycobacterium smegmatis* (*24*). Thus, the disruption of *cysQ* may have far-reaching consequences that extend beyond the confines of sulfur metabolism into other essential bacterial processes.

Though questions remain regarding the effects of CysQ on bacterial growth, its influence over mycobacterial sulfur metabolism is now more clearly defined. Loss of the enzyme decreases the biosynthesis of key sulfated metabolites, while the thiol composition of *Mtb* remains largely unchanged. These findings are consistent with the dysregulation of sulfation pathways in the absence of CysQ, most likely due to the inhibition of sulfotransferase activity by the accumulation of PAP. Thus, CysQ appears to specifically regulate the sulfation branch of the sulfate assimilation pathway, a nexus of biosynthetic enzymes whose metabolic potential remains largely unknown.

Materials and Methods

Bacterial strains and culture conditions

Wild-type *Mycobacterium tuberculosis* strain Erdman and its derivatives were cultured in Middlebrook 7H9 medium containing 10% oleic acid-albumin-dextrose-catalase (OADC) enrichment (Difco), 0.5% glycerol, and 0.05% Tween-80. Solid medium was prepared using Middlebrook 7H10 or 7H11 solid agar medium (Difco) with the same supplements. Cultures were grown in roller bottles or aerated shaker flasks incubated at 37 °C in either a roller bottle incubator or an orbital shaker set to 75 rpm, respectively. Where indicated, antibiotics were added at the following concentrations: hygromycin (50 μg/mL), kanamycin (25 μg/mL). Bacterial growth was monitored by measuring the optical density at 600 nm (OD_{600}) with a Thermo Scientific Genesys 20 Visible Spectrophotometer.

Construction of the cysQ *mutant*

A *cysQ*-deficient mutant, Δ*cysQ*, was generated from *Mtb* strain Erdman by homologous recombination as previously described (*25*). Briefly, specialized transduction phage phMWS120 was incubated with concentrated *Mtb* strain Erdman cells for 4 h at 39 ºC. Cells were then plated on 7H10 plates containing hygromycin. Colonies were picked and screened for the disruption by PCR, which confirmed the replacement of 340 bp of *cysQ* (amino acids 61 through 173) with a hygromycin resistance cassette. The Δ*cysQ*::*cysQ* complementation strain was created by cloning the *cysQ* gene from *Mtb* strain Erdman with an additional 350 bp at its 5' end and 80 bp at its 3' end into the mycobacterial expression vector pMV306, a derivative of the pMV361 vector (*26*) with a multiple cloning site in place of the expression cassette. The resulting plasmid was electroporated into Δ*cysQ* and transformants were selected on kanamycin-containing plates.

In vitro *growth studies*

Frozen stocks of wild-type, Δ*cysQ*, and Δ*cysQ*::*cysQ Mtb* were grown to log-phase and used to inoculate triplicate cultures of 30-mL 7H9 medium at an OD_{600} of 0.01. In addition, triplicate cultures of Δ*cysQ* in 7H9 medium supplemented with either 2 mM cysteine or 2 mM methionine were prepared. The cultures were incubated in aerated shaker flasks at 37 °C with shaking, and culture growth was monitored by calculating changes in OD_{600} over a period of five days.

Determination of thiol content

Samples for thiol analysis were prepared as previously described (*12*). Briefly, triplicate cultures of wild-type, Δ*cysQ*, and Δ*cysQ*::*cysQ Mtb* were grown to log-phase in 7H9 medium, and the OD_{600} of each was determined. The cultures were divided in two and pelleted for 5 min at 3500 rpm. Samples for thiol analysis were resuspended in 50% (v/v) acetonitrile in 20 mM HEPES (pH 8.0) containing 2 mM monobromobimane (Invitrogen). The remaining samples were resuspended in 50% (v/v) acetonitrile in 20 mM HEPES (pH 8.0) containing 5 mM *N*-ethylmaleimide (Sigma) prior to treatment with monobromobimane to serve as a thiol-blocked control. Bacteria were incubated for 15 min at 60 °C, and then pelleted for 5 min at 14,000 rpm. The supernatants were twice sterilized by filtration prior to removal from the biosafety level 3 facility and subsequently stored at -80 °C until analysis. High-performance liquid chromatography was used to determine the mycothiol, coenzyme A (CoA), cysteine, and hydrogen sulfide content of each sample as previously described (*27, 28*).

Analysis of sulfated glycolipids

A previously described TLC-based assay was used to analyze the relative levels of sulfated glycolipids in wild-type, Δ*cysQ*, and Δ*cysQ*::*cysQ Mtb* (*13*). Briefly, cultures were grown to log-phase in 7H9 medium, synchronized and grown to an OD_{600} of approximately 0.8. Cultures were normalized by cell density, pelleted for 5 min at 3500 rpm and resuspended in 10 mL of PBS containing 1 mg/mL sodium acetate. Each sample was labeled with 100 μCi of sodium [^{35}S]sulfate (PerkinElmer) for 16-18 h at 37 °C in a rotary shaker. Bacteria were pelleted for 5 min at 3500 rpm, extracted with chloroform:methanol (1:1), and subsequently analyzed by TLC (60:12:1 chloroform:methanol:water). Phosphorimaging, followed by densitometry analysis using ImageJ software, was used to quantify radioactivity. Three independent labeling experiments were analyzed and averaged to obtain the final data.

References

1. Bhave, D. P., Muse, W. B., 3rd, and Carroll, K. S. (2007) Drug targets in mycobacterial sulfur metabolism, *Infect. Disord. Drug Targets 7*, 140-158.

2. Schelle, M. W., and Bertozzi, C. R. (2006) Sulfate metabolism in mycobacteria, *Chembiochem 7*, 1516-1524.

3. Williams, S. J., Senaratne, R. H., Mougous, J. D., Riley, L. W., and Bertozzi, C. R. (2002) 5'-Adenosinephosphosulfate lies at a metabolic branch point in mycobacteria, *J. Biol. Chem. 277*, 32606-32615.

4. Mougous, J. D., Green, R. E., Williams, S. J., Brenner, S. E., and Bertozzi, C. R. (2002) Sulfotransferases and sulfatases in mycobacteria, *Chem. Biol. 9*, 767-776.

5. Pi, N., Hoang, M. B., Gao, H., Mougous, J. D., Bertozzi, C. R., and Leary, J. A. (2005) Kinetic measurements and mechanism determination of Stf0 sulfotransferase using mass spectrometry, *Anal. Biochem. 341*, 94-104.

6. Hatzios, S. K., Iavarone, A. T., and Bertozzi, C. R. (2008) Rv2131c from *Mycobacterium tuberculosis* is a CysQ 3'-phosphoadenosine-5'-phosphatase, *Biochemistry 47,* 5823-5831.

7. Neuwald, A. F., Krishnan, B. R., Brikun, I., Kulakauskas, S., Suziedelis, K., Tomcsanyi, T., Leyh, T. S., and Berg, D. E. (1992) *cysQ*, a gene needed for cysteine synthesis in *Escherichia coli* K-12 only during aerobic growth, *J. Bacteriol. 174*, 415-425.

8. Glaser, H. U., Thomas, D., Gaxiola, R., Montrichard, F., Surdin-Kerjan, Y., and Serrano, R. (1993) Salt tolerance and methionine biosynthesis in *Saccharomyces cerevisiae* involve a putative phosphatase gene, *EMBO J. 12*, 3105-3110.

9. Murguia, J. R., Belles, J. M., and Serrano, R. (1996) The yeast *HAL2* nucleotidase is an *in vivo* target of salt toxicity, *J. Biol. Chem. 271*, 29029-29033.

10. Senaratne, R. H., De Silva, A. D., Williams, S. J., Mougous, J. D., Reader, J. R., Zhang, T., Chan, S., Sidders, B., Lee, D. H., Chan, J., Bertozzi, C. R., and Riley, L. W. (2006) 5'-Adenosinephosphosulphate reductase (CysH) protects *Mycobacterium tuberculosis* against free radicals during chronic infection phase in mice, *Mol. Microbiol. 59*, 1744-1753.

11. Newton, G. L., Arnold, K., Price, M. S., Sherrill, C., Delcardayre, S. B., Aharonowitz, Y., Cohen, G., Davies, J., Fahey, R. C., and Davis, C. (1996) Distribution of thiols in microorganisms: mycothiol is a major thiol in most actinomycetes, *J. Bacteriol. 178*, 1990-1995.

12. Buchmeier, N. A., Newton, G. L., and Fahey, R. C. (2006) A mycothiol synthase mutant of *Mycobacterium tuberculosis* has an altered thiol-disulfide content and limited tolerance to stress, *J. Bacteriol. 188*, 6245-6252.

13. Kumar, P., Schelle, M. W., Jain, M., Lin, F. L., Petzold, C. J., Leavell, M. D., Leary, J. A., Cox, J. S., and Bertozzi, C. R. (2007) PapA1 and PapA2 are

acyltransferases essential for the biosynthesis of the *Mycobacterium tuberculosis* virulence factor Sulfolipid-1, *Proc. Natl. Acad. Sci. U. S. A. 104*, 11221-11226.

14. Hatzios, S. K., Schelle, M. W., Holsclaw, C. M., Behrens, C. R., Botyanszki, Z., Lin, F. L., Carlson, B. L., Kumar, P., Leary, J. A., and Bertozzi, C. R. (2009) PapA3 is an acyltransferase required for Polyacyltrehalose biosynthesis in *Mycobacterium tuberculosis*, *J. Biol. Chem. 284*, 12745-12751.

15. Converse, S. E., Mougous, J. D., Leavell, M. D., Leary, J. A., Bertozzi, C. R., and Cox, J. S. (2003) MmpL8 is required for Sulfolipid-1 biosynthesis and *Mycobacterium tuberculosis* virulence, *Proc. Natl. Acad. Sci. U. S. A. 100*, 6121-6126.

16. Mougous, J. D., Petzold, C. J., Senaratne, R. H., Lee, D. H., Akey, D. L., Lin, F. L., Munchel, S. E., Pratt, M. R., Riley, L. W., Leary, J. A., Berger, J. M., and Bertozzi, C. R. (2004) Identification, function and structure of the mycobacterial sulfotransferase that initiates Sulfolipid-1 biosynthesis, *Nat. Struct. Mol. Biol. 11*, 721-729.

17. Spiegelberg, B. D., Xiong, J. P., Smith, J. J., Gu, R. F., and York, J. D. (1999) Cloning and characterization of a mammalian lithium-sensitive bisphosphate 3'-nucleotidase inhibited by inositol 1,4-bisphosphate, *J. Biol. Chem. 274*, 13619-13628.

18. Movahedzadeh, F., Wheeler, P. R., Dinadayala, P., Av-Gay, Y., Parish, T., Daffe, M., and Stoker, N. G. (2010) Inositol monophosphate phosphatase genes of *Mycobacterium tuberculosis*, *BMC Microbiol. 10*, 50.

19. Mougous, J. D., Senaratne, R. H., Petzold, C. J., Jain, M., Lee, D. H., Schelle, M. W., Leavell, M. D., Cox, J. S., Leary, J. A., Riley, L. W., and Bertozzi, C. R. (2006) A sulfated metabolite produced by *stf3* negatively regulates the virulence of *Mycobacterium tuberculosis*, *Proc. Natl. Acad. Sci. U. S. A. 103*, 4258-4263.

20. Holsclaw, C. M., Sogi, K. M., Gilmore, S. A., Schelle, M. W., Leavell, M. D., Bertozzi, C. R., and Leary, J. A. (2008) Structural characterization of a novel sulfated menaquinone produced by *stf3* from *Mycobacterium tuberculosis*, *ACS Chem. Biol. 3*, 619-624.

21. Mechold, U., Ogryzko, V., Ngo, S., and Danchin, A. (2006) Oligoribonuclease is a common downstream target of lithium-induced pAp accumulation in *Escherichia coli* and human cells, *Nucleic Acids Res. 34*, 2364-2373.

22. Walsh, C. T., Gehring, A. M., Weinreb, P. H., Quadri, L. E., and Flugel, R. S. (1997) Post-translational modification of polyketide and nonribosomal peptide synthases, *Curr. Opin. Chem. Biol. 1*, 309-315.

23. Sassetti, C. M., Boyd, D. H., and Rubin, E. J. (2003) Genes required for mycobacterial growth defined by high density mutagenesis, *Mol. Microbiol. 48*, 77-84.

24. Chalut, C., Botella, L., de Sousa-D'Auria, C., Houssin, C., and Guilhot, C. (2006) The nonredundant roles of two 4'-phosphopantetheinyl transferases in vital processes of Mycobacteria, *Proc. Natl. Acad. Sci. U. S. A. 103*, 8511-8516.

25. Glickman, M. S., Cox, J. S., and Jacobs, W. R., Jr. (2000) A novel mycolic acid cyclopropane synthetase is required for cording, persistence, and virulence of *Mycobacterium tuberculosis*, *Mol. Cell 5*, 717-727.

26. Stover, C. K., de la Cruz, V. F., Fuerst, T. R., Burlein, J. E., Benson, L. A., Bennett, L. T., Bansal, G. P., Young, J. F., Lee, M. H., Hatfull, G. F., *et al.* (1991) New use of BCG for recombinant vaccines, *Nature 351*, 456-460.

27. Fahey, R. C., and Newton, G. L. (1987) Determination of low-molecular-weight thiols using monobromobimane fluorescent labeling and high-performance liquid chromatography, *Methods Enzymol. 143*, 85-96.

28. Buchmeier, N. A., Newton, G. L., Koledin, T., and Fahey, R. C. (2003) Association of mycothiol with protection of *Mycobacterium tuberculosis* from toxic oxidants and antibiotics, *Mol. Microbiol. 47*, 1723-1732.

Chapter 4: Biochemical characterization of the acyltransferase PapA3 and its contribution to Polyacyltrehalose biosynthesis in *Mycobacterium tuberculosis*[a]

Introduction

Mycobacterium tuberculosis (*Mtb*) has a complex cell wall that contains a number of unique glycolipids intimately linked to mycobacterial pathogenesis (*1, 2*). The biosynthesis of many of these virulence factors, including the trehalose mycolates, phenolic glycolipids, and Sulfolipid-1 (SL-1), is largely understood (*3-5*). In contrast, relatively little is known about the biosynthesis of other prominent *Mtb* glycolipids, such as di-, tri-, and polyacyltrehaloses. These acyltrehaloses are located in the outer surface of the cell wall and contain di- and tri-methyl-branched fatty acids that are only found in pathogenic species of mycobacteria (*6, 7*). Previous studies suggest a role for these glycolipids in anchoring the bacterial capsule, which impedes phagocytosis by host cells (*6*).

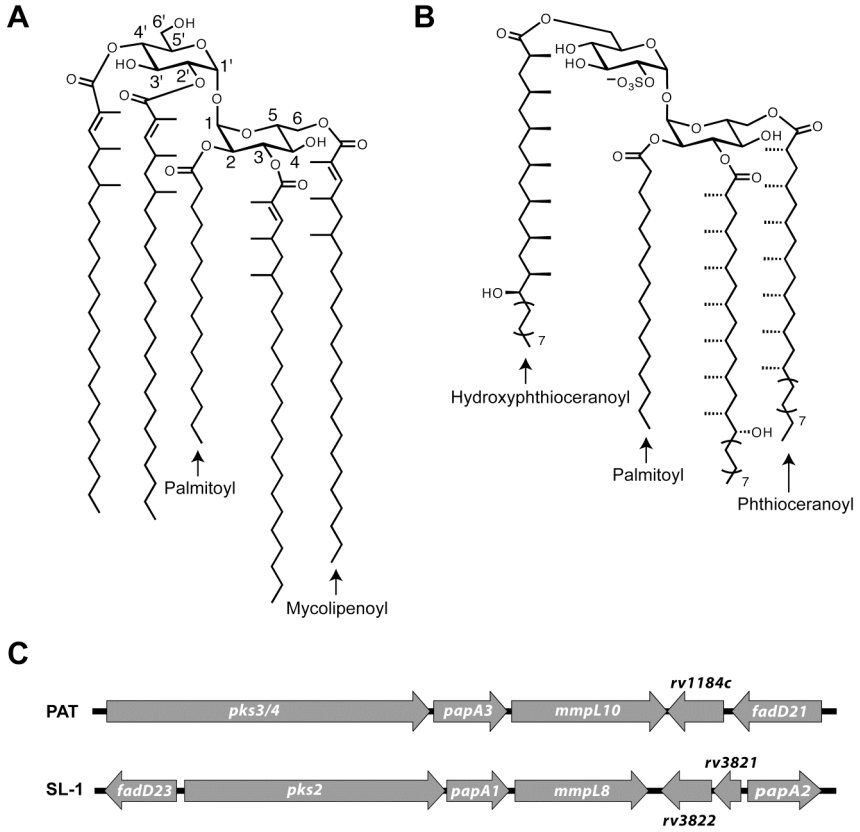

FIGURE 4-1. PAT and SL-1 share related structures and biosynthetic gene clusters. (**A**) Structure of PAT. (**B**) Structure of SL-1. (**C**) The genomic arrangement of the PAT and SL-1 biosynthetic gene clusters.

[a] Michael W. Schelle, Cynthia M. Holsclaw, Christopher R. Behrens, Zsofia Botyanszki, Fiona L. Lin, Brian L. Carlson, and Pawan Kumar contributed to the work presented in this chapter.

The major polyacyltrehalose (PAT) of *Mtb*, also referred to as pentaacyl or polypthienoyl trehalose, consists of five acyl chains--four mycolipenic (phthienoic) acids and one fully saturated fatty acid--linked to trehalose (Figure 4-1A) (*8*). The mycolipenic acid side chains of PAT are products of the polyketide synthase gene *pks3/4* (*7*). Disruption of *pks3/4* (also referred to as *msl3* (*7*)) abolishes PAT biosynthesis and causes cell aggregation. At present, the remaining proteins required for PAT assembly have not been characterized.

Interestingly, the PAT biosynthetic gene cluster strongly resembles that of SL-1, which is a structurally similar trehalose-based glycolipid unique to pathogenic mycobacteria (Figure 4-1B) (*9*). Both gene clusters contain polyketide synthase (*pks*), acyltransferase *(pap*), and lipid transport (*mmpL*) genes in a similar genomic arrangement (Figure 4-1C). The SL-1 locus encodes two acyltransferase genes, *papA1* and *papA2*, which are required for SL-1 biosynthesis (*5, 10*). These proteins belong to the mycobacterial-specific polyketide-associated protein (Pap) family of acyltransferases, which share a conserved $HX_3DX_{14}Y$ motif that is required for activity (*11*). The PapA2 enzyme catalyzes the esterification of the 2'-position of trehalose-2-sulfate with a saturated fatty acid. PapA1 mediates the subsequent esterification of this intermediate with a hydroxyphthioceranoyl group produced by Pks2 (*5*). Interestingly, the PAT locus contains a gene, *Rv1182*, that is homologous to both *papA1* and *papA2* (55% and 53% amino acid identity, respectively). This gene is annotated as *papA3* in the genome and was previously shown to encode a protein bearing the signature Pap motif (*11*).

In this chapter, we demonstrate that *papA3* encodes an acyltransferase essential for the biosynthesis of PAT. Disruption of the *papA3* gene resulted in loss of the glycolipid from *Mtb* lipid extracts, as determined by high-resolution mass spectrometry. Moreover, the purified enzyme was shown to selectively and sequentially acylate trehalose *in vitro*, generating a diacylated product similar to the 2,3-diacyltrehaloses of *Mtb*. Together, these data confirm that PapA3 plays a crucial role in PAT biosynthesis and highlight its potential involvement in the biosynthesis of related *Mtb* acyltrehaloses.

Results

Genomic analysis of the PAT biosynthetic locus

The *pap* gene family encodes polyketide synthase-associated acyltransferases that are involved in the synthesis of some of the complex lipids produced by *Mtb* (*5, 11*). In the *Mtb* genome, *papA3* is clustered with the polyketide synthase-encoding gene *pks3/4*. In some strains, including the sequenced H37Rv strain, there is an intervening stop codon in *pks3/4* which results in two separate open reading frames (termed *pks3* and *pks4*) (*7*). Strains containing this mutation do not synthesize PAT (*12*), indicating that an intact *pks3/4* gene is essential for the biosynthesis of this glycolipid. Within the same gene cluster resides *mmpL10*, which encodes a putative lipid transporter. MmpL10 belongs to the same protein family as MmpL8, which is required for SL-1 biosynthesis (*12, 13*). The genomic organization of *pks3/4*, *papA3*, and *mmpL10* parallels that of *pks2*, *papA1*, and *mmpL8* in the SL-1 biosynthetic gene cluster (Figure 4-1C). We previously demonstrated that *papA1* is the acyltransferase responsible for coupling the polyketide

product of Pks2 to a trehalose-based acceptor (*5*). By analogy, we hypothesized that PapA3 is essential for PAT biosynthesis, catalyzing trehalose acylation.

PapA3 is an acyltransferase that esterifies trehalose and trehalose-2-palmitate

The *papA3* gene from the H37Rv *Mtb* strain was expressed in *E. coli* BL21(DE3) as an N-terminal MBP-fusion protein. SDS-PAGE analysis revealed an apparent molecular mass of 95 kDa for the purified protein. Following TEV cleavage and subsequent removal of the protease and MBP by Ni^{2+}-affinity chromatography (Figure 4-2), the protein's identity was confirmed by mass spectrometry. The measured mass (51809 ± 3 Da) was consistent with the predicted molecular mass of the protein (51777.5 Da) oxidized at a single methionine residue. In addition, tryptic digestion and mass fingerprinting of the purified protein generated approximately 61% sequence coverage, providing further confirmation of the protein's identity (data not shown).

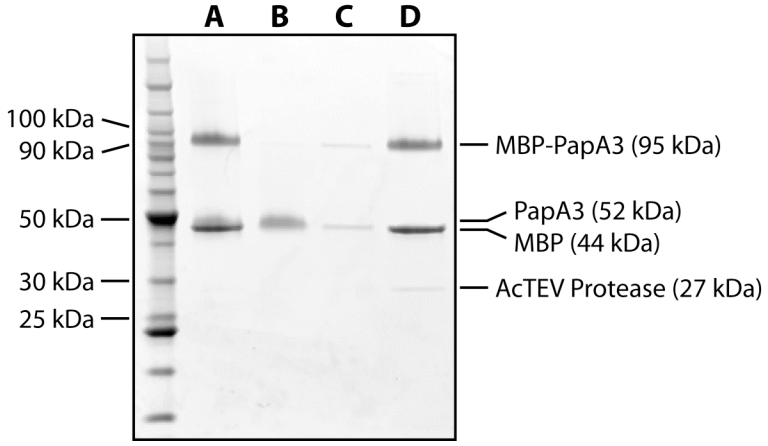

FIGURE 4-2. Purification of PapA3 from maltose-binding protein (MBP) using immobilized metal affinity chromatography. AcTEV cleavage of MBP-PapA3 resulted in a mixture of MBP, PapA3, and fusion protein, as indicated by SDS-PAGE analysis (**A**). PapA3 was purified from the mixture using Ni-NTA agarose, which selectively bound the His-tagged MBP, fusion protein, and protease while leaving PapA3 in solution (**B**). The resin was washed once with a buffer containing 30 mM imidazole (**C**), and the bound proteins were subsequently eluted with 300 mM imidazole (**D**).

Incubation of PapA3 with ^{14}C-PCoA and trehalose resulted in the formation of two unique products, as determined by silica gel thin-layer chromatography (TLC) and phosphorimaging (Figure 4-3A). Only the less polar product was formed by the reaction of PapA3 with ^{14}C-PCoA and synthetic trehalose-2-palmitate (T2P) (*14-16*). PapA3 showed no activity against several other saccharides, including T3P, trehalose-2-sulfate, α,β-trehalose, glucose, and maltose, suggesting that the enzyme is selective for trehalose and T2P (Table 4-1). Notably, PapA3 hydrolyzes ^{14}C-PCoA to ^{14}C-POH in the absence of another substrate (Figure 4-3A), similar to the other characterized Pap enzymes. Further kinetic analysis of the PapA3 reaction containing trehalose or T2P was precluded by the complexity of the product mixture.

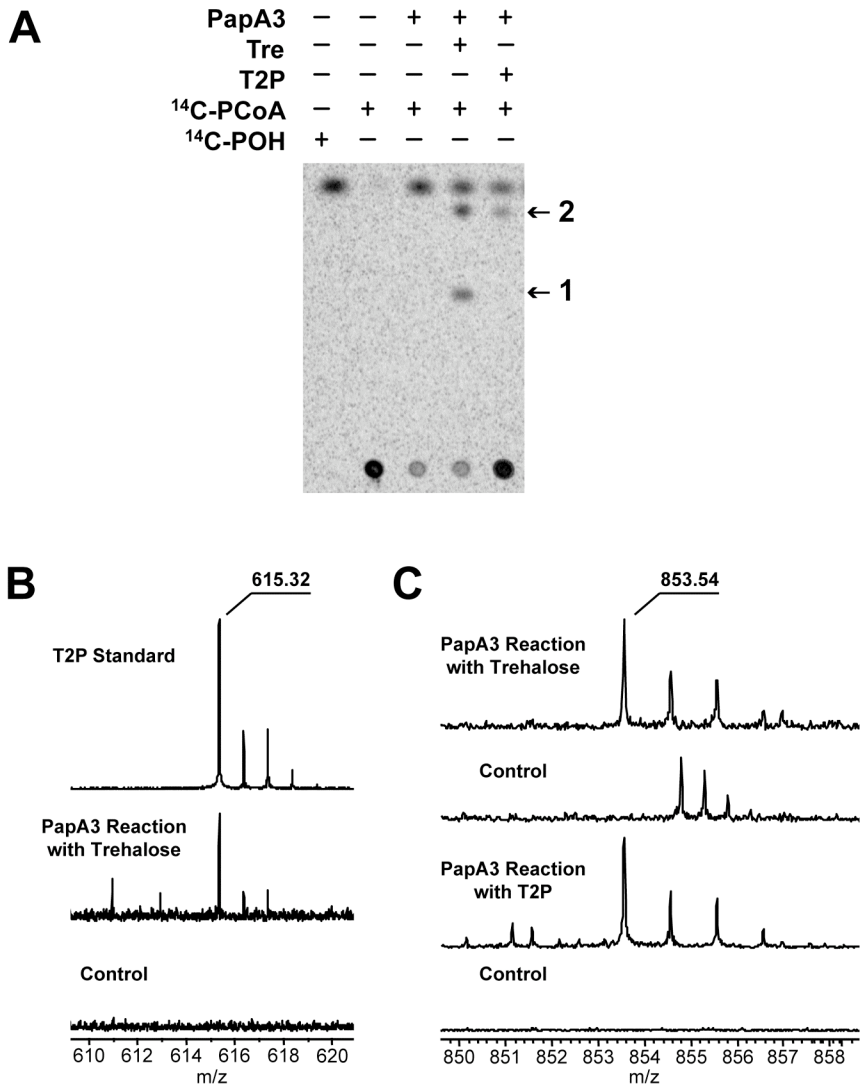

FIGURE 4-3. PapA3 is an acyltransferase that sequentially palmitoylates trehalose *in vitro*. (**A**) PapA3 was incubated with ^{14}C-PCoA and either trehalose (Tre) or T2P. The reactions were analyzed by TLC and phosphorimaging. Two new products (1 and 2) were observed in the reaction with Tre, but only product 2 was observed in the reaction with T2P. (**B**) ESI-FT-ICR MS analysis of product 1 from the PapA3 reaction with Tre. A product ion with *m/z* 615.32, corresponding to the *m/z* of a chloride adduct of synthetic T2P, was observed in the PapA3 reaction. In contrast, the control reaction lacking PapA3 showed no product at *m/z* 615. (**C**) ESI-FT-ICR MS analysis of product 2 from the PapA3 reaction with Tre and T2P. An ion with *m/z* 853.54 was observed in both reactions, but was not present in control reactions lacking PapA3.

Interestingly, no activity was detected with ^{14}C-butyryl coenzyme A or ^{14}C-crotonoyl coenzyme A, which contains a *trans*-2-ene functionality like the mycolipenoyl groups of PAT (Table 4-1). However, product formation was observed upon incubation of PapA3 with trehalose and ^{14}C-docosanoyl coenzyme A, which consists of a 22-carbon

saturated fatty acid conjugated to coenzyme A (data not shown). This suggests that PapA3 may also accept the 24-carbon backbone of mycolipenic acid. Taken together, these findings indicate that lipid chain length influences the substrate specificity of PapA3.

TABLE 4-1. Substrate specificity of PapA3

Substrate	Product Formation[c]
Nucleophile[a]	
Trehalose	Yes
T2P	Yes
T3P	ND
Trehalose-2-sulfate	ND
α,β-trehalose	ND
Glucose	ND
Maltose	ND
Acyl-CoA[b]	
Palmitoyl-CoA	Yes
Docosanoyl-CoA	Yes
Butyryl-CoA	ND
Crotonoyl-CoA	ND

ND, not detectable.
[a]Reactions were performed with 2 μM enzyme, 20 μM ^{14}C-palmitoyl-CoA, and 1 mM or 10 mM of each substrate in 100 mM ammonium bicarbonate (pH 7.2) at rt for 2 h.
[b]Reactions were performed with 2 μM enzyme, 20 μM ^{14}C-Acyl-CoA, and 1 mM of trehalose or T2P in 100 mM ammonium bicarbonate (pH 7.2) at rt for 2 h.
[c]Product formation was assessed by TLC and phosphorimaging.

Trehalose-2-palmitate and trehalose dipalmitate are products of PapA3

Products from the reaction of PapA3 with PCoA and either trehalose or T2P were characterized by electrospray ionization Fourier transform ion cyclotron resonance mass spectrometry (ESI-FT-ICR MS) and linear-ion trap MS operating in the negative ion mode. The reaction of PapA3 with trehalose yielded two unique products measured via FT-ICR MS at *m/z* 615.3153 and *m/z* 853.5447, corresponding to the exact masses of the chloride adducts of trehalose palmitate and trehalose dipalmitate, respectively (Figures 3B and 3C). The accurate mass spectra were calibrated internally, and both reaction products were measured to sub-ppm accuracy. The product ion at *m/z* 853.54 was also observed in the reaction of PapA3 with T2P (Figure 4-3C). Importantly, these products were not observed in the absence of enzyme. Linear-ion trap tandem mass spectrometry (MS^n) of the ion at *m/z* 615.32 yielded dissociation ions consistent with those derived from synthetic T2P (Figure 4-4). MS^n of the ion at *m/z* 853.54 was consistent with 2,3-dipalmitoylation of a single pyranose ring of trehalose (Figure 4-5), which was confirmed in the positive ion mode using lithium-ion coordination (Figure 4-6). Together, these data demonstrate that PapA3 sequentially acylates trehalose to form trehalose dipalmitate.

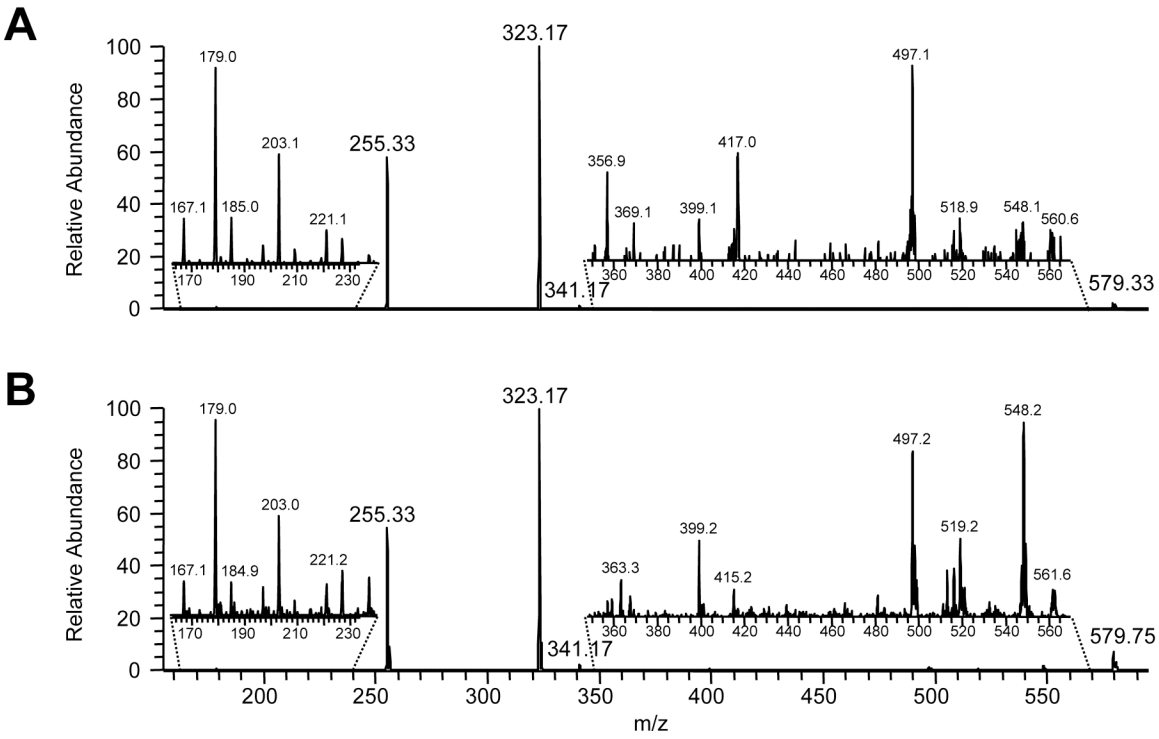

FIGURE 4-4. Linear-ion trap MS^n of synthetic T2P (**A**) is consistent with that of the product ion at *m/z* 615.32 in the reaction of PapA3 with trehalose (**B**). MS^n analysis was performed in the negative ion mode. Shown are the MS^3 spectra of the deprotonated ions, which were obtained after MS^2 dissociation of the adducted ions. The dissociation ions at *m/z* 255 and 323 are consistent with dissociation at the ester bond between palmitate and trehalose.

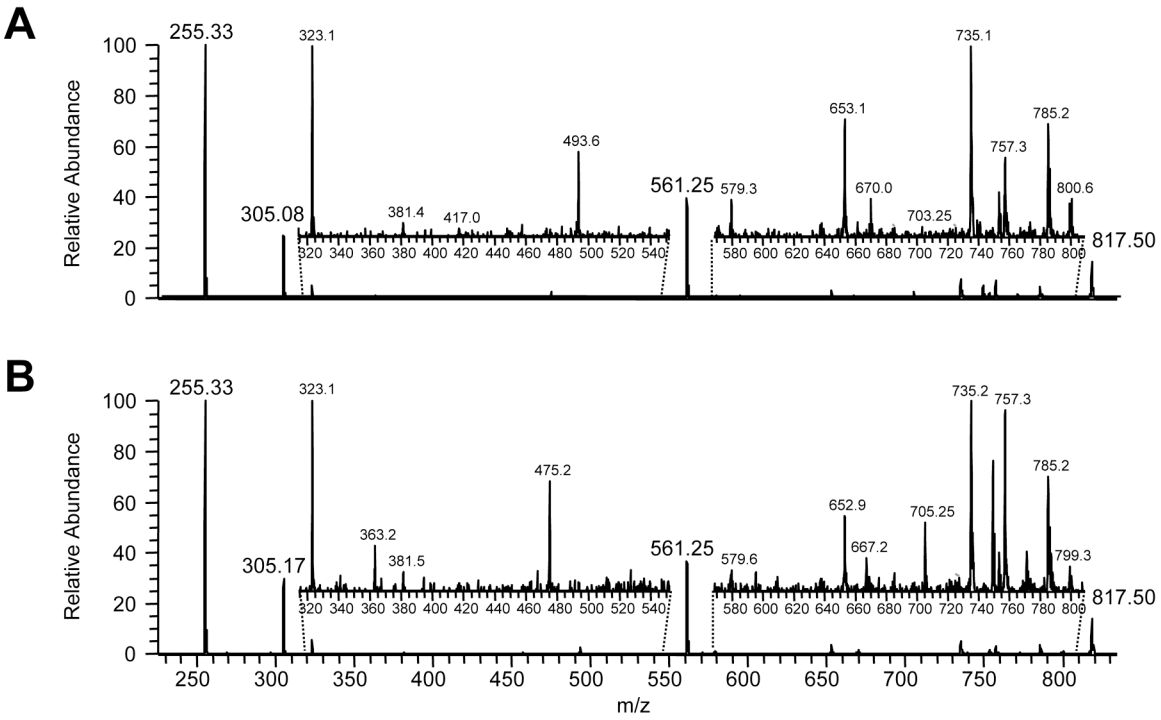

FIGURE 4-5. Linear-ion trap MS^n of the product ion at *m/z* 853.54 in the reaction of PapA3 with trehalose (**A**) and T2P (**B**) is consistent with 2,3-dipalmitoylation of trehalose. MS^n analysis was performed in the negative ion mode. The dissociation ions at *m/z* 561 and 305 are consistent with the loss of one or two palmitoyl groups from the trehalose moiety, respectively. The dissociation ion at *m/z* 653 is consistent with the loss of glucose, indicating both palmitoyl groups reside on the same pyranose ring of trehalose.

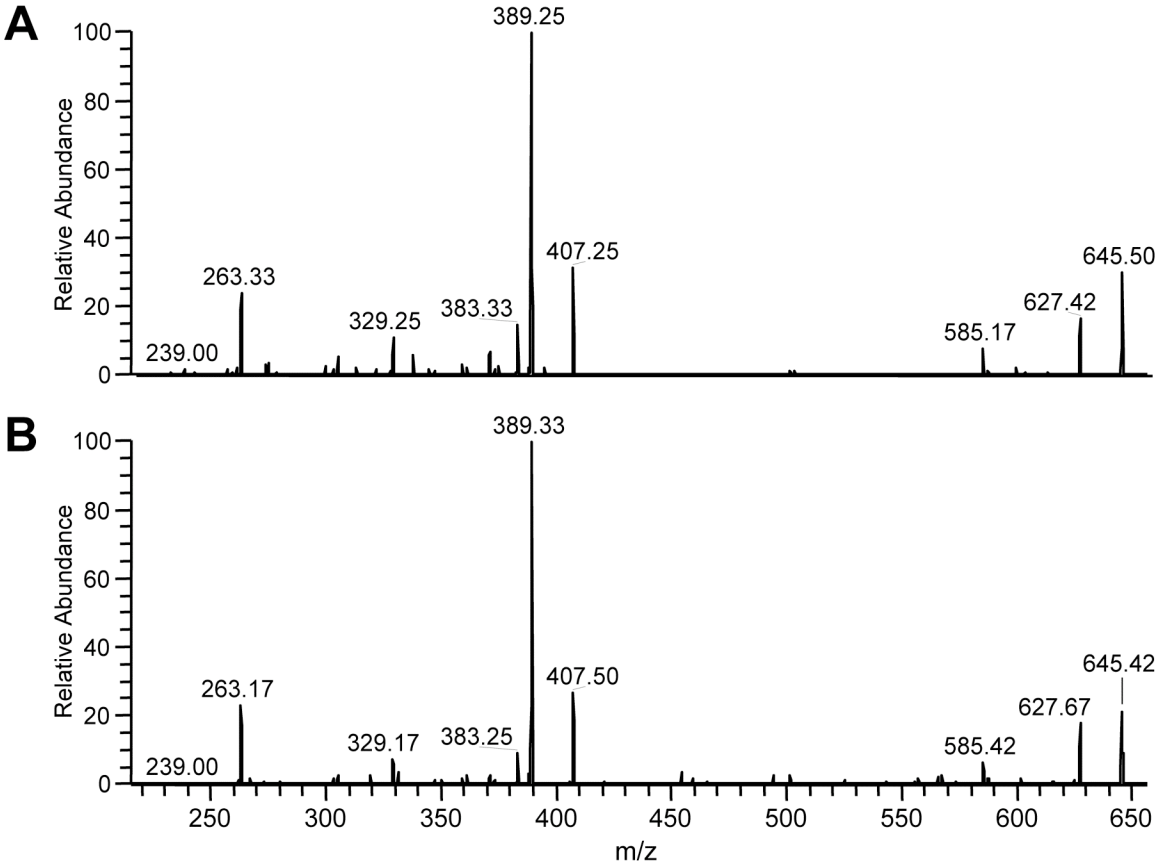

FIGURE 4-6. Linear-ion trap MS^n of the diacyl product ions from the reaction of PapA3 with trehalose (**A**) and T2P (**B**) is consistent with 2,3-dipalmitoylation of trehalose. MS^n analysis was performed in the positive ion mode using lithium-cation coordination. Two dissociation ions at *m/z* 663 and 645 were observed in the MS^2 spectra of these ions, corresponding to the cleavage of the glycosidic bond between the pyranose rings of trehalose (data not shown), and indicating that the acyl substituents are on the same pyranose ring. This confirms the data obtained in the negative ion mode (Figure 4-5). Shown are the MS^3 spectra of the dissociation ions obtained from the cleavage of the glycosidic bond between the individual pyranose rings of trehalose. Similar fragmentation patterns were observed between both substrates.

Trehalose-3-palmitate is not produced by PapA3

To rule out the possibility that the initial acylation product of PapA3 is trehalose-3-palmitate (T3P) or a mixture of 2- and 3-palmitoylated species, we synthesized T3P for additional biochemical and structural studies. To determine if T3P is a viable intermediate in the biosynthesis of trehalose dipalmitate, we incubated T3P with PapA3 and ^{14}C-PCoA. No product formation was detected following TLC and phosphorimaging (Figure 4-7), indicating that T3P is not a substrate for PapA3. Interestingly, the presence of T3P in the reaction mixture appears to diminish the hydrolysis of ^{14}C-PCoA by PapA3, suggesting it may instead inhibit the enzyme.

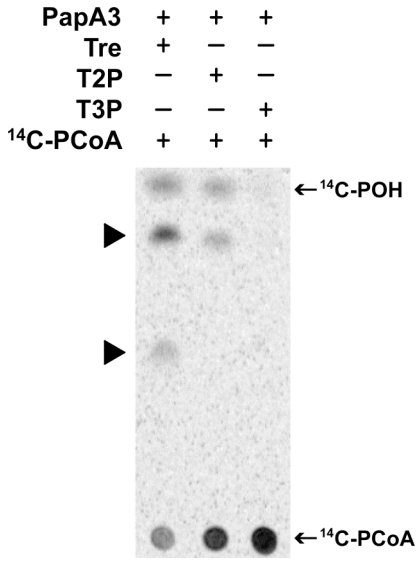

FIGURE 4-7. T3P is not a substrate for PapA3. PapA3 was incubated with ^{14}C-palmitoyl coenzyme A (^{14}C-PCoA) and either trehalose (Tre), T2P, or T3P. The reactions were analyzed by TLC and phosphorimaging. Product formation (denoted by the black triangles) was observed in the reactions with Tre and T2P, but not in the reaction with T3P. Hydrolysis of ^{14}C-PCoA to palmitic acid (^{14}C-POH) was dramatically reduced in the reaction with T3P.

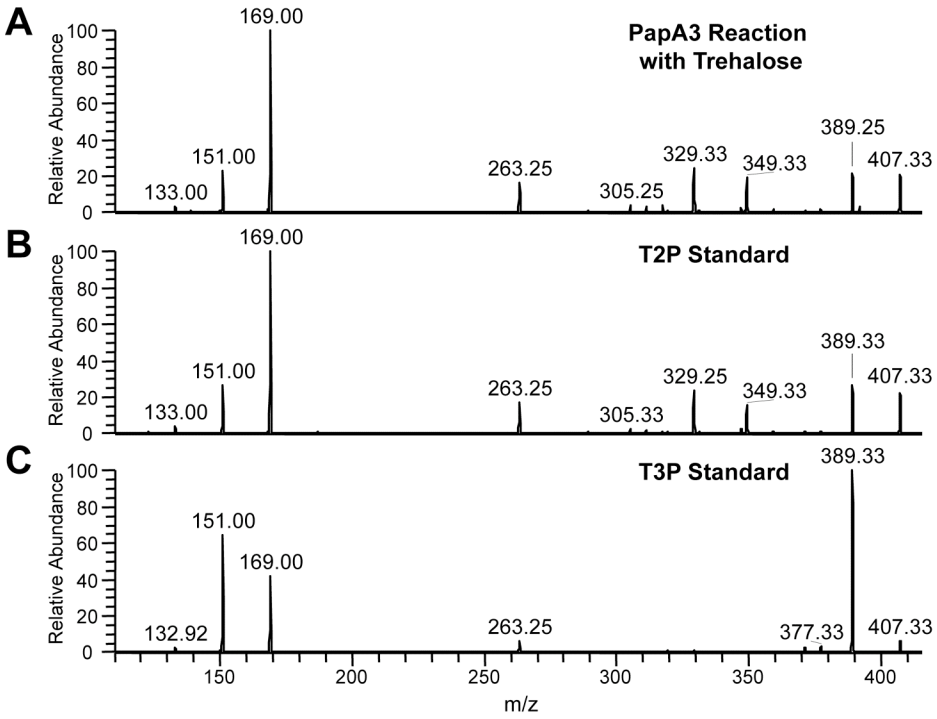

FIGURE 4-8. Linear-ion trap MS^n of the monoacyl product ion from the reaction of PapA3 with trehalose (**A**) is consistent with that of synthetic T2P (**B**) and not that of

synthetic T3P (**C**). MS^n analysis was performed in the positive ion mode using lithium-cation coordination. Shown are the MS^3 spectra of the dissociation ions obtained from the cleavage of the glycosidic bond between the individual pyranose rings of trehalose.

For further confirmation that the monoacyl product of PapA3 is not T3P, we analyzed T3P by MS^n in the positive ion mode using lithium-cation coordination and compared its fragmentation to that of T2P and the PapA3 monoacyl reaction product ion (Figure 4-8). T2P, T3P, and the monoacyl PapA3 reaction product were observed at *m/z* 587, corresponding to the lithium adducts of these molecules. Two dissociation ions at *m/z* 425 and 407 were observed in the MS^2 spectra of these ions, corresponding to the cleavage of the glycosidic bond between the pyranose rings of trehalose (data not shown). The MS^3 spectrum of the monoacyl PapA3 reaction product dissociation ion at *m/z* 407 was identical to that derived from synthetic T2P (Figures 4-8A and 4-8B) and dramatically distinct from the MS^3 spectrum derived from synthetic T3P (Figure 4-8C). These data clearly demonstrate that the monoacyl PapA3 reaction product is not T3P. Combined with the finding that T3P is not a substrate for PapA3, these data support the assignment of T2P as the initial acylation product of PapA3.

PapA3 is required for PAT biosynthesis in vivo

In order to determine whether PapA3 is required for PAT biosynthesis *in vivo*, a *papA3* deletion mutant, Δ*papA3*, was generated in the Erdman strain of *Mtb*. The H37Rv strain sequenced by Cole and colleagues (*17*) contains a stop codon in *pks3/4*, which truncates the encoded polyketide synthase and abolishes PAT biosynthesis. However, sequencing confirmed that the Erdman strain used in these studies encodes a single open reading frame for *pks3/4*, yielding a functional polyketide synthase (data not shown). Extraction of the crude lipids from wild-type Erdman cells with organic solvents followed by ESI-FT-ICR MS analysis confirmed the presence of the PAT lipid envelope in this strain of *Mtb* (Figure 4-9). In contrast, PAT was not observed in extracts from the Δ*papA3* mutant strain. Complementation of the Δ*papA3* mutant strain with a plasmid encoding *papA3* restored PAT production, demonstrating that PapA3 is essential for the biosynthesis of this glycolipid in *Mtb*.

PAT biosynthesis is independent of SL-1 biosynthesis

Given the similarities between the PAT and SL-1 genetic loci, we sought to determine if the two biosynthetic pathways shared common intermediates. The first committed step in SL-1 biosynthesis is the sulfation of trehalose at the 2-position of one of the glucose moieties by the sulfotransferase Stf0 (*18*). Thus, we analyzed the *Mtb* Δ*stf0* mutant strain, which lacks SL-1 as well as its upstream biosynthetic precursors, for the presence of PAT. FT-ICR MS analysis of crude lipid extracts clearly showed the presence of PAT in the Δ*stf0* mutant strain (Figure 4-9). Also, SL-1 synthesis was not perturbed in the Δ*papA3* mutant strain. These data indicate that the PAT biosynthetic pathway is independent of the SL-1 pathway and that these pathways share no intermediates other than the cellular pool of trehalose.

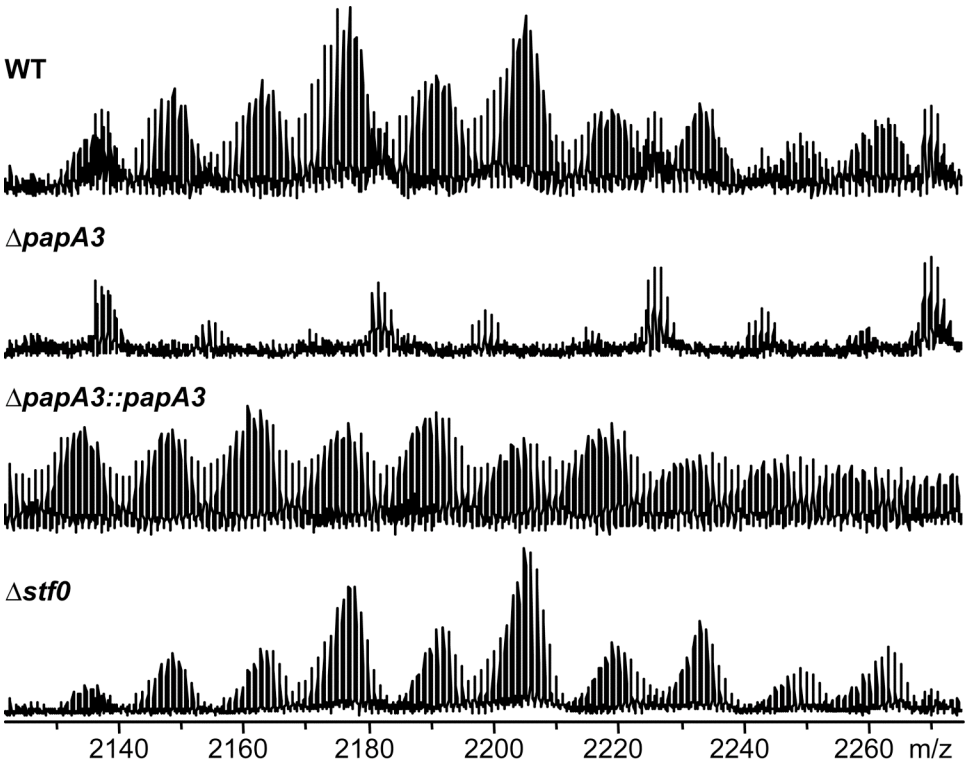

FIGURE 4-9. PAT biosynthesis requires *papA3*, but not *stf0*, *in vivo*. ESI-FT-ICR MS analysis of lipid extracts from WT, Δ*papA3::papA3*, and Δ*stf0 Mtb* strains revealed the presence of characteristic PAT lipoforms that are absent from Δ*papA3 Mtb* extracts.

Discussion

The data presented here establish that PapA3 is an acyltransferase required for PAT biosynthesis in *Mtb*. Recombinant PapA3 selectively acylates trehalose and T2P in a manner consistent with the structure of PAT. Also, deletion of *papA3* from *Mtb* prevents PAT synthesis *in vivo*. Furthermore, despite the genetic and structural similarities between PAT and SL-1, the biosynthetic pathways of these metabolites are independent. However, many questions remain about PapA3 and PAT biosynthesis.

In vitro, PapA3 catalyzes the sequential transfer of two palmitoyl groups onto a single glucose residue of trehalose, suggesting that PapA3 installs both the palmitoyl group at the 2-position of PAT and the 3-mycolipenoyl group (Figure 4-1A). It is possible that PapA3 associates with other proteins in the PAT biosynthetic pathway, forming a coordinate synthetic complex similar to that described for phthiocerol dimycocerosate biosynthesis (*19*). Such supramolecular assemblies may influence substrate availability and orientation in the PapA3 active site, thereby conferring this unique activity.

Whether PapA3 is truly a bifunctional acyltransferase remains unclear. PapA3 may only install the palmitoyl group of PAT *in vivo*, in which case the formation of trehalose dipalmitate by the purified enzyme is an *in vitro* artifact. Such activity has been observed with the lauroyltransferase of *E. coli* Lipid A biosynthesis, which transfers two

lauroyl groups *in vitro* but only one *in vivo* (*20*). Alternatively, the mycolipenoyl groups found at the 3-, 6-, 2'-, and 4'-positions of PAT may all be physiological products of PapA3. This hypothesis is supported by the genetic association between *papA3* and the mycolipenate synthase *pks3/4* and the promiscuity of PapA3 towards the acylation state of trehalose. Unfortunately, our analysis of the acylation events catalyzed by PapA3 is limited by the lack of a commercially available mycolipenoyl substrate and our limited capability to detect either T2P or trehalose mycolipenates *in vivo*.

The chemical similarities between PAT and SL-1 suggest that the biosynthesis of these molecules may be comparable. However, the SL-1 gene locus encodes two Pap proteins, PapA2 and PapA1, which sequentially install a palmitoyl group and a methyl-branched hydroxyphthioceranoyl group, respectively. By comparison, the PAT gene locus encodes only PapA3. Previously, we showed that PapA2 does not recognize trehalose and cannot account for T2P synthesis (*5*). We initially hypothesized that the SL-1 precursor trehalose-2-sulfate-2'-palmitate (termed SL_{659}) may be desulfated by a sulfatase to form T2P, thus negating the need for a committed trehalose palmitoyl transferase. However, the Δ*stf0* mutant strain, which lacks SL_{659}, maintained the ability to synthesize PAT. We therefore conclude that SL-1 and PAT biosynthesis are independent.

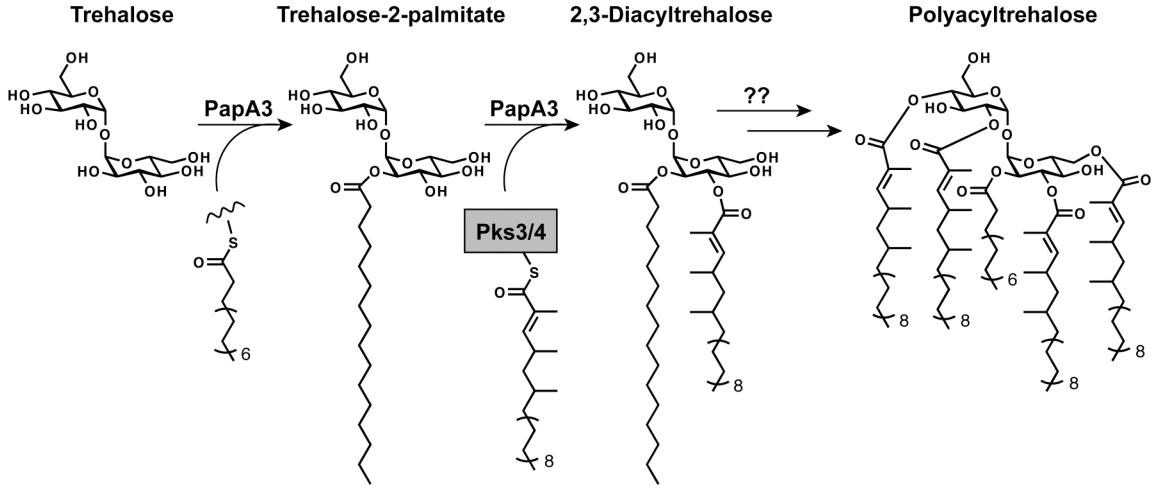

FIGURE 4-10. Proposed PAT biosynthetic pathway. PapA3 first acylates the 2-position of one of the glucose residues of trehalose with a palmitoyl group to form T2P. A mycolipenoyl group, synthesized by Pks3/4, is then transferred to the 3-position of T2P by PapA3 to generate 2,3-diacyltrehalose. 2,3-Diacyltrehalose may either be transported to the cell surface or serve as a biosynthetic intermediate that is further elaborated with mycolipenic acids to give PAT.

On the basis of our biochemical and genetic data, we propose the model for PAT biosynthesis shown in Figure 4-10. Initially, PapA3 modifies the 2-position of one of the glucose residues of trehalose with a palmitoyl group from an unknown acyl donor, most likely PCoA or an acyl pantotheine-based cofactor. A mycolipenoyl group is then transferred to the 3-position of T2P by PapA3, which may associate directly with Pks3/4

or an unknown acyl carrier protein to initiate this second acylation step. The resulting 2,3-diacyltrehalose may be transported to the cell surface without further modification through an unknown pathway. Alternatively, it may serve as a biosynthetic intermediate that is elaborated either intracellularly or extracellularly with the three remaining mycolipenoyl groups of PAT by means of PapA3 or an unidentified acyltransferase. By analogy to other *Mtb* lipid biosynthetic pathways, transport of PAT or its precursor to the cell surface is most likely accomplished by MmpL10.

Clearly, several questions regarding the biosynthesis of PAT remain unanswered. The synthesis of physiological substrates for *in vitro* assays and the comparative lipid analysis of a panel of PAT biosynthetic mutants, including Δ*mmpL10* and Δ*pks3/4*, may resolve some of these issues. While genes from the PAT biosynthetic gene cluster are upregulated under various conditions of environmental stress, including phagosomal acidification and nutrient starvation (*21, 22*), the role of PAT in *Mtb* pathogenesis remains a mystery. Notably, a recent study of an *Mtb* strain deficient in PAT biosynthesis suggests PAT does not contribute to virulence in mice (*23*). However, the phenotype of SL-1-deficient *Mtb* strains is also indistinguishable from wild type in the murine model of infection (*5*), suggesting the function of these glycolipids may be host-specific. Thus, a more appropriate model of tuberculosis may be key to elucidating the role of these lipids in *Mtb* pathogenesis.

Materials and Methods

Reagents and chemicals

Pfu DNA polymerase was from Stratagene (La Jolla, CA). Oligonucleotides were from Elim Biopharmaceuticals, Inc. (Hayward, CA). Restriction enzymes were from New England Biolabs (Ipswich, MA). Qiagen (Valencia, CA) kits were used for plasmid DNA purification and the extraction of DNA from agarose gels. T4 DNA ligase and BL21(DE3) chemically competent cells were purchased from Invitrogen (Carlsbad, CA). DNA sequencing was performed by Elim Biopharmaceuticals, Inc. ^{14}C-Palmitoyl coenzyme A (^{14}C-PCoA), ^{14}C-palmitic acid (^{14}C-POH), ^{14}C-butyryl coenzyme A, ^{14}C-crotonoyl coenzyme A, and ^{14}C-docosanoyl coenzyme A were purchased from ARC Radiolabeled Chemicals (St. Louis, MO; 50-55 mCi/mmol). Unlabeled palmitoyl coenzyme A (PCoA) was purchased from Avanti Polar Lipids, Inc. (Alabaster, AL). T2P and trehalose-2-sulfate were synthesized as previously described (*14-16, 24*). Glass-backed Silica Gel 60 HPTLC plates were purchased from EMD Chemicals (Gibbstown, NJ). All other chemicals were purchased from Sigma-Aldrich (St. Louis, MO) or Fluka (St. Louis, MO) and used without further purification.

Chemical synthesis and structural characterization of trehalose-3-palmitate

All chemical reagents were of analytical grade, obtained from commercial suppliers and used without further purification. Anhydrous dimethylformamide (DMF) and methanol (MeOH) were purchased from Aldrich or Acros in sealed bottles. In all cases, magnesium sulfate was used as a drying agent and solvent was removed by reduced pressure with a Buchi Rotovapor R-114 equipped with a Welch self-cleaning dry

vacuum. Flash chromatography was performed using Sorbent Technologies 60 Å 40-63 μm (230-400 mesh) silica. All ^{1}H and ^{13}C NMR spectra are reported in ppm and referenced to solvent peaks ($CDCl_3$: δ 7.24, 3:1 CD_3OD:$CDCl_3$: δ 4.78). Spectra were obtain on a Bruker DRX-500® and AVB-400® instruments. Low and high-resolution fast-atom bombardment (FAB) spectra were obtained from the UC Berkeley Mass Spectrometry Laboratory.

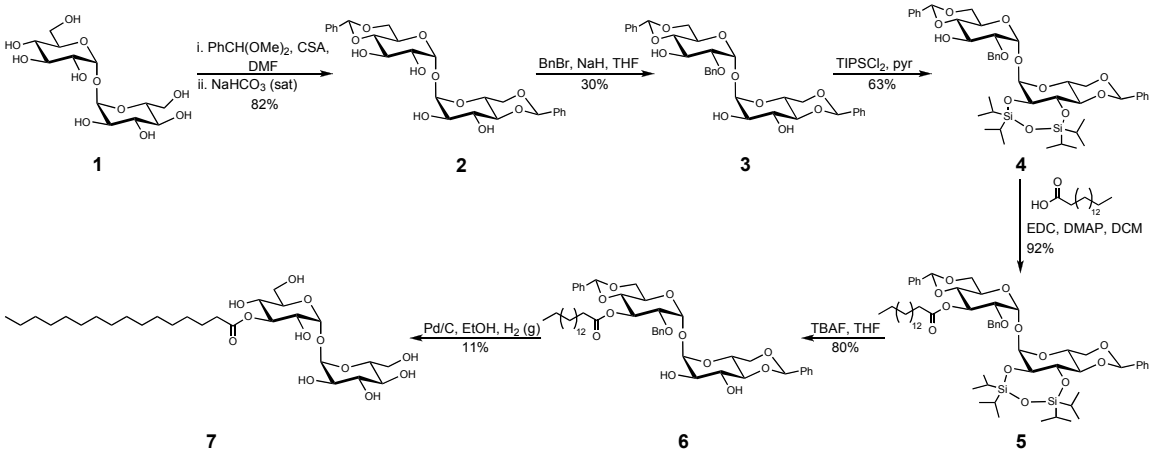

SCHEME 4-1. Synthesis of 3-O-palmitoyl-α,α-D-trehalose.

4,6,4',6'-di-O-benzylidine-α,α-D-trehalose (2). Anhydrous trehalose **1** (1.02 g, 2.98 mmol) was suspended in DMF (15 mL) (Scheme 4-1). (1*S*)-(+)-10-camphorsulfonic acid (34.6 mg, 0.15 mmol, 0.05 eq) and benzaldehyde dimethyl acetal (0.67 mL, 4.47 mmol, 1.5 eq) were added at rt. The flask was attached to a rotary evaporator and warmed to 40 °C under vacuum for 3 h. DMF was evaporated off, and the remaining residue was suspended in saturated $NaHCO_3$ (15 mL). The product precipitated out while the reaction was stirred overnight at rt. The white solid was filtered through a Buckner funnel and column purified in 1:3 hexanes:ethyl acetate to obtain product **2** (1.28 g, 2.47 mmol, 82%). ^{1}H NMR (500 MHz, CD_3OD): δ 3.39 (t, 2H, *J*=9.5 Hz), 3.53 (dd, 2H, *J*=9.5, 4.0 Hz), 3.63 (t, 2H, *J*=10.2 Hz), 3.93 (t, 2H, *J*=9.4 Hz), 4.02 (m, 2H), 4.12 (dd, 2H, *J*=10.0, 5.0 Hz), 5.03 (d, 2H, *J*=3.9 Hz), 5.48 (s, 2H), 7.24 (m, 6H), 7.39 (m, 4H). ^{13}C NMR (125 MHz, 1:1 CD_3OD:$CDCl_3$): δ 62.7, 68.6, 70.0, 72.3, 81.5, 94.9, 101.6, 126.1, 127.7, 128.6, 137.6. HRMS (FAB) calcd. for $C_{26}H_{31}O_{11}$ [M+H$^+$]: 519.1816; found: 519.1879.

2-O-benzyl-4,6,4',6'-di-O-benzylidine-α,α-D-trehalose (3). Compound **2** (0.216 g, 0.416 mmol) was dissolved in tetrahydrofuran (THF) (7 mL) at rt. Sodium hydride (16.6 mg, 60% dispersion in oil, 0.416 mmol, 1 eq) was added to the solution, which was stirred for 2 h. Benzyl bromide (0.0494 mL, 0.416 mmol, 1 eq) was added dropwise. The reaction was stirred overnight. The THF was evaporated off and the crude material was purified via column chromatography in 1:1 hexanes:ethyl acetate to afford compound **3** (74.1 mg, 0.123 mmol, 30%) and starting material **2** (71.7 mg, 0.138 mmol, 33.2%). ^{1}H NMR (500 MHz, $CDCl_3$): δ 3.47 (app. t, 1H, *J*=9.2 Hz), 3.51 (app. t, 1H, *J*=9.6 Hz), 3.56 (dd, 1H, *J*=9.3, 3.7 Hz), 3.68 (m, 3H), 4.03 (m, 2H), 4.11 (m, 3H), 4.19

(m, 1H), 4.28 (dd, 1H, *J*=10.3, 4.9 Hz), 4.75 (s, 2H), 5.15 (d, 1H, *J*=3.8 Hz), 5.18 (d, 1H, *J*=3.7 Hz), 5.48 (s, 1H), 5.51 (s, 1H), 7.36 (m, 11H), 7.44 (m, 2H), 7.48 (m, 2H). ^{13}C NMR (100 MHz, $CDCl_3$): δ 63.0, 63.1, 68.8, 68.9, 70.4, 71.3, 72.4, 73.6, 78.9, 81.0, 81.3, 93.7, 95.2, 102.1, 126.4, 126.5, 128.0, 128.2, 128.3, 128.4, 128.8, 129.3, 129.4, 137.0, 137.1, 137.5. HRMS (FAB) calcd. for $C_{33}H_{37}O_{11}$ [M+H$^+$]: 609.2330; found: 609.2319.

2-O-benzyl-4,6,4',6'-di-O-benzylidine-2',3'-O-(1,1,3,3-tetraisopropyldisiloxane)-α,α-D-trehalose (4). Compound **3** (30.3 mg, 0.050 mmol) was dissolved in pyridine (4 mL). 1,3-Dichloro-1,1,3,3-tetraisopropyldisiloxane (0.040 mL, 0.125 mmol, 2.5 eq) was added dropwise at rt. The reaction mixture was stirred overnight at 40 °C. Pyridine was evaporated off, and the crude material was purified via column chromatography in 4:1 hexanes:ethyl acetate to afford an inseparable mixture of compound **4** (26.7 mg, 0.031 mmol, 63%) and protecting group (1,3-dichloro-1,1,3,3-tetraisopropyldisiloxane). ^{1}H NMR (500 MHz, $CDCl_3$): δ 0.92 (m, 6H-**4**+protecting group), 0.95-1.10 (m, 69H-**4**+protecting group), 3.50 (m, 3H), 3.66 (m, 1H), 3.71 (m, 1H), 3.88 (dd, 1H, *J*=8.5, 4.1 Hz), 4.18 (m, 6H), 4.68 (d, 1H, *J*=11.8 Hz), 4.76 (d, 1H, *J*=11.8 Hz), 5.13 (d, 1H, *J*=4.1 Hz), 5.19 (d, 1H, *J*=3.5 Hz), 5.48 (s, 1H), 5.54 (s, 1H), 7.27 (m, 2H), 7.34 (m, 9H), 7.44 (m, 4H). ^{13}C NMR (125 MHz, $CDCl_3$): δ 11.6, 12.2, 12.6, 12.8, 13.0, 17.0, 17.1, 17.2, 17.3, 17.4, 62.3, 62.6, 69.0, 70.2, 73.1, 73.3, 75.3, 78.7, 81.3, 81.4, 92.9, 94.8, 101.1, 102.2, 126.0, 126.4, 128.0, 128.2, 128.6, 129.2, 137.1, 137.4, 137.7. HRMS (FAB) calcd. for $C_{45}H_{62}NaO_{12}Si_2$ [M+Na$^+$]: 873.3672; found: 873.3675.

2-O-benzyl-4,6,4',6'-di-O-benzylidine-2',3'-O-(1,1,3,3-tetraisopropyldisiloxane)-3-O-palmitoyl-α,α-D-trehalose (5). Compound **4** (41.4 mg, 0.049 mmol) was dissolved in dichloromethane (DCM) (2 mL). Palmitic acid (25.1 mg, 0.098 mmol, 2 eq) was added to the stirring solution at rt. A solution of 1-ethyl-3-(3-dimethylaminopropyl)carbodiimide hydrochloride (93.9 mg, 0.49 mmol, 10 eq) and 4-dimethylaminopyridine (59.9 mg, 0.49 mmol, 10 eq) in DCM (1 mL) was added dropwise to the reaction mixture. The reaction was stirred for 4 h. The solvent was evaporated off, and the crude material was purified via column chromatography in 8:1 hexanes:ethyl acetate to give product **5** (49.1 mg, 0.045 mmol, 92%). ^{1}H NMR (500 MHz, $CDCl_3$): δ 0.86 (t, 3H, *J*=6.8 Hz), 0.97 (m, 3H), 1.06-1.11 (m, 24H), 1.13-1.29 (m, 26H), 1.56 (m, 3H), 2.26 (m, 2H), 3.50 (app. q, 2H, *J*=9.7 Hz), 3.66 (m, 3H), 3.90 (dd, 1H, *J*=8.4, 4.3 Hz), 4.15 (m, 3H), 4.23 (t, 1H, *J*=8.6 Hz), 4.27 (m, 1H), 4.58 (d, 1H, *J*=12.3 Hz), 4.65 (d, 1H, *J*=12.3 Hz), 5.13 (d, 1H, *J*=4.22 Hz), 5.18 (d, 1H, *J*=3.6 Hz), 5.40 (s, 1H), 5.51 (s, 1H), 5.59 (t, 1H, *J*=9.7 Hz), 7.31 (m, 11H), 7.38 (m, 2H), 7.46 (m, 2H). ^{13}C NMR (125 MHz, $CDCl_3$): δ 11.6, 12.6, 12.8, 14.1, 16.9, 17.0, 17.1, 17.2, 17.3, 17.4, 22.7, 25.0, 29.0, 29.3, 29.4, 29.6, 29.7, 31.9, 34.4, 62.4, 68.9, 70.4, 72.6, 73.3, 75.4, 76.4, 76.7, 77.0, 77.2, 79.6, 81.3, 93.1, 94.7, 101.2, 101.5, 126.1, 126.2, 127.8, 127.9, 128.0, 128.5, 128.6, 128.8, 137.2, 137.4, 172.4. HRMS (FAB) calcd. for $C_{61}H_{92}NaO_{13}Si_2$ [M+Na$^+$]: 1111.5969; found: 1111.5949.

2-O-benzyl-4,6,4',6'-di-O-benzylidine-3-O-palmitoyl-α,α-D-trehalose (6). Compound **5** (49.1 mg, 0.045 mmol) was dissolved in THF (3 mL). Tetrabutylammonium fluoride (0.1 mL, 1 M in THF, 0.1 mmol) was added dropwise at rt. The reaction was run for 10

min and then the solvent was evaporated off. The crude material was purified via column chromatography in 3:1 hexanes:ethyl acetate to yield compound **6** (30.5 mg, 0.036 mmol, 80%). Longer reaction times led to decomposition. ^{1}H NMR (500 MHz, $CDCl_3$): δ 0.86 (t, 3H, *J*=6.8 Hz), 1.18-1.28 (m, 26H), 1.59 (m, 3H), 2.30 (t, 1H, *J*=7.5 Hz), 2.31 (t, 1H, *J*=7.5 Hz), 3.45 (t, 1H, *J*=9.4 Hz), 3.54 (t, 1H, *J*=9.7 Hz), 3.65 (m, 4H), 4.07 (m, 3H), 4.13 (m, 1H), 4.29 (dd, 1H, *J*=10.2, 5.0 Hz), 4.63 (d, 1H, *J*=12.0 Hz), 4.66 (d, 1H, *J*=12.0 Hz), 5.16 (d, 1H, *J*=3.9 Hz), 5.20 (d, 1H, *J*=3.7 Hz), 5.45 (s, 1H), 5.46 (s, 1H), 5.59 (t, 1H, *J*=9.7 Hz), 7.33 (m, 11H), 7.42 (m, 4H). ^{13}C NMR (125 MHz, $CDCl_3$): δ 14.1, 22.7, 25.1, 29.0, 29.3, 29.6, 29.7, 31.9, 34.4, 63.0, 63.1, 68.8, 70.5, 71.0, 72.4, 73.1, 76.7, 77.0, 77.2, 79.5, 81.0, 93.7, 95.2, 101.3, 102.0, 126.0, 126.5, 127.7, 128.0, 128.1, 128.2, 128.6, 128.9, 129.2, 136.9, 137.0, 137.2, 172.7. HRMS (FAB) calcd. for $C_{49}H_{66}NaO_{12}$ [M+Na^+]: 869.4446; found: 869.4424.

3-O-palmitoyl-α,α-D-trehalose (7). Compound **6** (30.5 mg, 0.036 mmol) was dissolved in ethanol (EtOH) (4 mL) at rt. 10% palladium on charcoal (10 mg) was added under N_2. The mixture was stirred under a H_2 balloon overnight. The catalyst was removed by filtration, and the solvent was evaporated off. The residue was redissolved in 1:1 MeOH:EtOH. 10% palladium on charcoal (10 mg) was added, and the mixture was stirred under H_2 overnight. The catalyst was removed by filtration despite an incomplete reaction, and the solvent was evaporated off. The crude material was purified via column chromatography in 10:1 chloroform:MeOH to afford compound **7** (2.38 mg, 0.0041 mmol, 11%). ^{1}H NMR (500 MHz, 3:1 CD_3OD:$CDCl_3$): δ 0.83 (app. t, 3H, *J*=13.0 Hz), 1.15-1.31 (m, 26 H), 1.60 (m, 2H), 2.34 (app. t, 2H, *J*=7.5 Hz), 3.42 (m, 2H), 3.57 (dd, 1H, *J*=10.0, 3.8 Hz), 3.62 (m, 2H), 3.74 (m, 3H), 3.80 (m, 2H), 5.08 (d, 1H, *J*=3.6 Hz), 5.09 (d, 1H, *J*=3.7 Hz), 5.23 (app. t, 1H, *J*=10.9 Hz). ^{13}C NMR (125 MHz, 3:1 CD_3OD:$CDCl_3$): δ 13.2, 22.3, 24.7, 28.8, 29.1, 29.2, 29.3, 29.4, 31.7, 34.0, 60.9, 61.3, 68.4, 70.1, 70.6, 71.8, 72.2, 72.4, 73.0, 75.0, 93.4, 93.5, 174.3. HRMS (FAB) calcd. for $C_{28}H_{52}NaO_{12}$ [M+Na^+]: 603.3351; found: 603.3348.

Electrospray ionization Fourier transform ion cyclotron resonance mass spectrometry

Mass spectra were obtained on an Apex II FT-ICR mass spectrometer equipped with a 7 T actively-shielded superconducting magnet (Bruker Daltonics, Billerica, MA). Ions were introduced into the ion source via direct injection at a rate of 1 μL/min. Ions were generated with an Apollo pneumatically-assisted electrospray ionization source (Analytica, Branford, CT) operating in the negative ion mode and were accumulated in an rf-only external hexapole for 0.5-2 s before being transferred to the ion cyclotron resonance cell for mass analysis. Mass spectra consist of 512k data points and are an average of between 28-128 scans. The spectra were acquired using XMASS version 6.0.0 or 7.0.8 (Bruker Daltonics). All spectra were internally calibrated with at least four known compounds.

Electrospray ionization linear-ion trap mass spectrometry

Additional mass spectra were obtained on an LTQ ion trap mass spectrometer equipped with an ESI source (ThermoFinnigan) operating in either the negative or positive ion mode. Ions were introduced into the ion source via direct injection at a rate of 5 μL/min. For linear-ion trap tandem mass spectrometry (MS^n) experiments, the precursor ions were isolated with an isolation width of 1-3 Da, the ions were activated with a 13-20% normalized collision energy for 100 ms, and the q_z value was maintained at 0.250. Spectra are an average of 100 scans, acquired using Xcalibur, version 1.4 (ThermoFinnigan).

Preparation of protein expression vector

The *papA3* gene (*Rv1182*, encoding residues 2-472) was amplified from *Mtb* H37Rv genomic DNA with the primers 5'-TACTGTAGTC**GAATTC**TTGCGGGTTGGACCGTTGAC-3' (EcoRI) and 5'-GATTACAGGT**CTGCAG**TCAGGCAACATTCTGCTGCT-3' (PstI). *Rv1182* was ligated into a modified pMAL-C2X vector (New England Biolabs) encoding an N-terminal His_7-tag and TEV cleavage site. The TEV cleavage site was introduced by site directed mutagenesis using the QuikChange PCR mutagenesis kit (Stratagene), and the His_7-tag was annealed to the 5' end of the maltose-binding protein (MBP)-coding region. DNA sequencing was performed to confirm the successful construction of the protein-encoding plasmid.

Protein expression and purification

E. coli BL21(DE3) cells were transformed with the protein expression plasmid. Transformants were used to inoculate 1 L cultures of LB medium containing 100 mg/L ampicillin and 2 g/L glucose. The cultures were incubated at 37 ºC for approximately 2.5 h with shaking until an OD_{600} of 0.6-0.8 was attained. Protein expression was induced by the addition of IPTG to a final concentration of 100 μM. After 18-20 h at 18 ºC, cells from each liter of culture were harvested and suspended in 30 mL of lysis buffer (20 mM Tris, pH 7.4, 200 mM NaCl, 1 mM EDTA, 1 mM DTT, 1 mM TCEP) supplemented with 5 μg/mL lysozyme and 5 μg/mL DNase. Cells were lysed using a high-pressure homogenizer (Avestin EmulsiFlex-C5). The lysate was cleared by centrifugation and applied to amylose resin (New England Biolabs) equilibrated with lysis buffer. After washing the resin with additional lysis buffer, MBP-PapA3 was eluted in lysis buffer containing 10 mM maltose. The eluted protein was diluted approximately 1:15 in low salt buffer (50 mM Tris, pH 7.4, 1 mM DTT, 1 mM TCEP, 10% glycerol) and loaded onto a MonoQ HR 5/5 column (GE Healthcare Biosciences Corp.) equilibrated with the same buffer. The protein was purified using a gradient of 1.5-100% high salt buffer (50 mM Tris, pH 7.4, 1 M NaCl, 1 mM DTT, 1 mM TCEP, 10% glycerol) over 40 min at a constant temperature of 4 ºC. Fractions (0.5 mL each) were analyzed by SDS-PAGE, and those containing pure protein were pooled and analyzed by the Bradford protein assay to determine protein concentration. MBP was cleaved from PapA3 using AcTEV protease

(Invitrogen) and removed using Ni-NTA resin (Qiagen), which bound the His-tagged MBP and protease while leaving the desired protein in solution. PapA3 was subsequently concentrated and stored at -80 ºC.

To confirm the protein's identity, the purified sample was desalted on a microbore reversed-phase column (Bruker Agilent) and characterized using a Bruker Hewlett-Packard ESI-Ion Trap mass spectrometer. Tryptic digestion and mass fingerprinting using a LTQ mass spectrometer provided further confirmation of the protein's identity. Protein concentration was determined by UV absorption at 280 nm using a calculated extinction coefficient of 57,340 M^{-1} cm^{-1}.

Biochemical characterization of PapA3

A previously described TLC-based assay (*5*) was used to characterize the acyltransferase activity of PapA3. Briefly, PapA3 (2 μM) was incubated with 20 μM ^{14}C-PCoA and 1 mM of the desired sugar substrate in reaction buffer (100 mM ammonium bicarbonate, pH 7.2) for 2 h at rt. Alternate ^{14}C-labeled acyl donors were screened at a concentration of 20 μM. The reactions were quenched by the addition of an equal volume of ethanol and subsequently analyzed by TLC (35:65 methanol:chloroform) and phosphorimaging. Stocks of each sugar substrate were prepared in water with the exception of T2P and T3P, which were dissolved in dimethyl sulfoxide (DMSO). The amount of DMSO in any given reaction did not exceed 5% of the reaction volume.

Mass spectrometry characterization of reaction products

PapA3 (1 μM) was incubated with 20 μM unlabeled PCoA and 1 mM trehalose or T2P in reaction buffer for 6 h at rt. Control reactions without enzyme were also prepared. Samples were lyophilized and stored at -20 ºC prior to analysis by ESI-FT-ICR and linear ion-trap MS.

Construction of M. tuberculosis *mutants*

Mtb cells (Erdman strain) were cultured in 7H9 medium supplemented with 10% OADC, 0.5% glycerol, and 0.05% Tween-80, or on 7H10 solid agar medium supplemented with 10% OADC and 0.5% glycerol. Hygromycin (50 μg/mL) or kanamycin (25 μg/mL) was used when necessary. The Δ*papA3* mutant strain was created by homologous recombination as previously described (*25*). Briefly, specialized transduction phage phMWS120 was incubated with concentrated wild-type Erdman *Mtb* cells for 4 h at 39 ºC. Cells were then plated on 7H10 plates containing hygromycin. Colonies were picked and screened for the deletion by PCR. The resulting deletion replaced 1136 bp of *papA3* (amino acids 45-423) with a hygromycin resistance cassette. The Δ*papA3*::*papA3* complementation strain was created by cloning the *papA3* gene from *Mtb* (Erdman strain) into the mycobacterial expression vector pMV261 (*26*) under the control of the *groEL* promoter, resulting in the complementation plasmid pMWS149. This plasmid was electroporated into the Δ*papA3* strain and transformants were selected on kanamycin-containing plates. The Δ*stf0* mutant was created by homologous

recombination using transduction phage phMWS102 as described above. The resulting deletion replaced 600 bp of *stf0* (amino acids 22-222) with a hygromycin resistance cassette.

Preparation of M. tuberculosis *lipid extracts*

Mtb cultures were synchronized and grown in 7H9 media to OD_{600} = 0.6. Cultures (50 mL) were transitioned to Tween-80-free 7H9 media and grown at 37 °C for 1 d. Surface lipids were extracted with hexane (1 mL) as described previously (*27*). The remaining cell pellets were extracted with 4 mL of chloroform:methanol (2:1).

Sample preparation for mass spectrometry

PapA3 reaction product samples were resuspended in 1 mL of 100% methanol (MeOH) for ESI-FT-ICR MS analysis. For linear-ion trap MS analysis of PapA3 reaction product samples, 500 μL of the resuspended volume were concentrated to dryness and resuspended in 3 mL of chloroform ($CHCl_3$):isopropyl alcohol (IPA) (2:1). *Mtb* cell surface extracts were concentrated to dryness under nitrogen and resuspended in 3 mL of $CHCl_3$:IPA (2:1).

Lipids in each sample were separated using a modification of the method of Kaluzny *et al*. (*28*). Samples were passed over a solid-phase extraction column (Sep-Pak Vac, NH_2 resin, Waters) that had been pre-charged with 3 mL of 0.1 M ammonium acetate in MeOH. The column was eluted using 3 mL of each of the following solvents: 1) $CHCl_3$:IPA (2:1), 2) diethyl ether:acetic acid (98:2), 3) 100% MeOH, and 4) 0.1 M ammonium acetate in MeOH. Column fractions from the PapA3 reaction product samples were concentrated to dryness and resuspended in 1 mL of $CHCl_3$:MeOH (2:1). Acyltrehaloses eluted in solvent 3. For linear-ion trap MS^n experiments, lithium acetate was added to the PapA3 reaction products and the T2P and T3P standards to a final concentration of 1 mM. Column fractions from *Mtb* cell surface extracts were concentrated to dryness under nitrogen and resuspended in either 200 μL $CHCl_3$:MeOH (2:1) (fractions from solvents 1 and 2) or 400 μL $CHCl_3$:MeOH (2:1) (fractions from solvents 3 and 4) for mass spectrometry analysis. PAT eluted in solvent 1, and SL-1 eluted in solvent 4.

References

1. Brennan, P. J., and Nikaido, H. (1995) The envelope of mycobacteria, *Annu. Rev. Biochem. 64*, 29-63.

2. Minnikin, D. E., Kremer, L., Dover, L. G., and Besra, G. S. (2002) The methyl-branched fortifications of *Mycobacterium tuberculosis*, *Chem. Biol. 9*, 545-553.

3. Takayama, K., Wang, C., and Besra, G. S. (2005) Pathway to synthesis and processing of mycolic acids in *Mycobacterium tuberculosis*, *Clin. Microbiol. Rev. 18*, 81-101.

4. Ferreras, J. A., Stirrett, K. L., Lu, X., Ryu, J. S., Soll, C. E., Tan, D. S., and Quadri, L. E. (2008) Mycobacterial phenolic glycolipid virulence factor biosynthesis: mechanism and small-molecule inhibition of polyketide chain initiation, *Chem. Biol. 15*, 51-61.

5. Kumar, P., Schelle, M. W., Jain, M., Lin, F. L., Petzold, C. J., Leavell, M. D., Leary, J. A., Cox, J. S., and Bertozzi, C. R. (2007) PapA1 and PapA2 are acyltransferases essential for the biosynthesis of the *Mycobacterium tuberculosis* virulence factor Sulfolipid-1, *Proc. Natl. Acad. Sci. U. S. A. 104*, 11221-11226.

6. Rousseau, C., Neyrolles, O., Bordat, Y., Giroux, S., Sirakova, T. D., Prevost, M. C., Kolattukudy, P. E., Gicquel, B., and Jackson, M. (2003) Deficiency in mycolipenate- and mycosanoate-derived acyltrehaloses enhances early interactions of *Mycobacterium tuberculosis* with host cells, *Cell. Microbiol. 5*, 405-415.

7. Dubey, V. S., Sirakova, T. D., and Kolattukudy, P. E. (2002) Disruption of *msl3* abolishes the synthesis of mycolipanoic and mycolipenic acids required for polyacyltrehalose synthesis in *Mycobacterium tuberculosis* H37Rv and causes cell aggregation, *Mol. Microbiol. 45*, 1451-1459.

8. Daffe, M., Lacave, C., Laneelle, M. A., Gillois, M., and Laneelle, G. (1988) Polyphthienoyl trehalose, glycolipids specific for virulent strains of the tubercle bacillus, *Eur. J. Biochem. 172*, 579-584.

9. Schelle, M. W., and Bertozzi, C. R. (2006) Sulfate metabolism in mycobacteria, *Chembiochem 7*, 1516-1524.

10. Bhatt, K., Gurcha, S. S., Bhatt, A., Besra, G. S., and Jacobs, W. R., Jr. (2007) Two polyketide-synthase-associated acyltransferases are required for sulfolipid biosynthesis in *Mycobacterium tuberculosis*, *Microbiology 153*, 513-520.

11. Onwueme, K. C., Ferreras, J. A., Buglino, J., Lima, C. D., and Quadri, L. E. (2004) Mycobacterial polyketide-associated proteins are acyltransferases: proof of principle with *Mycobacterium tuberculosis* PapA5, *Proc. Natl. Acad. Sci. U. S. A. 101*, 4608-4613.

12. Domenech, P., Reed, M. B., and Barry, C. E., 3rd. (2005) Contribution of the *Mycobacterium tuberculosis* MmpL protein family to virulence and drug resistance, *Infect. Immun. 73*, 3492-3501.

13. Domenech, P., Reed, M. B., Dowd, C. S., Manca, C., Kaplan, G., and Barry, C. E., 3rd. (2004) The role of MmpL8 in sulfatide biogenesis and virulence of *Mycobacterium tuberculosis*, *J. Biol. Chem. 279*, 21257-21265.

14. Wallace, P. A., and Minnikin, D. E. (1994) Synthesis of 4,6:2',3':4',6'-tri-O-cyclohexylidene-alpha,alpha'-trehalose 2-palmitate: an intermediate for the synthesis of mycobacterial 2,3-di-O-acyl-alpha,alpha'-trehalose antigens, *Carbohydr. Res. 263*, 43-59.

15. Wallace, P. A., Minnikin, D. E., and Ridell, M. (1994) Synthesis and structure of 2,3-di-*O*-acyl-α,α-trehalose lipid antigens from *Mycobacterium fortuitum*, *J. Chem. Soc., Chem.Commun.*, 329-330.

16. Wang, C. C., Lee, J. C., Luo, S. Y., Fan, H. F., Pai, C. L., Yang, W. C., Lu, L. D., and Hung, S. C. (2002) Synthesis of biologically potent alpha1-->2-linked disaccharide derivatives via regioselective one-pot protection-glycosylation, *Angew. Chem. Int. Ed. Engl. 41*, 2360-2362.

17. Cole, S. T., Brosch, R., Parkhill, J., Garnier, T., Churcher, C., Harris, D., Gordon, S. V., Eiglmeier, K., Gas, S., Barry, C. E., 3rd, Tekaia, F., Badcock, K., Basham, D., Brown, D., Chillingworth, T., Connor, R., Davies, R., Devlin, K., Feltwell, T., Gentles, S., Hamlin, N., Holroyd, S., Hornsby, T., Jagels, K., Krogh, A., McLean, J., Moule, S., Murphy, L., Oliver, K., Osborne, J., Quail, M. A., Rajandream, M. A., Rogers, J., Rutter, S., Seeger, K., Skelton, J., Squares, R., Squares, S., Sulston, J. E., Taylor, K., Whitehead, S., and Barrell, B. G. (1998) Deciphering the biology of *Mycobacterium tuberculosis* from the complete genome sequence, *Nature 393*, 537-544.

18. Mougous, J. D., Petzold, C. J., Senaratne, R. H., Lee, D. H., Akey, D. L., Lin, F. L., Munchel, S. E., Pratt, M. R., Riley, L. W., Leary, J. A., Berger, J. M., and Bertozzi, C. R. (2004) Identification, function and structure of the mycobacterial sulfotransferase that initiates Sulfolipid-1 biosynthesis, *Nat. Struct. Mol. Biol. 11*, 721-729.

19. Jain, M., and Cox, J. S. (2005) Interaction between polyketide synthase and transporter suggests coupled synthesis and export of virulence lipid in *M. tuberculosis*, *PLoS Pathog. 1*, e2.

20. Six, D. A., Carty, S. M., Guan, Z., and Raetz, C. R. (2008) Purification and mutagenesis of LpxL, the lauroyltransferase of *Escherichia coli* lipid A biosynthesis, *Biochemistry 47*, 8623-8637.

21. Rohde, K. H., Abramovitch, R. B., and Russell, D. G. (2007) *Mycobacterium tuberculosis* invasion of macrophages: linking bacterial gene expression to environmental cues, *Cell Host Microbe 2*, 352-364.

22. Hampshire, T., Soneji, S., Bacon, J., James, B. W., Hinds, J., Laing, K., Stabler, R. A., Marsh, P. D., and Butcher, P. D. (2004) Stationary phase gene expression of *Mycobacterium tuberculosis* following a progressive nutrient depletion: a model for persistent organisms?, *Tuberculosis 84*, 228-238.

23. Chesne-Seck, M. L., Barilone, N., Boudou, F., Gonzalo Asensio, J., Kolattukudy, P. E., Martin, C., Cole, S. T., Gicquel, B., Gopaul, D. N., and Jackson, M. (2008) A point mutation in the two-component regulator PhoP-PhoR accounts for the absence of polyketide-derived acyltrehaloses but not that of phthiocerol dimycocerosates in *Mycobacterium tuberculosis* H37Ra, *J. Bacteriol. 190*, 1329-1334.

24. Langston, S., Bernet, B., and Vasella, A. (1994) Temporary protection and activation in the regioselective synthesis of saccharide sulfates, *Helv. Chim. Acta 77*, 2341-2353.

25. Glickman, M. S., Cox, J. S., and Jacobs, W. R., Jr. (2000) A novel mycolic acid cyclopropane synthetase is required for cording, persistence, and virulence of *Mycobacterium tuberculosis*, *Mol. Cell 5*, 717-727.

26. Stover, C. K., de la Cruz, V. F., Fuerst, T. R., Burlein, J. E., Benson, L. A., Bennett, L. T., Bansal, G. P., Young, J. F., Lee, M. H., Hatfull, G. F., *et al.* (1991) New use of BCG for recombinant vaccines, *Nature 351*, 456-460.

27. Converse, S. E., Mougous, J. D., Leavell, M. D., Leary, J. A., Bertozzi, C. R., and Cox, J. S. (2003) MmpL8 is required for sulfolipid-1 biosynthesis and Mycobacterium tuberculosis virulence, *Proc. Natl. Acad. Sci. U. S. A. 100*, 6121-6126.

28. Kaluzny, M. A., Duncan, L. A., Merritt, M. V., and Epps, D. E. (1985) Rapid separation of lipid classes in high yield and purity using bonded phase columns, *J. Lipid Res. 26*, 135-140.

Chapter 5: Discovery of a novel osmoregulatory pathway in *Mycobacterium tuberculosis*

Introduction

Bacterial pathogens must overcome a complex arsenal of environmental pressures in order to mount a successful infection. Acidification, oxidative stress, and nutrient depravation are just a few of the strategies employed by macrophages to destroy microbial invaders (*1, 2*). Bacteria must also cope with changes in environmental osmolarity, which may vary widely over the course of a pathogen's life cycle (*3*). For example, there is a ten-fold difference in the concentration of potassium, sodium, calcium, and chloride ions between the cytosol of mammalian cells and the surrounding extracellular space (*4*). Bacteria typically respond to such fluctuations through the compensatory accumulation or expulsion of compatible solutes that restores osmotic balance to the cell (*5*). These osmoregulatory mechanisms are often triggered at the transcriptional level by osmotic stress and are in many cases associated with bacterial virulence (*3, 6, 7*).

Mycobacterium tuberculosis (*Mtb*), the intracellular pathogen that causes tuberculosis, is notoriously adept at surmounting conditions of environmental stress and establishing long-term residence in the host (*8*). Though its osmoregulatory pathways are poorly defined, *Mtb* undoubtedly confronts numerous osmotic challenges during the course of infection. Indeed, a recent study indicates that the pathogen encounters osmotic stress upon phagocytosis (*7*). Moreover, *Mtb* is subject to the diverse environmental demands of airborne droplet nuclei, the mucosal epithelia of the lung, phagosomes, necrotic cells, and caseous granulomas. This necessitates facile adaptation to changes in external osmolarity via signal transduction pathways.

Two types of regulatory networks typically mediate the bacterial response to environmental stress: two-component systems and alternative sigma factors (also known as extracytoplasmic function (ECF) sigma factors) (*9-11*). Two-component systems consist of a membrane-associated sensor histidine kinase and cognate response regulator protein (*10*). The sensor kinase responds to an external stimulus by phosphorylating the response regulator, which subsequently alters gene expression. Alternative sigma factors regulate transcription by binding RNA polymerase and recruiting it to specific promoters (*11*). This activity is tightly controlled by anti-sigma factors, which bind cognate sigma factors and prevent their association with RNA polymerase. A third group of proteins, the anti-anti-sigma factors, facilitate dissociation of this inhibitory complex by binding the anti-sigma factor (*12, 13*). The anti-sigma factor can, in turn, phosphorylate the anti-anti-sigma factor on a conserved serine or threonine residue, liberating itself for another round of protein-protein interactions.

In addition to two-component systems and alternative sigma factors, *Mtb* encodes a third class of proteins involved in modulating the bacterial response to external stimuli: the eukaryotic-like receptor serine/threonine protein kinases (STPKs) (*14, 15*). STPKs regulate a variety of cellular functions, such as cell wall biosynthesis and cell division, via phosphorylation. Recent studies also support a role for these enzymes in the regulation of alternative sigma factors (*16-18*). However, the precise environmental signals that govern STPK activity are largely unknown.

Thus far, two regulatory networks from *Mtb* have been indirectly implicated in the response to osmotic stress. The KdpD/KdpE two-component system, by analogy to the homologous system from *Escherichia coli*, is believed to modulate intracellular potassium concentration in response to changes in environmental osmolarity (*4*). Consistent with this hypothesis, Steyn *et al.* have demonstrated that the *kdpFABC* operon, which is transcriptionally regulated by KdpD/KdpE in *E. coli*, is highly induced at low potassium concentration in *Mtb*. A second two-component system, MtrA/MtrB, is involved in the transcriptional regulation of osmoprotective genes from *Corynebacterium glutamicum*, a gram-positive soil bacterium closely related to *Mtb* (*19*). Thus far, no alternative sigma factors or STPKs have been ascribed osmoregulatory functions.

We sought to explore the mechanisms governing the adaptation of *Mtb* to changes in environmental osmolarity by profiling the global transcriptional response to osmotic stress. The most highly induced gene in our analysis, *Rv0516c*, encodes an anti-anti-sigma factor homolog previously shown to be phosphorylated by the STPK PknD *in vivo* (*16*). Remarkably, we discovered that PknD regulates expression of this protein in response to osmotic stress. Further, we discovered that deletion of *Rv0516c* from *Mtb* significantly improves recovery from osmotic shock. The *Rv0516c* mutant is also more resistant to vancomycin, suggesting that the encoded protein may mediate the response to osmotic stress by modifying the peptidoglyan architecture of the cell wall. We also found that *Rv0516c* deletion enhances the transcription of several osmotically regulated genes, supporting a role for the protein in modulating the transcriptional response to osmotic stress. One of these genes, *espA*, encodes a substrate of the virulence-associated ESX-1 secretion system that has recently been implicated in the maintenance of cell wall integrity (*20*). Interestingly, both PknD and Rv0516c were found to influence the expression and secretion of EspA. Taken together, these findings support the existence of a novel osmoregulatory network in *Mtb* that is mediated by PknD phosphorylation of Rv0516c and influences ESX-1 secretion.

Results

Osmotic stress elicits a significant transcriptional response from M. tuberculosis

We hypothesized that *Mtb* might adapt to changes in environmental osmolarity by modulating gene expression. To explore this possibility, we determined the global transcriptional profile of *Mtb* in response to osmotic stress. Microarray analysis was performed following 1-h exposure of *Mtb* to 140 mM sodium chloride, a sodium concentration typical of the phagosome (*21, 22*), the membrane-bound organelle formed upon macrophage engulfment. Over 100 significantly induced genes were identified in this analysis (Table 5-1), many of them coordinately regulated by the same promoter. Notably, the entire *arg* operon, which is required for the *de novo* biosynthesis of arginine (*23*), was induced by osmotic stress, as well as the *Rv3616c-Rv3614c* operon, which encodes components of the ESX-1 secretion system that are required for full *Mtb* virulence (*24-26*). Several genes involved in sulfur metabolism (e.g., *cysA3*, *csd*, and *sirA*) were also osmotically regulated, as well as an abundance of genes involved in ribosomal assembly. These findings imply that external osmolarity can activate a unique

transcriptional program in *Mtb* that may influence bacterial virulence and facilitate survival during the course of infection.

TABLE 5-1. Genes showing greatest upregulation in *M. tuberculosis* strain CDC1551 upon exposure to osmotic stress[a]

Gene number	Fold change	Gene name	Gene number	Fold change	Gene name	Gene number	Fold change	Gene name
Rv0516c	21.2		Rv2412	2.9	rpsT	Rv3810	2.4	pirG
MT1178	11.0		Rv0747	2.9	PE_PGRS10	Rv1980c	2.3	mpt64
Rv1653	7.0	argJ	Rv1642	2.9	rpmI	Rv0702	2.3	rplD
Rv3615c	6.5	espC	Rv2890c	2.9	rpsB	Rv0475	2.3	hbhA
Rv3118	5.3	sseC1	MT2420	2.9		Rv0227c	2.3	
Rv1654	5.1	argB	MT1448	2.9		MT2516	2.3	obg
Rv1655	4.9	argD	Rv3460c	2.8	rpsM	MT3693	2.3	
MT0066.2	4.8		Rv0263c	2.8		Rv1659	2.3	argH
Rv3613c	4.3		Rv1641	2.8	infC	Rv0709	2.3	rpmC
MT0066.1	4.0		Rv3418c	2.7	groES	Rv3443c	2.3	rplM
Rv1078	4.0	pra	Rv2271	2.7		Rv0440	2.3	groEL2
Rv3614c	3.9	espD	Rv3459c	2.7	rpsK	Rv2783c	2.2	gpsI
Rv2348c	3.8		Rv1466	2.7		Rv0716	2.2	rplE
Rv0683	3.8	rpsG	Rv0950c	2.7		Rv0761c	2.2	adhB
Rv0701	3.7	rplC	MT0835	2.7		Rv0055	2.2	rpsR1
Rv0703	3.6	rplW	Rv2441c	2.7	rpmA	Rv1657	2.2	argR
Rv0682	3.6	rpsL	Rv1886c	2.6	fbpB	MT3562	2.2	truA
Rv3616c	3.6	espA	MT2460	2.6		Rv0211	2.1	pckA
Rv3117	3.5	cysA3	Rv2301	2.6	cut2	Rv0009	2.1	ppiA
MT2422	3.4		MT3217	2.6		Rv1072	2.1	
Rv1464	3.3	csd	Rv1462	2.6		Rv0719	2.1	rplF
MT2421	3.3		Rv1643	2.6	rplT	Rv0352	2.1	dnaJ1
Rv3219	3.3	whiB1	MT2245	2.6		Rv0952	2.1	sucD
Rv3442c	3.2	rpsI	Rv3924c	2.5	rpmH	Rv1996	2.1	
Rv0652	3.1	rplL	Rv1652	2.5	argC	Rv1656	2.1	argF
Rv0700	3.1	rpsJ	Rv3131	2.5		Rv3029c	2.1	fixA
Rv1463	3.1		Rv3457c	2.4	rpoA	Rv0714	2.1	rplN
Rv3458c	3.0	rpsD	Rv0706	2.4	rplV	Rv0056	2.1	rplI
Rv0718	3.0	rpsH	Rv2391	2.4	sirA	Rv2889c	2.1	tsf
Rv2442c	3.0	rplU	Rv2190c	2.4		Rv3763	2.1	lpqH
Rv2050	3.0		Rv1297	2.4	rho	Rv3130c	2.1	tgs1
Rv0704	3.0	rplB	Rv0867c	2.4	rpfA	Rv2745c	2.1	
Rv0684	3.0	fusA1	Rv3028c	2.4	fixB	Rv0350	2.1	dnaK
Rv1658	3.0	argG	Rv0708	2.4	rplP	Rv0721	2.0	rpsE
Rv0717	3.0	rpsN1	Rv1908c	2.4	katG	Rv0676c	2.0	mmpL5
Rv0667	2.9	rpoB	Rv0479c	2.4		Rv0707	2.0	rpsC

[a]DNA microarray analysis was used to identify *Mtb* genes significantly induced following 1-h exposure to 140 mM NaCl. Arrays from four biological replicates were analyzed using the Significance Analysis of Microarrays (SAM) program from Stanford University. Genes having a mean $\log_2$ fold change of 1 or higher with a SAM-assigned q-value of zero were deemed significant. Gene annotations were obtained from TubercuList (http://tuberculist.epfl.ch/) and the JCVI Comprehensive Microbial Resource (http://cmr.jcvi.org/cgi-bin/CMR/CmrHomePage.cgi).

The anti-anti-sigma factor homolog Rv0516c is highly induced by osmotic stress

The most highly induced gene in our microarray analysis, *Rv0516c*, encodes a protein homologous to SpoIIAA, the canonical anti-anti-sigma factor that regulates sporulation in *Bacillus subtilis* (*16, 27*). Our findings are consistent with a previous study in which quantitative real-time PCR analysis revealed a 14.5-fold induction of *Rv0516c* following treatment with 400 mM NaCl for 1 h (*28*). To validate our microarray results

at the protein level, we constructed an *Rv0516c* expression construct encoding a C-terminal $(DDDDK)_3$ tag (*Rv0516c* Tn::*pRv0516c*). We observed a sharp increase in *Rv0516c* expression following exposure to 140 mM NaCl for 3 h (Figure 5-1A). Similar expression levels resulted from treatment with two other osmolytes, potassium chloride and sucrose, at equal osmolarity (140 mM and 280 mM, respectively). These findings confirm that osmotic stress induces Rv0516c expression *in vivo*.

We next investigated whether the *Rv0516c* promoter could be used to enhance the expression of a reporter gene in response to increasing osmolarity. We introduced a GFP expression plasmid under the control of the *Rv0516c* promoter into the CDC1551 strain of *Mtb* and quantified fluorescence following incubation with NaCl, KCl, or sucrose at equal osmolarity for a period of 2 days. In all cases, osmolyte addition increased GFP fluorescence by roughly the same amount relative to an untreated control (Figure 5-1B). While the amount of fluorescence produced by the control was somewhat surprising given the low level of Rv0516c expression observed in the absence of osmotic stress, this can most likely be attributed to the distinct post-transcriptional and post-translational mechanisms that regulate the expression of these two proteins. Overall, these findings suggest that the *Rv0516c* promoter is recognized by a transcriptional element from *Mtb* that is activated by osmotic stress.

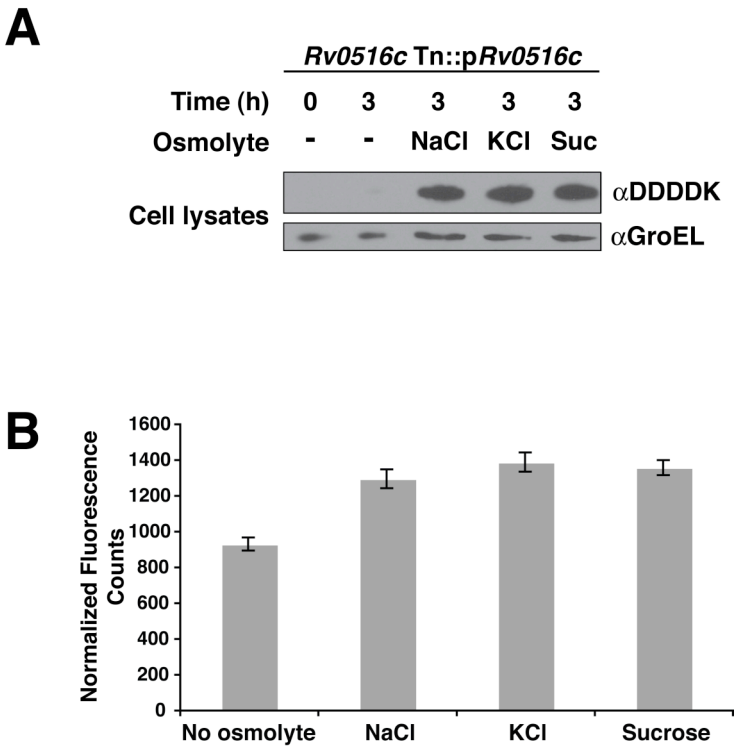

FIGURE 5-1. *Rv0516c* is induced by osmotic stress. (**A**) Western blot analysis of Rv0516c expression following *Mtb* exposure to NaCl, KCl, or sucrose (suc) applied at equal osmolarity. (**B**) Mean fluorescence intensity of *Mtb* expressing GFP under the control of the *Rv0516c* promoter following treatment with various osmolytes applied at

equal osmolarity. $P < 0.02$ for all conditions relative to control (no osmolyte) by two-tailed Student's *t* test.

Rv0516c *deletion enhances resistance to high osmolarity and vancomycin*

The homology between Rv0516c and SpoIIAA led us to consider a possible role for this protein in regulating the *Mtb* response to osmotic stress. To explore this possibility, we obtained an *Rv0516c* transposon mutant, *Rv0516c* Tn, and evaluated its growth kinetics following hyperosmotic shock with 0.5 M NaCl. Surprisingly, we discovered that the ability of *Rv0516c* Tn to withstand osmotic shock was far superior to that of wild-type *Mtb*, which exhibited an apparent decline in bacterial replication (Figure 5-2A). Notably, complementation of *Rv0516c* Tn under control of the native *Rv0516c* promoter restored the wild-type response to NaCl treatment. Both the wild-type and complemented strains tended to aggregate following approximately 1-2 days of NaCl exposure, a phenotype observed previously in other bacteria in response to osmotic stress (*29-31*). In contrast, the mutant strain remained relatively well suspended in the culture medium. In light of this observation, we were unable to distinguish whether the apparent decline in the growth kinetics of the wild-type and complemented strains was the result of reduced bacterial replication or clumping.

We subsequently considered whether *Rv0516c* Tn might also be more resistant to other types of cell wall stress. To this end, we determined the minimal inhibitory concentrations (MICs) of isoniazid, sodium dodecyl sulfate (SDS), NaCl, D-cycloserine, and vancomycin for the mutant, wild-type, and complemented (*Rv0516c* Tn::p*Rv0516c*) strains (Figure 5-2B). The sole variation in these MICs was observed with vancomycin, whose MIC for *Rv0516c* Tn was four-fold higher than those for the other two strains. To provide further confirmation of this phenotype, we enumerated the colony-forming units (CFUs) of each strain following treatment with 1.5 μg/mL vancomycin for four days (Figure 5-2C). The CFUs/mL produced by *Rv0516c* Tn exceeded that of the wild-type strain by approximately three orders of magnitude. A similar difference was observed between the mutant and complemented strains. These data suggest *Rv0516c* may somehow suppress bacterial resistance to osmotic stress, perhaps by affecting peptidoglycan (PGN) biosynthesis. However, D-cycloserine, which inhibits PGN biosynthesis by preventing the racemization of L-alanine (*32*), was equally effective at inhibiting growth of the wild-type and mutant strains. This may imply that *Rv0516c* affects one of the later stages of PGN assembly, which are inhibited by vancomycin (*33*).

A

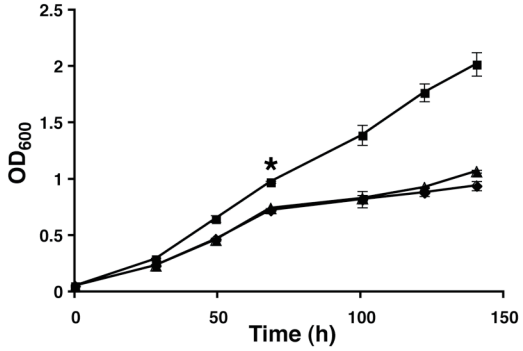

B

Strain	Minimal Inhibitory Concentration (MIC)[a] Isoniazid (μg/mL)	SDS (%, v/v)	NaCl (M)	D-cycloserine (μg/mL)	Vancomycin (μg/mL)
Wild-type CDC1551	0.0313	0.01	1	3.9	0.78
Rv0516c Tn	0.0313	0.01	1	3.9	3.13
Rv0516c Tn::p*Rv0516c*	0.016	0.01	1	3.9	0.78

[a]MIC values represent the lowest concentration of drug that visibly inhibited growth of the indicated strain after 1 or 2 weeks. These values were consistent among 3 biological replicates.

C

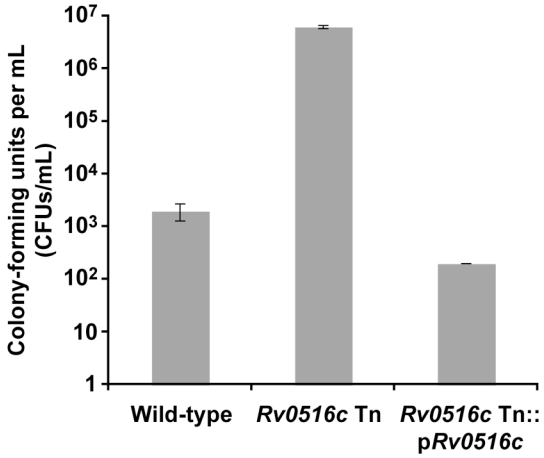

FIGURE 5-2. *Rv0516c* enhances sensitivity to osmotic stress and vancomycin. (**A**) Disruption of *Rv0516c* (■) significantly decreases the growth attenuation observed in wild-type (●) and complemented (▲) *Mtb* strains following treatment with 0.5 M NaCl (*). (**B**) Minimal inhibitory concentrations of various cell wall-perturbing agents. (**C**) Wild-type, *Rv0516c* Tn, and complemented strains were grown in medium containing 1.5 μg/mL vancomycin for three days, serially diluted, and plated for the enumeration of colony-forming units. These results represent the average of two biological replicates.

PknD phosphorylation regulates Rv0516c expression under osmotic stress

SpoIIAA regulates sporulation in *B. subtilis* by sequestering the anti-sigma factor SpoIIAB from the alternative sigma factor σ^F, an association that is abolished by phosphorylation of SpoIIAA (*27*). Previous work by Greenstein *et al.* established that the membrane-associated PknD STPK phosphorylates Rv0516c at Thr2 *in vivo*, and that

increasing PknD activity enhances *Rv0516c* transcription (*16*). Given the high degree of predicted structural homology between Rv0516c and SpoIIAA (Figure 5-3A), we hypothesized that phosphorylation of Rv0516c might also affect its biological activity.

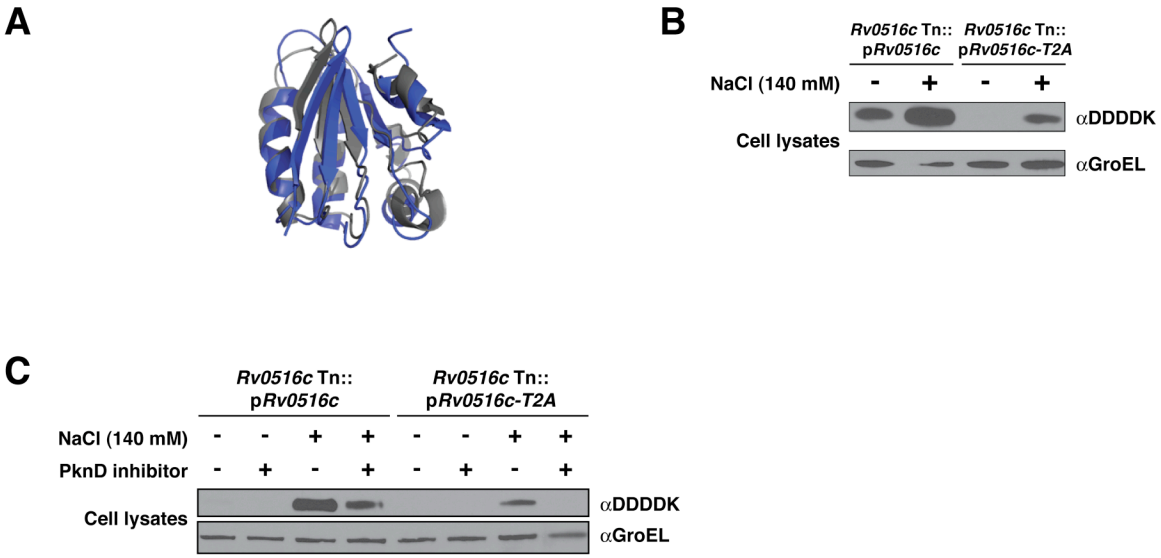

FIGURE 5-3. Rv0516c is an anti-anti-sigma factor homolog whose expression under osmotic stress is mediated by PknD phosphorylation. (**A**) The predicted fold of Rv0516c (gray) is similar to that of a well-characterized anti-anti-sigma factor from *Bacillus subtilis* (blue). (**B**) Phosphorylation of Rv0516c at Thr2 regulates its expression. (**C**) Inhibition of PknD decreases Rv0516c expression under osmotic stress and abrogates expression of the phosphorylation-deficient T2A mutant.

We therefore introduced a phosphorylation-deficient (T2A) copy of *Rv0516c* under the control of the gene's native promoter into *Rv0516c* Tn (*Rv0516c* Tn::p*Rv0516c-T2A*) and evaluated its response to increasing osmolarity. We discovered that phosphorylation at this site enhances Rv0516c expression (Figure 5-3B), which is consistent with the finding by Greenstein *et al*. that overexpression of PknD induces *Rv0516c* (*16*). Notably, we also found that in the absence of Thr2 phosphorylation, the amount of Rv0516c protein produced in the presence of osmolyte is less than that generated by cells expressing wild-type Rv0516c. Though this finding suggests that phosphorylation is required for full induction of *Rv0516c* by osmotic stress, we cannot rule out the possibility that the T2A mutation compromises protein stability, which could result in a global reduction of Rv0516c protein levels.

We next sought to establish a link between PknD activity and *Rv0516c* induction by osmotic stress. To this end, we used a PknD inhibitor to specifically evaluate the role of PknD phosphorylation on Rv0516c expression in the presence of osmolyte. We found that PknD inhibition was accompanied by a modest decrease in the induction of wild-type *Rv0516c* in response to osmotic stress (Figure 5-3C). In contrast, inhibition of PknD completely abrogated expression of the T2A mutant under these conditions. Taken together, these findings suggest that PknD regulates the induction of *Rv0516c* by osmotic

stress both through direct phosphorylation of the encoded protein and by phosphorylating at least one other protein required for this response. Previous studies suggest that Rv0516c can also be phosphorylated by the PknE and PknB STPKs *in vitro*, which may explain why PknD inhibition does not result in a complete loss of wild-type *Rv0516c* expression. However, the lack of expression observed in the T2A mutant strain in the presence of PknD inhibitor implies that the remaining PknD substrate(s) involved in this pathway are exclusively phosphorylated by PknD. Again, we cannot rule out the possibility that the Thr2 mutation is deleterious to the stability of Rv0516c, which could also account for the observed decline in expression of the mutant protein.

Rv0516c influences the transcriptional response to osmotic stress

To determine whether the effects of *Rv0516c* on the recovery of *Mtb* from osmotic shock might be mediated by transcriptional events, we compared the transcriptional response of *Rv0516c* Tn to wild-type *Mtb* following treatment with 140 mM NaCl. Surprisingly, the overall expression profiles of these two strains were similar, though more genes were upregulated in the mutant strain (data not shown). Further analysis revealed that a subset of osmotically regulated genes was significantly more induced by osmotic stress in the mutant strain (Figure 5-4). Notably, these genes were among those most highly induced by NaCl treatment in the wild-type strain, and included all of the genes from the *arg* and *Rv3616c* operons of *Mtb*. These findings suggest that *Rv0516c* deletion enhances the transcriptional response of *Mtb* to osmotic stress, and that these changes may partially account for the improved tolerance of *Rv0516c* Tn to conditions of high osmolarity.

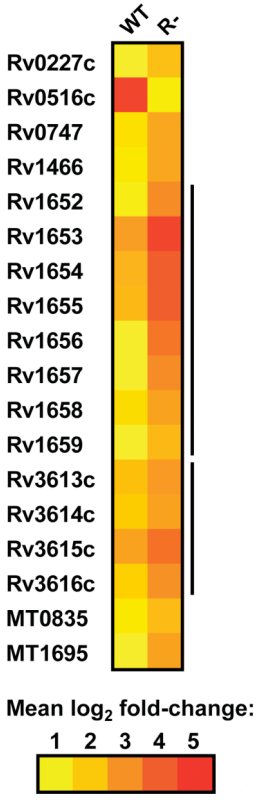

FIGURE 5-4. *Rv0516c* deletion enhances transcription of some of the most highly induced genes in the osmotic stress regulon of *M. tuberculosis*. Genes induced following 1-h treatment with 140 mM NaCl in both wild-type (WT) and *Rv0516c* Tn (R-) strains are color-coded by their respective mean $\log_2$ fold-change values. The genes shown here are those for which the fold-change ratio of R- to WT was ≥ 1.7, with the exception of *Rv0516c*, the only gene for which the ratio of WT to R- was ≥ 1.7.

Expression of the virulence factor EspA is induced by osmotic stress

The finding that the *Rv3616c-Rv3614c* operon, which plays a significant role in *Mtb* virulence (*24-26*), was highly induced by osmotic stress prompted us to explore the relationship between *Rv3616c*, which encodes the EspA protein, and osmolarity in more detail. We evaluated EspA levels in wild-type cell lysates and observed a marked increase in EspA expression following treatment with 140 mM NaCl by Western blot analysis (Figure 5-5A). Interestingly, the expression of ESAT-6, another substrate of the ESX-1 secretion system, was unaffected by osmotic stress. This phenotype was also manifest upon exposure of *Mtb* to other osmolytes (data not shown), providing further validation that osmotic stress specifically regulates EspA expression.

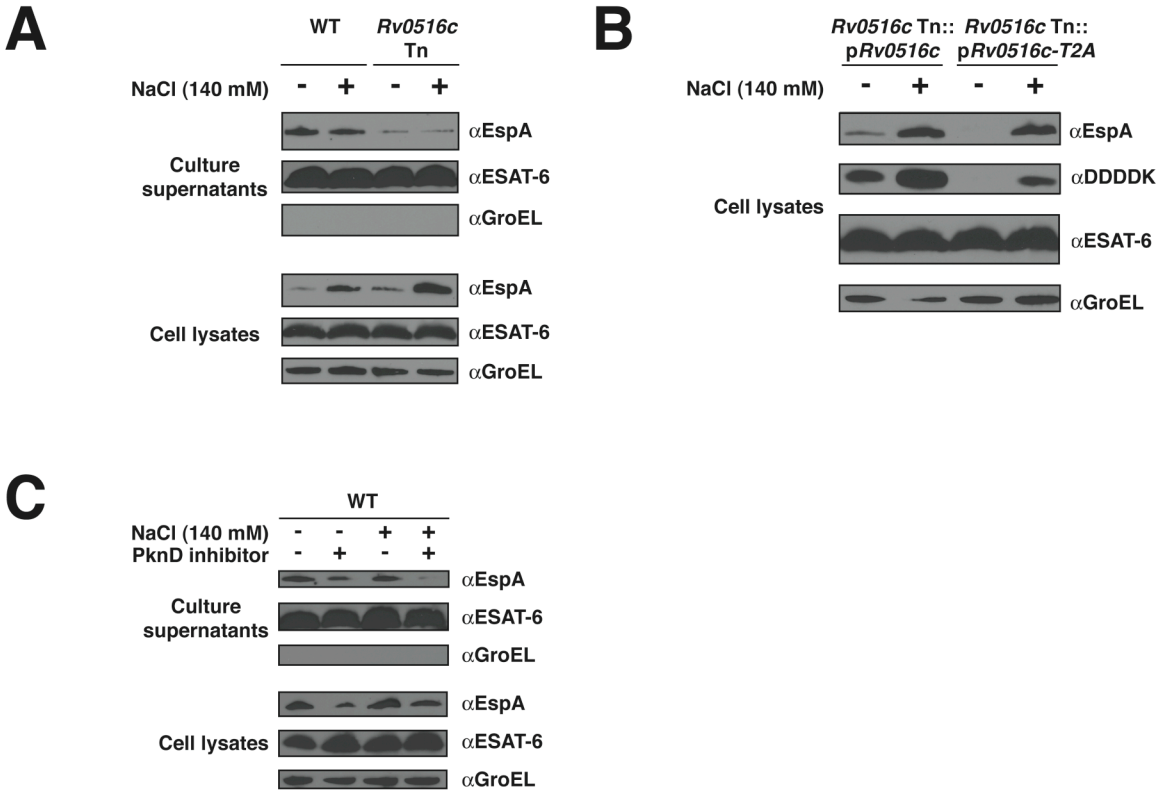

FIGURE 5-5. Osmotic stress, Rv0516c, and PknD regulate expression of the virulence factor EspA. (**A**) EspA expression is induced by osmotic stress, and its secretion is decreased by disruption of *Rv0516c*. (**B**) Phosphorylation of Rv0516c affects EspA expression. (**C**) Inhibition of PknD decreases expression and secretion of EspA.

Rv0516c and PknD regulate EspA expression and secretion

Because our microarray analysis revealed that Rv0516c affects the response of the *Rv3616c-Rv3614c* operon to osmotic stress, we hypothesized that Rv0516c, or perhaps PknD, might influence the expression or secretion of EspA. To investigate this possibility, we compared EspA expression and secretion in *Rv0516c* Tn to that of wild-

type *Mtb* in the presence or absence of osmotic stress by Western blot analysis. We discovered that while EspA was still induced by NaCl treatment in *Rv0516c* Tn, its secretion was substantially diminished (Figure 5-5A). Remarkably, this phenotype was independent of culture osmolarity and specific to EspA, as no change in ESAT-6 secretion was observed in the mutant strain. Further, loss of Rv0516c phosphorylation at Thr2 was accompanied by a sharp decrease in EspA expression (Figure 5-5B), while ESAT-6 levels remained unaffected.

The apparent link between Rv0516c phosphorylation and EspA expression prompted us to evaluate whether inhibition of PknD kinase activity might also correlate with reduced EspA levels. As anticipated, treatment with PknD inhibitor in both the presence and absence of osmotic stress diminished EspA expression. Moreover, PknD inhibition appeared to reduce EspA secretion, particularly in response to NaCl treatment. Again, the expression and secretion of ESAT-6 were unaffected by exposure to osmotic stress or treatment with PknD inhibitor. In sum, these findings suggest that Rv0516c and PknD phosphorylation selectively influence the expression and secretion of a particular ESX-1 substrate.

Discussion

The data presented here support a model in which Rv0516c represses the transcriptional response to osmotic stress (Figure 5-6). This effect may be mediated by the binding of unphosphorylated Rv0516c to an alternative sigma factor, preventing its association with RNA polymerase. In this model, PknD is activated by conditions of heightened environmental osmolarity and phosphorylates Rv0516c, triggering the release of the sequestered sigma factor and subsequent transcription of osmotically regulated genes, such as *Rv0516c* and the *espA* operon. Presumably, induction of *Rv0516c* affords a degree of feedback inhibition that is crucial to the tight regulation of this signal transduction pathway. Notably, this is the first report of a transcriptional protein directly involved in regulating the osmotic stress response of *Mtb*, and the first study to implicate osmotic stress in the activation of PknD.

This model is consistent with several of our findings. First, that *Rv0516c* bears homology to a sigma factor regulator, influences the transcriptional response to osmotic stress, and is itself highly induced by increasing environmental osmolarity supports its involvement in a transcriptional network that is responsive to osmotic stress. Second, Rv0516c is a well-characterized substrate for PknD *in vivo*, and we have shown that PknD phosphorylation mediates changes in the expression of both Rv0516c and EspA under conditions of osmotic stress. Consistent with this finding, mutation of the PknD phosphorylation site on Rv0516c affects the expression of these two proteins.

Despite the high degree of predicted structural homology between Rv0516c and SpoIIAA, the prototypical anti-anti-sigma factor from *B. subtilis*, we propose that Rv0516c acts as an anti-sigma factor. Though we initially anticipated that these proteins might play similar roles in the context of alternative sigma factor regulation, the apparent repression of certain osmotically regulated genes by Rv0516c argues against this assignment. Indeed, deletion of *Rv0516c* enhances both the transcriptional response and resistance of *Mtb* to osmotic stress; these phenotypes are consistent with the role of an anti-sigma factor. Moreover, the regulation of alternative sigma factors by STPKs has

thus far only been shown to occur via phosphorylation of their cognate anti-sigma factor proteins (*17, 18*). Our model is consistent with this regulatory framework. Finally, despite the apparent structural similarities between Rv0516c and SpoIIAA, it is important to note that the phosphorylation site of the former, Thr2, lies in a presumably unstructured, Ser/Thr-rich N-terminal region of the protein that is excluded from its predicted structural alignment with SpoIIAA (Figure 5-3A). In contrast, the phosphorylation site of SpoIIAA, Ser58, lies at the base of an alpha-helix on the opposing face of the protein (*34*). This distinction may be responsible for the apparent functional divergence of these two proteins.

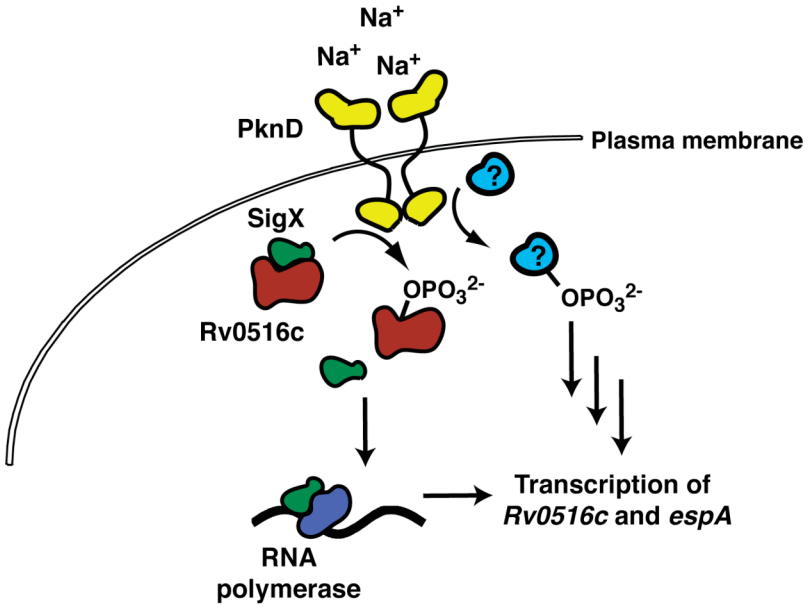

FIGURE 5-6. Model of the Rv0516c osmoregulatory pathway. Unphosphorylated Rv0516c binds and inhibits an alternative sigma factor (SigX) from interacting with RNA polymerase. Osmotic stress activates PknD phosphorylation of Rv0516c, which induces the release of the sigma factor and enables the transcription of osmotically regulated genes such as *Rv0516c* and *espA*. Phosphorylation of a second, unidentified substrate by PknD may also influence the expression of these genes in response to osmotic stress.

Though the identity of Rv0516c's putative cognate sigma factor remains unknown, only two alternative sigma factors from *Mtb* have been shown to directly induce *Rv0516c* expression (*35, 36*). The first, SigE, responds to various forms of cell wall stress and has been shown to enhance *Mtb* resistance to treatment with detergent and exposure to oxidative stress or high temperature (*37*). It is also required for full *Mtb* virulence. Likewise, SigF, the second candidate sigma factor, has been shown to be important for virulence, but the environmental conditions that regulate its activity have not been well characterized (*37*). Interestingly, the promoter region of *Rv0516c* contains sequences resembling the SigF-recognition motif, and a previous yeast two-hybrid study revealed an interaction between Rv0516c and this sigma factor (*36, 38*). Further, induction of *Rv0516c* by overexpression of PknD coincides with the induction of several

SigF-regulated genes (*16*). Notably, both SigE and SigF modulate the transcription of several *Mtb* genes that are also regulated by osmotic stress (*35, 36*).

We hypothesize that the primary transcriptional influence of Rv0516c is directed through an alternative sigma factor such as SigE or SigF, but it is also likely that Rv0516c interacts with a larger network of proteins that may or may not be integral to its involvement in the osmotic stress response. For example, the putative anti-anti-sigma factor Rv2638 associates with Rv0516c in yeast two-hybrid assays, and the *in vitro* binding of these two proteins is abolished by Rv0516c phosphorylation (*16, 38*). In addition, the STPKs PknB and PknE have been shown to phosphorylate Rv0516c *in vitro* (*16*), suggesting the potential involvement of Rv0516c in additional signaling pathways. PknB, which regulates cell wall morphology, phosphorylates RseA, the anti-sigma factor of SigE, in response to vancomycin treatment (*18*). Interestingly, microarray analysis has shown that vancomycin induces *Rv0516c* expression (*39*), though we were unable to detect induction at the protein level by Western blot analysis (data not shown).

Just as Rv0516c may participate in additional stress response pathways, we anticipate the involvement of other, as yet unidentified proteins in the osmotic stress response that may act independently of Rv0516c. Indeed, our findings suggest that PknD phosphorylates at least one other protein that induces Rv0516c expression upon NaCl treatment (c.f., blue protein in Figure 7). Other putative *Mtb* transcription factors induced by osmotic stress (e.g., WhiB1 and Rv2745c, Table 5-1) may also play a role in regulating bacterial osmoadaptation (*40, 41*). Regardless, it is evident that Rv0516c makes a significant contribution to the osmotic stress response of *Mtb*.

The transcriptional program initiated in part by Rv0516c has important consequences for bacterial metabolism. Several genes involved in protein biosynthesis (e.g., *rps*, *rpl*, and *arg* operons) are highly induced by osmotic stress and may compensate for the increase in protein misfolding that typically accompanies exposure to high osmolarity (*42*). These transcriptional changes are partially regulated by Rv0516c, whose deletion dramatically alters the bacterial response to osmotic stress. In the absence of *Rv0516c*, *Mtb* becomes more resistant to increasing osmolarity, suggesting the bacteria may be less sensitive to changes in turgor pressure. Indeed, the reduced proclivity of the mutant strain to aggregate following NaCl treatment may imply that the structure of the cell wall has been modified in a way that renders the bacteria less susceptible to osmotic challenge. This advantage may result from modifications to the peptidoglycan architecture of the cell wall that also confer enhanced resistance to vancomycin. Consistent with this hypothesis, PbpB, a protein involved in peptidoglycan biosynthesis, is upregulated by osmotic stress upon disruption of *Rv0516c* (data not shown). Moreover, *espA*, which has recently been shown to enhance the cell wall integrity of *Mtb* (*20*), is more highly transcribed by the mutant strain in response to NaCl treatment. These measures, all of which are likely to protect the cell wall from osmotic stress, are negatively regulated by Rv0516c, which supports its assignment as a transcriptional repressor.

It is not immediately clear why *Mtb* would choose to suppress its response to osmotic stress. Several considerations have likely influenced the evolution of this pathway. First, alternative sigma factors are tightly regulated to avoid aberrant transcription and carefully tune the bacterial response to diverse environmental conditions. Rv0516c may maintain that delicate transcriptional balance under conditions

of osmotic stress. Second, as increasing osmolarity results in the upregulation of several energetically taxing metabolic pathways, such as those involved in protein biosynthesis, it is logical for *Mtb* to suppress this response. Finally, the activation of EspA expression by osmotic stress must be tightly regulated as secretion of this virulence factor has significant immunological consequences that may interfere with the pathogen's life cycle.

Notably, the apparent regulation of EspA expression by Rv0516c and osmotic stress are consistent with the recent findings of Garces *et al*. that this virulence factor contributes to the cell wall integrity of *Mtb* (*20*). It is particularly striking that expression of EspA, but not ESAT-6, is affected by osmolarity. To our knowledge, this is the first example of a discrete environmental signal selectively regulating the expression of an ESX-1 substrate. Perhaps of greater interest is the finding that *Rv0516c* deletion and PknD inhibition reduce EspA secretion, but not that of ESAT-6. The current paradigm for ESX-1 secretion holds that each of these proteins forms a heterodimeric complex (ESAT-6 binds CFP-10, EspA binds EspC), and that each dimer is dependent on the other for secretion; the ESAT-6/CFP-10 heterodimer cannot be secreted in the absence of the EspA/EspC heterodimer, and vice versa (*24, 25*). However, the fact that EspA secretion is selectively regulated by Rv0516c and PknD, and its expression selectively induced by osmotic stress, suggests EspA may have a function distinct from its role in ESX-1 secretion that is responsive to environmental conditions affecting cell wall integrity.

Taken together, these data establish the framework for an unprecedented osmoregulatory pathway in *Mtb* that modulates the transcriptional and physiological response of the pathogen to osmotic stress. In addition, we have demonstrated the selective environmental regulation of an ESX-1 substrate that is mediated by components of this pathway, which may have implications for its role in *Mtb* biology. We conclude that *Mtb* has evolved a complex network of proteins to adapt to external osmolarity, and that this network may represent a new paradigm for bacterial adaptation to osmotic stress.

Materials and Methods

Bacterial strains and culture conditions

Mtb strains CDC1551 and *Rv0516c* Tn, a CDC1551 mutant with a Himar1 transposon insertion in the *Rv0516c* gene (JHU0516c-101) (*43*), were obtained from the Tuberculosis Animal Research and Gene Evaluation Taskforce (NIH/NIAID contract number N01 AI-30036). *Escherichia coli* strains used for the preparation of mycobacterial plasmids were grown in LB broth or agar with the appropriate antibiotics. *Mtb* strain CDC1551 and its derivatives were cultured in Middlebrook 7H9 medium (Difco) containing 10% oleic acid-albumin-dextrose-catalase (OADC) enrichment (Difco), 0.5% glycerol, and 0.05% Tween-80, or in Sauton medium (0.5 g KH_2PO_4, 0.5 g $MgSO_4$, 4.0 g L-asparagine, 60 mL glycerol, 0.05 g ferric ammonium citrate, 2.0 g citric acid, 0.1 mL 1% (w/v) $ZnSO_4$ in 900 mL H_2O supplemented with 0.05% Tween-80 and adjusted to pH 7 with 10 M KOH). Solid medium was prepared using Middlebrook 7H11 solid agar (Difco) and the same supplements as the 7H9-based medium with the addition of 100 μg/mL cycloheximide (Sigma). Antibiotics were used to maintain episomal plasmids at the following concentrations: hygromycin (150 μg/mL for *E. coli*,

50 μg/mL for *Mtb*), kanamycin (50 μg/mL for *E. coli*, 25 μg/mL for *Mtb*). Unless otherwise indicated, cultures were grown in roller bottles or aerated shaker flasks incubated at 37 °C in either a roller bottle incubator or an orbital shaker, respectively. Bacterial growth was monitored by measuring the optical density at 600 nm (OD_{600}) with a Thermo Scientific Genesys 20 Visible Spectrophotometer.

Plasmid preparation

All DNA constructs were derived from the mycobacterial shuttle vector pMV261. The *egfp* gene from pEGFP (Clontech), which contains two fluorescence-enhancing mutations (F64L and S65T), was subcloned into pMV261-kan to generate pMWS114. *Rv0516c* promoter and coding sequences were amplified from *Mtb* strain CDC1551 genomic DNA isolated using the cetyltrimethylammonium bromide (CTAB)-lysozyme method (*44*). Genomic DNA was similarly isolated from *Rv0516c* Tn and analyzed by PCR to verify the presence of the Himar1 transposon in the *Rv0516c* gene (data not shown). The p*Rv0516c-T2A* plasmid was generated by introducing a T2A mutation into the *Rv0516c* gene encoded by p*Rv0516c* using QuikChange mutagenesis (Stratagene). All constructs were confirmed by DNA sequencing.

Sample preparation for microarray and protein analysis

Mtb cultures were grown to mid-log phase from frozen stocks in Middlebrook 7H9-based medium. The cells were washed once in Sauton medium and then diluted to an OD_{600} of 0.05 (*Rv0516c* Tn), 0.1 (CDC1551), or 0.12 (*Rv0516c* Tn::p*Rv0516c* and *Rv0516c* Tn::p*Rv0516c*-T2A) and grown to mid-log phase in the same medium. The bacteria were subsequently pelleted for 5 min at 500 rpm at rt to remove clumps, diluted to an OD_{600} of 0.1, and grown for a period of 2 days to early log phase. Samples for microarray analysis were divided into two 30-mL cultures, the first of which was centrifuged for 10 min at 3500 rpm at rt. After gently decanting the culture supernatant, the cell pellet was frozen on dry ice and stored at -80 °C until future RNA extraction (t=0 sample). The remaining culture was treated with a concentrated solution of NaCl in Sauton medium to give a final concentration of 140 mM NaCl and incubated for an additional hour at 37 °C prior to harvesting and freezing the cells (t=1 h sample).

Samples for protein analysis were divided into two 30-mL cultures, one of which was treated with a concentrated solution of either NaCl, KCl, or sucrose in Sauton medium to give a final concentration of 140 mM (NaCl or KCl) or 280 mM (sucrose) prior to incubating the cultures at 37 °C for an additional 3 h. The cells were then harvested by centrifugation (3500 rpm for 10 min at rt) and stored at -80 °C. Culture supernatants were twice sterilized by filtration through 0.2-μm filters prior to removal from the biosafety level 3 facility, concentrated by centrifugation using 3 kDa molecular weight cut-off filter units (Millipore), and stored at -20 °C. Cell lysates for protein analysis were prepared as previously described and stored at -20 °C (*25*). Briefly, frozen cell pellets were resuspended in 500 μL resuspension buffer (50 mM Tris pH 7.5, 5 mM EDTA, 1 mM β-mercaptoethanol, 1 complete, mini EDTA-free protease inhibitor cocktail tablet (Roche)), boiled for 20 min, disrupted by two 45-sec cycles of bead-

beating, and centrifuged for 1 min at 14,000 rpm at rt to clarify the lysates prior to removal from the biosafety level 3 facility.

RNA extraction and microarray analysis

RNA extraction and microarray analysis were performed as previously described (*45*). Briefly, cell pellets were resuspended in TRIzol reagent (Invitrogen), disrupted by bead-beating, and centrifuged to clarify the cellular lysates, which were subsequently transferred to tubes containing Heavy Phase Lock Gel (5 PRIME) and chloroform. Each sample was inverted for 2 min prior to centrifugation and removal of the aqueous layer, which was then precipitated by treatment with isopropanol and high salt. RNA purification and DNase treatment were performed using the RNeasy kit (Qiagen) according to the manufacturer's instructions. Five micrograms of each RNA sample were reverse transcribed in the presence of aminoallyl dUTP (Fermentas) and covalently labeled with either Cy3 or Cy5 dyes. Pairs of differentially labeled cDNA were prepared from the RNA of corresponding t=0 and t=1 h samples. Probe pairs were hybridized overnight at 42 °C to whole-genome *Mtb* arrays provided by the Pathogen Functional Genomics Resource Center under the NIAID contract number N01 AI-15447. Arrays were scanned with a GenePix 4000B scanner and analyzed using GenePix 6.0 and Acuity 4.1 software. Lowess-normalized data from four biological replicates were analyzed using the Significance Analysis of Microarrays (SAM) program from Stanford University (*46*). Genes with a mean $\log_2$ fold change of at least 1 with a q-value of zero were deemed significant. Genes whose transcriptional regulation is affected by *Rv0516c* were defined as having a mean $\log_2$ fold change ratio of *Rv0516c* Tn to wild-type ≥ 1.7.

Western blot analysis

Proteins from cell lysate and culture supernatant samples were analyzed by SDS-PAGE and Western blotting. Total protein concentrations were determined by Bradford assay (Bio-Rad). Equal amounts of each culture supernatant (10 μg) and cell lysate (1-5 μg) sample were separated by SDS-PAGE, and immunoblotting was performed to detect proteins of interest. Antibodies against ESAT-6 (mouse monoclonal, HYB 076-08, ab26246), GroEL (mouse monoclonal, ab20519), and the DDDDK tag (rabbit polyclonal, ab1162) were purchased from Abcam and used at dilutions of 1:500, 1:200, and 1:50,000, respectively. The EspA antibody (rabbit polyclonal serum) was a kind gift from S. Fortune at Harvard University. Horseradish peroxidase-conjugated secondary antibodies (SouthernBiotech) were used at a dilution of 1:5000 and detected using chemiluminescent reagents (Pierce). Equal protein loading was confirmed using GroEL, a cytosolic molecular chaperone, as a loading control for cell lysate samples and by assessing the total protein content of culture supernatants with India ink (data not shown). The absence of GroEL in overexposed blots of culture supernatant samples was also verified to ensure that cell lysis was not responsible for any observed differences in protein secretion.

GFP reporter assays

The 1000-bp promoter region of *Rv0516c* followed by an ATG start site was inserted immediately upstream of the *egfp* gene in pMWS114. This construct was transformed into *Mtb* strain CDC1551 to generate CDC1551::p*Rv0516c*-GFP. CDC1551::p*Rv0516c*-GFP was grown to mid-log phase in Middlebrook 7H9-based medium, washed once in Sauton medium, diluted to an OD_{600} of 0.1 and grown to mid-log phase in the same medium. Cells were pelleted for 5 min at 500 rpm at rt to remove clumps and used to inoculate triplicate cultures at an OD_{600} of 0.1, which were grown for 2 days to early log phase. Each culture was then divided into four 10-mL aliquots in 50-mL conical tubes, three of which were treated with a concentrated solution of either NaCl, KCl, or sucrose in Sauton medium to achieve a final concentration of 140 mM (NaCl or KCl) or 280 mM (sucrose). The cultures were then incubated at 37 °C for an additional 2 days in an orbital shaker, at which point the OD_{600} was determined. A 1-mL aliquot was removed from each culture and centrifuged for 1 min at 14,000 rpm at rt. The supernatant was discarded and the cells resuspended in 200 μL of 10% buffered formalin phosphate containing 0.05% Tween-80. The samples were removed from the biosafety level 3 facility after 1 h to allow sufficient time for bacterial sterilization. The cells were then transferred to a 96-well plate in a biosafety level 2 hood. The total cellular fluorescence of each sample was measured and normalized by cell density.

In vitro *growth studies*

CDC1551, *Rv0516c* Tn, and *Rv0516c* Tn::p*Rv0516c* strains were grown to mid-log phase from frozen stocks in Middlebrook 7H9-based medium. Cells were pelleted for 5 min at 500 rpm at rt to remove clumps and used to inoculate triplicate 15-mL cultures of the same medium at an OD_{600} of 0.05 in aerated shaker flasks. Once the cells had reached mid-log phase, they were treated with a concentrated solution of NaCl in 7H9-based medium to give a final concentration of 500 mM NaCl and incubated for an additional 3 days at 37 °C. Bacterial growth was monitored daily for the duration of the study.

Cell wall stress resistance assays

Minimal inhibitory concentrations were determined using the broth microdilution method as previously described with minor modifications (*47*). CDC1551, *Rv0516c* Tn, and *Rv0516c* Tn::p*Rv0516c* strains were grown to mid-log phase from frozen stocks in Middlebrook 7H9-based medium. Cells were pelleted for 5 min at 500 rpm at rt to remove clumps and used to inoculate triplicate wells of a 96-well plate containing two-fold serial dilutions of each drug (i.e., isoniazid, SDS, NaCl, D-cycloserine, or vancomycin) in 150 μL medium at an OD_{600} of 0.02. Cultures were incubated for 7 and 14 d at 37 °C. The minimal inhibitory concentration was defined as the lowest concentration of drug that visibly inhibited bacterial growth.

To evaluate vancomycin resistance, CDC1551, *Rv0516c* Tn, and *Rv0516c* Tn::p*Rv0516c* strains were grown to mid-log phase from frozen stocks in Middlebrook

7H9-based medium, pelleted for 5 min at 500 rpm at rt to remove clumps, and used to inoculate triplicate 10-mL cultures in 50-mL conical tubes at an OD_{600} of 0.05 in 7H9-based medium containing 1.5 μg/mL vancomycin. The cultures were incubated at 37 °C on an orbital shaker for 3 days and then centrifuged at 3500 rpm for 5 min at rt. The harvested cells were resuspended in 10 mL of 7H9-based medium, serially diluted, and plated for the enumeration of colony-forming units.

Structural modeling

The protein structure of Rv0516c was modeled using the freely available PHYRE Protein Fold Recognition server (http://www.sbg.bio.ic.ac.uk/~phyre/) (*48*). The estimated precision value of the SpoIIAA protein from *B. subtilis* (PDB: 1auz) was 100%. MacPyMOL was used to align the Rv0516c model with the structure of SpoIIAA.

PknD inhibition assays

CDC1551, *Rv0516c* Tn::p*Rv0516c* and *Rv0516c* Tn::p*Rv0516c*-T2A *Mtb* cultures were grown to mid-log phase from frozen stocks in Middlebrook 7H9-based medium, washed once in Sauton medium and then diluted to an OD_{600} of 0.1 (CDC1551) or 0.12 (*Rv0516c* Tn::p*Rv0516c* and *Rv0516c* Tn::p*Rv0516c*-T2A) and grown to mid-log phase in the same medium. The bacteria were subsequently pelleted for 5 min at 500 rpm at rt to remove clumps, diluted to an OD_{600} of 0.1, and grown for a period of 2 days to early log phase. Each culture was divided into four 30-mL cultures, two of which were treated with 60 μM SP600125 ("InSolution JNK Inhibitor II", EMD Chemicals). SP600125 is a c-Jun N-terminal kinase (JNK) inhibitor that specifically inhibits phosphorylation by the STPK PknD for at least 8 h at this concentration (*16*). Following 2 h at 37 °C, a concentrated solution of NaCl in Sauton medium was added to one of the untreated cultures and to one of the SP600125-treated cultures, giving a final concentration of 140 mM NaCl. All four cultures were incubated for an additional 3 h at 37 °C, and then culture supernatants and cell lysates were prepared for SDS-PAGE and Western blot analysis as already described.

References

1. Rohde, K., Yates, R. M., Purdy, G. E., and Russell, D. G. (2007) *Mycobacterium tuberculosis* and the environment within the phagosome, *Immunol. Rev. 219*, 37-54.

2. Appelberg, R. (2006) Macrophage nutriprive antimicrobial mechanisms, *J. Leukoc. Biol. 79*, 1117-1128.

3. Sleator, R. D., and Hill, C. (2002) Bacterial osmoadaptation: the role of osmolytes in bacterial stress and virulence, *FEMS Microbiol. Rev. 26*, 49-71.

4. Steyn, A. J., Joseph, J., and Bloom, B. R. (2003) Interaction of the sensor module of *Mycobacterium tuberculosis* H37Rv KdpD with members of the Lpr family, *Mol. Microbiol. 47*, 1075-1089.

5. Csonka, L. N. (1989) Physiological and genetic responses of bacteria to osmotic stress, *Microbiol. Rev. 53*, 121-147.

6. Sleator, R. D., and Hill, C. (2005) A novel role for the LisRK two-component regulatory system in listerial osmotolerance, *Clin. Microbiol. Infect. 11*, 599-601.

7. Price, C. T., Bukka, A., Cynamon, M., and Graham, J. E. (2008) Glycine betaine uptake by the ProXVWZ ABC transporter contributes to the ability of *Mycobacterium tuberculosis* to initiate growth in human macrophages, *J. Bacteriol. 190*, 3955-3961.

8. Russell, D. G. (2001) *Mycobacterium tuberculosis*: here today, and here tomorrow, *Nat. Rev. Mol. Cell Biol. 2*, 569-577

9. Jordan, S., Hutchings, M. I., and Mascher, T. (2008) Cell envelope stress response in Gram-positive bacteria, *FEMS Microbiol. Rev. 32*, 107-146.

10. Hoch, J. A. (2000) Two-component and phosphorelay signal transduction, *Curr. Opin. Microbiol. 3*, 165-170.

11. Bashyam, M. D., and Hasnain, S. E. (2004) The extracytoplasmic function sigma factors: role in bacterial pathogenesis, *Infect. Genet. Evol. 4*, 301-308.

12. Helmann, J. D. (1999) Anti-sigma factors, *Curr. Opin. Microbiol. 2*, 135-141.

13. Yudkin, M. D., and Clarkson, J. (2005) Differential gene expression in genetically identical sister cells: the initiation of sporulation in *Bacillus subtilis*, *Mol. Microbiol. 56*, 578-589.

14. Greenstein, A. E., Grundner, C., Echols, N., Gay, L. M., Lombana, T. N., Miecskowski, C. A., Pullen, K. E., Sung, P. Y., and Alber, T. (2005) Structure/function studies of Ser/Thr and Tyr protein phosphorylation in *Mycobacterium tuberculosis*, *J. Mol. Microbiol. Biotechnol. 9*, 167-181.

15. Molle, V., and Kremer, L. (2010) Division and cell envelope regulation by Ser/Thr phosphorylation: Mycobacterium shows the way, *Mol. Microbiol. 75*, 1064-1077.

16. Greenstein, A. E., MacGurn, J. A., Baer, C. E., Falick, A. M., Cox, J. S., and Alber, T. (2007) *M. tuberculosis* Ser/Thr protein kinase D phosphorylates an anti-anti-sigma factor homolog, *PLoS Pathog. 3*, e49.

17. Park, S. T., Kang, C. M., and Husson, R. N. (2008) Regulation of the SigH stress response regulon by an essential protein kinase in *Mycobacterium tuberculosis*, *Proc. Natl. Acad. Sci. U. S. A. 105*, 13105-13110.

18. Barik, S., Sureka, K., Mukherjee, P., Basu, J., and Kundu, M. (2010) RseA, the SigE specific anti-sigma factor of *Mycobacterium tuberculosis*, is inactivated by phosphorylation-dependent ClpC1P2 proteolysis, *Mol. Microbiol. 75*, 592-606.

19. Moker, N., Brocker, M., Schaffer, S., Kramer, R., Morbach, S., and Bott, M. (2004) Deletion of the genes encoding the MtrA-MtrB two-component system of *Corynebacterium glutamicum* has a strong influence on cell morphology, antibiotics susceptibility and expression of genes involved in osmoprotection, *Mol. Microbiol. 54*, 420-438.

20. Garces, A., Atmakuri, K., Chase, M. R., Woodworth, J. S., Krastins, B., Rothchild, A. C., Ramsdell, T. L., Lopez, M. F., Behar, S. M., Sarracino, D. A., and Fortune, S. M. (2010) EspA acts as a critical mediator of ESX1-dependent virulence in *Mycobacterium tuberculosis* by affecting bacterial cell wall integrity, *PLoS Pathog. 6*, e1000957.

21. Carrithers, M. D., Dib-Hajj, S., Carrithers, L. M., Tokmoulina, G., Pypaert, M., Jonas, E. A., and Waxman, S. G. (2007) Expression of the voltage-gated sodium channel NaV1.5 in the macrophage late endosome regulates endosomal acidification, *J. Immunol. 178*, 7822-7832.

22. Hackam, D. J., Rotstein, O. D., Zhang, W. J., Demaurex, N., Woodside, M., Tsai, O., and Grinstein, S. (1997) Regulation of phagosomal acidification. Differential targeting of Na+/H+ exchangers, Na+/K+-ATPases, and vacuolar-type H+-atpases, *J. Biol. Chem. 272*, 29810-29820.

23. Xu, Y., Labedan, B., and Glansdorff, N. (2007) Surprising arginine biosynthesis: a reappraisal of the enzymology and evolution of the pathway in microorganisms, *Microbiol. Mol. Biol. Rev. 71*, 36-47.

24. MacGurn, J. A., Raghavan, S., Stanley, S. A., and Cox, J. S. (2005) A non-RD1 gene cluster is required for Snm secretion in *Mycobacterium tuberculosis*, *Mol. Microbiol. 57*, 1653-1663.

25. Fortune, S. M., Jaeger, A., Sarracino, D. A., Chase, M. R., Sassetti, C. M., Sherman, D. R., Bloom, B. R., and Rubin, E. J. (2005) Mutually dependent secretion of proteins required for mycobacterial virulence, *Proc. Natl. Acad. Sci. U. S. A. 102*, 10676-10681.

26. Raghavan, S., Manzanillo, P., Chan, K., Dovey, C., and Cox, J. S. (2008) Secreted transcription factor controls *Mycobacterium tuberculosis* virulence, *Nature 454*, 717-721.

27. Duncan, L., Alper, S., and Losick, R. (1996) SpoIIAA governs the release of the cell-type specific transcription factor sigma F from its anti-sigma factor SpoIIAB, *J. Mol. Biol. 260*, 147-164.

28. Dhandayuthapani, S. (2007) Stress response of genes encoding putative stress signaling molecules of *Mycobacterium tuberculosis*, *Front. Biosci. 12*, 4676-4681.

29. Jung, J. U., Gutierrez, C., Martin, F., Ardourel, M., and Villarejo, M. (1990) Transcription of *osmB*, a gene encoding an *Escherichia coli* lipoprotein, is regulated by dual signals. Osmotic stress and stationary phase, *J. Biol. Chem. 265*, 10574-10581.

30. Siegel, S. M., and Roberts, K. (1966) The microbiology of saturated salt solutions and other harsh environments, I. Growth of a salt-dependent bacterial form in LiCL-saturated nutrient broth, *Proc. Natl. Acad. Sci. U. S. A. 56*, 1505-1508.

31. Wai, S. N., Mizunoe, Y., Takade, A., Kawabata, S. I., and Yoshida, S. I. (1998) *Vibrio cholerae* O1 strain TSI-4 produces the exopolysaccharide materials that determine colony morphology, stress resistance, and biofilm formation, *Appl. Environ. Microbiol. 64*, 3648-3655.

32. David, S. (2001) Synergic activity of D-cycloserine and beta-chloro-D-alanine against *Mycobacterium tuberculosis*, *J. Antimicrob. Chemother. 47*, 203-206.

33. Kahne, D., Leimkuhler, C., Lu, W., and Walsh, C. (2005) Glycopeptide and lipoglycopeptide antibiotics, *Chem. Rev. 105*, 425-448.

34. Kovacs, H., Comfort, D., Lord, M., Campbell, I. D., and Yudkin, M. D. (1998) Solution structure of SpoIIAA, a phosphorylatable component of the system that regulates transcription factor sigmaF of *Bacillus subtilis*, *Proc. Natl. Acad. Sci. U. S. A. 95*, 5067-5071.

35. Manganelli, R., Voskuil, M. I., Schoolnik, G. K., and Smith, I. (2001) The *Mycobacterium tuberculosis* ECF sigma factor sigmaE: role in global gene expression and survival in macrophages, *Mol. Microbiol. 41*, 423-437.

36. Geiman, D. E., Kaushal, D., Ko, C., Tyagi, S., Manabe, Y. C., Schroeder, B. G., Fleischmann, R. D., Morrison, N. E., Converse, P. J., Chen, P., and Bishai, W. R. (2004) Attenuation of late-stage disease in mice infected by the *Mycobacterium tuberculosis* mutant lacking the SigF alternate sigma factor and identification of SigF-dependent genes by microarray analysis, *Infect. Immun. 72*, 1733-1745.

37. Manganelli, R., Provvedi, R., Rodrigue, S., Beaucher, J., Gaudreau, L., and Smith, I. (2004) Sigma factors and global gene regulation in *Mycobacterium tuberculosis*, *J. Bacteriol. 186*, 895-902.

38. Parida, B. K., Douglas, T., Nino, C., and Dhandayuthapani, S. (2005) Interactions of anti-sigma factor antagonists of *Mycobacterium tuberculosis* in the yeast two-hybrid system, *Tuberculosis 85*, 347-355.

39. Provvedi, R., Boldrin, F., Falciani, F., Palu, G., and Manganelli, R. (2009) Global transcriptional response to vancomycin in *Mycobacterium tuberculosis*, *Microbiology 155*, 1093-1102.

40. Agarwal, N., Raghunand, T. R., and Bishai, W. R. (2006) Regulation of the expression of *whiB1* in *Mycobacterium tuberculosis*: role of cAMP receptor protein, *Microbiology 152*, 2749-2756.

41. Mehra, S., Dutta, N. K., Mollenkopf, H. J., and Kaushal, D. (2010) *Mycobacterium tuberculosis* MT2816 encodes a key stress-response regulator, *J. Infect. Dis. 202*, 943-953.

42. Ignatova, Z., and Gierasch, L. M. (2007) Effects of osmolytes on protein folding and aggregation in cells, *Methods Enzymol. 428*, 355-372.

43. Lamichhane, G., Zignol, M., Blades, N. J., Geiman, D. E., Dougherty, A., Grosset, J., Broman, K. W., and Bishai, W. R. (2003) A postgenomic method for predicting essential genes at subsaturation levels of mutagenesis: application to *Mycobacterium tuberculosis*, *Proc. Natl. Acad. Sci. U. S. A. 100*, 7213-7218.

44. Larsen, M. H., Biermann, K., Tandberg, S., Hsu, T., and Jacobs, W. R., Jr. (2007) Genetic Manipulation of *Mycobacterium tuberculosis*, *Curr. Protoc. Microbiol. Chapter 10*, Unit 10A 12.

45. Rustad, T. R., Harrell, M. I., Liao, R., and Sherman, D. R. (2008) The enduring hypoxic response of *Mycobacterium tuberculosis*, *PLoS ONE 3*, e1502.

46. Tusher, V. G., Tibshirani, R., and Chu, G. (2001) Significance analysis of microarrays applied to the ionizing radiation response, *Proc. Natl. Acad. Sci. U. S. A. 98*, 5116-5121.

47. Hugonnet, J. E., Tremblay, L. W., Boshoff, H. I., Barry, C. E., 3rd, and Blanchard, J. S. (2009) Meropenem-clavulanate is effective against extensively drug-resistant *Mycobacterium tuberculosis*, *Science 323*, 1215-1218.

48. Kelley, L. A., and Sternberg, M. J. (2009) Protein structure prediction on the Web: a case study using the Phyre server, *Nat. Protoc. 4*, 363-371.